Physics Investigations of a Compact Simulation of a Large Fast Breeder Reactor

SNEAK-Assembly 10

compiled by
H. Giese
Institut für Neutronenphysik und Reaktortechnik
Projekt Schneller Brüter

Kernforschungszentrum Karlsruhe

KERNFORSCHUNGSZENTRUM KARLSRUHE

Institut für Neutronenphysik und Reaktortechnik
Projekt Schneller Brüter

KfK 2573

Physics Investigations of a Compact
Simulation of a Large Fast
Breeder Reactor

SNEAK-Assembly 10

compiled by

H. Giese

with contributions from

F. Helm, G. Henneges, U. v. Möllendorff
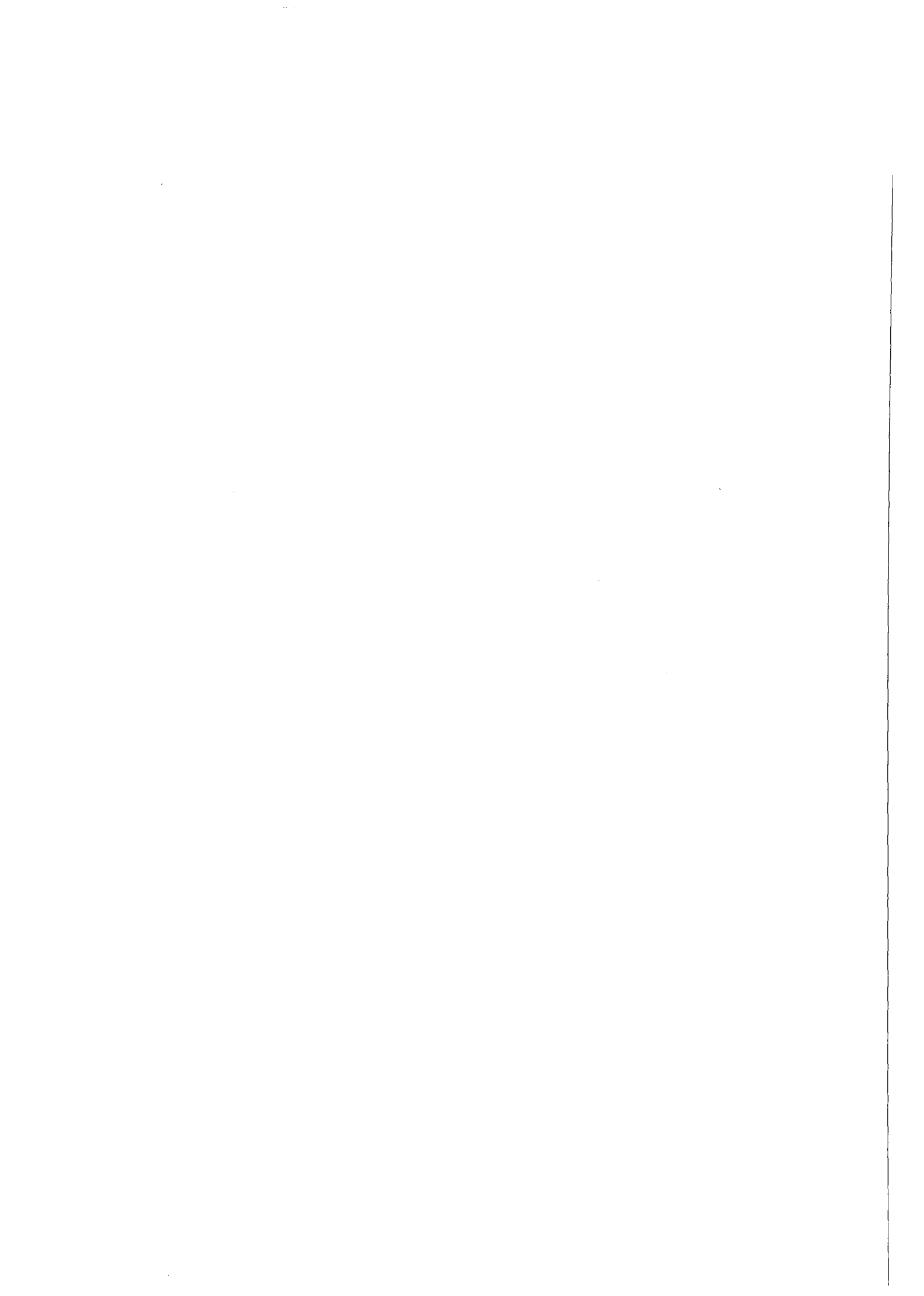
Physics Investigations of a Compact Simulation of a Large Fast
Breeder Reactor - SNEAK-Assembly 10

Abstract

SNEAK-10 was the first SNEAK assembly devoted to the investigation
of certain neutronic properties of breeder reactors with a nominal
power of $\sim$ 1200 MW$_{el}$. The investigations were concentrated on
flux tilts and related mutual control rod interactions, occurring
upon changes of control insertion depths.

As the physical size and fuel inventory of such reactors signifi-
cantly exceed the capacity of SNEAK the investigated cores had to
be compacted by a factor of approximately 2, without affecting the
phenomena of interest. This was achieved by the use of densified
compositions without sodium and adequate reduction of the physical
dimensions. Lacking sufficient amounts of plutonium, uranium fuel
was used in all investigated configurations.

The measured and calculated results indicate to what extent various
calculational methods are able to predict criticality, control rod
worthsand flux distributions in large fast reactors. In particular
they show where the use of a synthesis method or a direct three-
dimensional calculation is advantageous. The KFKINR cross section
set was used as a data base.

Physikalische Untersuchungen an einer kompakten Simulation eines
großen Schnellbrüter-Cores - Anordnung SNEAK-10

Zusammenfassung

SNEAK-10 war die erste SNEAK-Anordnung, die der Untersuchung bestimmter
neutronenphysikalischer Eigenschaften von Brutreaktoren mit einer
nominellen Leistung von $\sim$ 1200 MW_{el} gewidmet war. Die Untersuchungen
konzentrierten sich auf Flußverwerfungen und Kontrollstab-Wechselwir-
kungseffekte, wie sie beim Verändern der Eintauchtiefe der Regelbänke
auftreten.

Da sowohl die Coreabmessungen als auch das Brennstoffinventar solcher
Reaktoren die bei SNEAK zur Verfügung stehende Kapazität deutlich über-
steigen, mußten die zu untersuchenden Cores um etwa einen Faktor 2
kompaktiert werden, ohne dabei jedoch die interessierenden Phänomene
zu verfälschen. Dies wurde erreicht durch Verdichtung der Original-
kompositionen ohne Natrium und angemessene Reduktion aller linearen
Dimensionen. Da keine ausreichenden Mengen Plutonium zur Verfügung
standen, wurde in allen untersuchten Corekonfigurationen Uran-Brenn-
stoff verwendet.

Die gemessenen und berechneten Resultate vermitteln einen Überblick
darüber, inwieweit die verwendeten Rechenmethoden imstande sind,
bestimmte Größen wie Kritikalität, Kontrollstabwerte und Flußver-
teilungen in großen Brutreaktoren vorherzusagen. Insbesondere wird
demonstriert, in welchen Fällen die Anwendung von Syntheserechnungen
oder direkten dreidimensionalen Rechnungen zu bevorzugen ist. Als
Datenbasis wurde in allen Rechnungen der KFKINR-Querschnittsatz
verwendet.

Table of Contents

1. Introduction

During the last years various studies were performed with the objective
to predict the neutronic properties of "second generation" breeder
reactors having a nominal electrical power in the region of 1000 -
2000 MW.

It was found in these studies that cores of this size will exhibit
certain neutronic phenomena which are not known from breeder reactors
of smaller size, i.e.

    i) flux shifts over the whole core rather than only
       local flux depressions upon control rod insertion

    ii) strong mutual interaction of distantly spaced
       control rods as a direct consequence of i).

It is evident that special consideration must be given to these effects
when assessing the operational characteristics and safety of such reac-
tors. E.g., a precise prediction of control rod worths is essential to
assure sufficient shutdown margins, precluding accidental criticality
or supercriticality during reactor maintenance and refueling operations.

An investigation in a critical facility was supposed to be helpful in
getting a more precise knowledge of the magnitude of the above mentioned
effects, and in testing the ability of present reactor computational
tools to predict them. However, a real-size mock-up of such a large
reactor in SNEAK was not possible because of insufficient core matrix
dimensions and lack of an adequate fuel inventory. Therefore the
dimensions of the reference core under investigation had to be reduced
in order to suit the SNEAK matrix dimensions, without affecting the
phenomena of interest.

As was described in /1,2/ this can be done by using the core compositions without sodium, increasing the density by compaction, and reducing all linear core dimensions by the same factor. This procedure results in a compact core that has dimensions comparable to those of the reference core in terms of neutron migration length and should therefore exhibit similar distance dependent control rod influences and interactions.

The spectral effect of the missing sodium content of the reference core can be partially compensated by introduction of adequate amounts of higher-density scattering materials such as graphite into the compacted compositions.

The SNEAK-10 experimental program comprised the investigation of three uranium fueled compact core configurations with the following objectives:

SNEAK-10-A was built to study the neutronic properties of a typical large breeder core in the "follower state". The designation "follower state" indicates that all control rods are totally withdrawn (parked) and the respective positions are filled with sodium (Fig. 4). In this configuration measurements of the central material worth, the flux distribution, importance profiles, and the reactivity effect of various control rod insertion patterns were performed.

SNEAK-10-B had basically the same core design like 10-A, but the inner control rod ring was inserted to about the core midplane and the reactivity loss was compensated by filling 8 of the 12 outer follower positions with core material (Fig. 5). This modification of the core was built in order to study the change of axial and radial flux distributions with respect to the all-follower configuration. The experimental program in this assembly was therefore concentrated on the measurement of axial and radial fission rate distributions.

SNEAK-10-C had an arrangement of Na-followers which was selected so that the core was a (uranium fueled) compact mock-up of the BIZET-assembly BZ-A /20/ which was built in ZEBRA as a British German Common Experiment (Fig. 6). The investigations in 10-C encompassed the measurement of fission rate profiles and the reactivity of various control rod configurations. With respect to the other SNEAK-10 assemblies, 10-C offers the advantage that comparing the experimental results with those of BZ-A will help to clarify the transferability of compact-core characteristics to a breeder of actual size.

2.   Description of the assemblies

2.1   Adaptation to a large breeder core

The reference breeder core chosen for investigation in SNEAK-10-A and 10-B was taken from a preliminary design study of the SNR-2 with a nominal power of $\sim$ 1200 MW$_{el}$ /3/. In accordance with this reference core, both assemblies had two cylindrical core zones containing two concentric rings of control rods, one located in the inner core zone close to the core center, and the other in the outer core zone adjacent to the inner boundary.

The choice of the compact core compositions was ruled by the following aspects:

a) Fuel
   Since no sufficient amounts of Pu fuel were available all SNEAK-10 assemblies had to be fueled with uranium.

b) Compaction factor

   The reference core should be compacted by about a factor
   of 2, in order to suit the SNEAK-matrix dimensions and
   fuel inventory.

c) Adjustment of spectra

   The neutron spectra of the compact and reference core
   should resemble each other as closely as possible.

The reference composition used for the adjustment was an SNR-2 compo-
sition which had been proposed by Interatom for the generation of
weighting spectra for the KFKINR-002 cross section set /4/.

In order to select the most suitable compact composition, 1-D homogene-
ous diffusion calculations in spherical geometry were performed, yielding
the following parameters for a comparison with the reference core:

a) Spectral indices: σ_{f8}/σ_{f5}, σ_{c8}/σ_{f5}

b) The radius r_K of a critical sphere consisting of the
   respective material, being correlated with the
   material buckling via
   $$B_m^2 = \frac{\pi}{r_K}^2$$

c) The one-group condensed cross sections $\nu\Sigma_f$ and Σ_c

A comparison of the corresponding parameters of the inner core compo-
sition that was chosen for SNEAK-10 under consideration of the above
mentioned aspects, and the SNR-2 reference composition is given in
Table 2.1.

The remaining discrepancies are caused by unavoidable changes of
composition, such as the use of uranium instead of plutonium fuel and

Table 2.1 Comparison of neutronic Parameters of Reference and Compact Core

	SNR-2	SNR-2 fuelled with U235 $(1.5*N_{Pu239+241}=N_{U235})$	SNEAK-10	Resulting Compaction Factor
1 group cross sections $[cm^{-1}]$				
$\nu\Sigma_f$	.620-2	.731-2	.137-1	2.21
Σ_c	.285-2	.272-2	.509-2	1.79
Critical parameters				
$B_m^2 [m^{-2}]$	8.35	11.18	29.78	
r_K (unreflected sphere) $[m]$	1.087	.940	.576	1.89
Reaction rate balance				
$\frac{1}{\nu\Sigma_f} * \begin{bmatrix} \Sigma_f \\ \Sigma_c \\ DB^2 \end{bmatrix}$ Σ_f	.341	.396	.396	
Σ_c	.460	.373	.371	
DB^2	.199	.231	.233	
Spectral indices				
σ_{f8}/σ_{f5}	.0207	.0248	.0305	
σ_{c8}/σ_{f5}	.141	.140	.134	

the replacement of the sodium and part of the steel by graphite. In order to demonstrate this for the effect of the fuel, column 2 shows the nuclear parameters for the SNR-2 composition when fueled with uranium. They show considerably reduced differences to the parameters of the compact composition used in SNEAK-10.

2.2 Unit cells and general geometrical properties

Fig. 1 shows the core unit cells, "window cells", and the fuel element loading schemes. Window cells are necessary to build up a horizontal channel for the measurement of radial fission-chamber and importance traverses. The aluminium spacers replaced 2 graphite platelets and 1 UO_2 platelet.

All assemblies had the same core height of approximately 48.9 cm and were surrounded by a radial blanket of about 30 cm thickness con- sisting of depleted uranium. The height of the axial blanket, also consisting of depleted uranium, varied slightly for the different core regions, because no sufficient amounts of uniform material (platelets, blocks, rodlets) were available.

Figs. 2 and 3 show the cell structures and loading schemes of the SNEAK shim and safety rods. Special consideration was given to the design of the different unit cells with respect to minimum reactivity disturbance of the surrounding core.

2.3 SNEAK-10-A

A horizontal cross section of the clean critical core SNEAK-10-A is given in Fig. 4. The term "clean critical" designates the core requi- ring a minimum of shim rod (absorber part) insertion to establish criticality.

For the simulation of a completely withdrawn control rod system, SNEAK-10-A contained 16 blocks, each consisting of 4 SNEAK elements, which were loaded with Na platelets over the total core and axial blanket height and absorber material above the upper axial blanket. As an absorber, steel boxes containing B_4C of natural enrichment (19.6 % ^{10}B) were used. These simulated control rods were distributed in two rings with average radii of r_i = 19.23 cm and r_a = 65.39 cm.

For the investigation of control rod reactivities the Na loading at specific positions had to be replaced by an absorber loading. This was accomplished by lowering the whole element loading by a special mechanism installed in the bottom of the element tubes, thus driving the B_4C boxes located on top of the sodium platelets into the core region.

Because of the insufficient dimensions of the SNEAK matrix, the absorber loading height as well as the available space for lowering the loading was limited to 80 cm. Thus only the core and upper axial blanket portion of the simulated control rods could be loaded with absorber material, whereas the lower axial blanket portion still contained sodium. This fact was taken into account in the comparison of measured and calculated control rod worths by an adequate reduction of the calculated values (section 5.4).

2.4   SNEAK-10-B

The core cross section of SNEAK-10-B is shown in Fig. 5. As already mentioned in the introduction, this core was designed to study the change of axial and radial flux distributions with respect to the follower core, when the inner control rod ring is partially inserted.

The following modifications were applied to SNEAK-10-A. The absorber part of the 4 inner simulated control rods was lowered to 5 cm above the core midplane. In order to reestablish criticality, eight of the initially twelve rod positions in the outer ring were filled up with fuel. The core and blanket dimensions were nearly identical with those of SNEAK-10-A.

2.5 SNEAK-10-C

The core unit cells and element loading schemes were identical with those of SNEAK-10-A.

As can be seen in Fig. 6, the core contained 15 simulated control rods, distributed over the core in a similar way as in the BZ-A assembly.

The core and blanket dimensions closely resembled those of the other SNEAK-10 assemblies.

3. Analysis of critical experiments

3.1 Experiment

The core configurations shown in Figs. 4 - 6 were slightly supercritical when all SNEAK shim rods had the absorber part withdrawn, i.e., were in their most reactive position. To establish criticality the excess reactivity had to be compensated by partial absorber insertion of one or more (to minimize flux tilts) shim rods. For the different core configurations this excess reactivity as well as the resulting k_{eff} of the respective configuration is given below:

SNEAK-10-A: ρ = 8.77 ¢ k_{eff} = 1.0006

SNEAK-10-B: ρ = 31.88 ¢ k_{eff} = 1.0022

SNEAK-10-C: ρ = 5.54 ¢ k_{eff} = 1.0004

Since the k_{eff} calculations were performed on the basis of the core
cross sections of Figs. 4 - 6 the calculated results had to be
compared to the k_{eff} values listed above.

3.2 Calculations

For each critical configuration a set of calculations was performed
which can principally be separated into the following blocks:

a) A 2-dim. diffusion calculation in RZ-geometry using the
   code DIXY /5/ with homogenized cross sections of the
   unit cells prepared by the NUSYS module 446. NUSYS is a
   modular reactor calculation code used at the GfK-Karlsruhe.

b) A 3-dim. synthesis diffusion calculation using the code
   KASY /6/, in order to check the agreement of 2-dim. and
   3-dim. criticality prediction.

c) Calculation of corrections which have to be added to the
   k_{eff} values of a) and b) in order to take into account
   effects (transport, heterogeneity...) which are neglected
   in these calculations.

The microscopic cross sections used in the calculations were based upon
the 26-group cross section set KFKINR001 /7/.

For the use in the basic calculation (a) this cross section set was
condensed to 12 energy groups in order to reduce computer time con-
sumption. The following condensation scheme was applied:

   4 5 6 7 8 9 10 11 12 13 14 26

The numbers denote the highest-numbered group of the 26-group set in
each of the groups of the 12 group set.

The 3-dim. synthesis calculations (b) used 6-group cross sections,
which were derived using the condensation scheme

$$4 \quad 6 \quad 9 \quad 11 \quad 14 \quad 26$$

The fluxes needed for the cross section condensation were taken from
1-dim. diffusion calculations in cylinder geometry using the same radial
model as the basic RZ calculation. In the vicinity of the simulated
control rods, the core regions were divided into subzones where the
cross sections were condensed separately with the individual flux
spectra of these regions.

The geometrical models of the basic RZ calculations are shown in Figs. 7 - 9.
For optimal geometrical resolution mesh widths of $\Delta s \approx 1$ cm were chosen
throughout the core region and of $\Delta s = 2$ cm in the blanket region.

The KASY calculations were carried out on the basis of the critical core
cross sections of Figs. 4 - 6, using a vertical geometry according to
Figs. 7 - 9. In these calculations a mesh width of 2.72 cm was chosen
throughout the core and blanket. (For further remarks on KASY calculations
see section 8.2.)
A survey of the compositions used in the calculations is given in
Table 3.1 (for clarification of abbreviations see legend on page 11).

The major difficulty of calculations in RZ geometry is the necessity of
cylindrisation. Basically the cylindrical radii are defined by equa-
ting cylindrical and real cross section areas. In SNEAK-10 an additional
problem arose from the complicated azimuthal structure of the core,
caused by the presence of the simulated control rods. Since azimuthal
structures cannot be represented in a RZ cylinder model, these control
rods had:

Legend of abbreviations

Core subzones containing identical composition are indicated by
index i in Figs. 7, 8, 9

CI_i	inner core zone (containing SNEAK control rods)
CA_i	outer core zone (containing SNEAK control rods)
CF1	core region of inner simulated control rod ring containing 4 Na followers; central follower in 10-C
CF2	core region of outer simulated control rod ring containing 12 Na followers
CF3	core region of outer simulated control rod ring containing 4 Na followers
CAB	core region of inner simulated control rod ring containing 4 absorbers
BA BB BC	axial blankets containing slightly different materials
BR	radial blanket
BF1 BF2 BF3 BAB	blanket compositions corresponding to CF1, CF2, CF3, CAB
FO	Na follower
AB	B_4C Absorber
TI,TA	SNEAK shim rods of inner/outer core zone
SI,SA	SNEAK safety rods of inner/outer core zone

Table 3.1 Atomic Compositions (10^{22} atoms/cm^3) SNEAK-10   – Part 1 –

Comp. / Isotope	CI	CA	CF1	CF2	CF3	CAB	TI	TA	SI	SA
Al	.03547	.005928	.02098	.003753	.004452	.02098	.6586	.6807		
B10						.3306				
B11						1.3566				
C	1.9538	1.9421	1.1622	1.2309	1.7065	1.5847	1.9754	.6331	1.9762	1.9767
Cr+Mn	.2093	.2073	.2530	.2476	.2205	.2350	.2312	.2900	.2900	.2900
Fe	.7067	.6999	.8569	.8382	.7454	.7795	.7809	.9853	.9851	.9851
H	.000710	.000757	.000422	.000479	.000666	.000422	.002506	.002591		
Mg	.000379	.000283	.000225	.000179	.000246	.001020				
Mo	.001374	.001464	.001797	.001813	.001584	.001221				
Na			.6767	.6117	.2039					
Nb	.000811	.000865	.000829	.000861	.000865	.000829				
Ni	.1216	.1199	.1475	.1439	.1278	.1231	.1463	.1571	.1568	.1571
O	1.6928	1.7458	1.0058	1.1053	1.5324	1.0058	.9904	2.1899	1.1652	1.1655
Si	.008411	.008380	.01158	.01125	.009337	.01369	.008887	.008887	.008887	.008887
Ti	.000297	.000061	.000176	.000039	.000045	.001869	.003880	.003880	.003880	.003880
U235	.26167	.31315	.15545	.19825	.27485	.15545	.26365	.31316	.26302	.31296
U238	1.60437	1.56459	.95316	.99051	1.37384	.95316	1.43880	1.29301	1.34190	1.29216

Table 3.1 Atomic Compositions (10^{22} atoms/cm^3) SNEAK-10   – Part 2 –

Comp. / Isotope	BA	BB	BC	BR	BF1	BF2	BF3	BAB	FO	AB
Al				.5155						
B10								.3306		.8236
B11								1.3566		3.3795
C	.001356	.02047	.001356		.002316	.001432	.01842	.4248	.003720	1.0558
Cr+Mn	.1196	.1196	.1196	.000038	.1998	.1920	.1437	.1817	.3171	.2618
Fe	.3955	.3955	.3955		.6721	.6455	.4788	.5947	1.0769	.8521
H										
Mg				.003750				.000795		.001281
Mo	.000997	.000997	.000997		.001573	.001517	.001170	.000997	.002415	.000997
Na					.6767	.6117	.2039		1.6671	
Nb	.000854	.000854	.000854		.000854	.000854	.000854	.000854	.000854	.000854
Ni	.08052	.06578	.09845	.04122	.1201	.1097	.08041	.09869	.1854	.1206
O					.000013	.000011			.000031	
Si	.004532	.004532	.004532	.001150	.009272	.008816	.005960	.01139	.01621	.01980
Ti				.000058				.001693		.003881
U235	.016668	.016718	.016245	.016245	.009902	.010584	.014673	.009902		
U238	4.09417	4.11014	3.99400	3.99400	2.43226	2.60205	3.60743	2.43226		

(model 1)   either to be represented by rings with a cross section
            area equal to the cross section sum of all control rods
            represented by the respective ring

(model 2)   or to be smeared into the core compositions over
            appropriate ring areas.

While in model 1 the original compositions remain unchanged since only
the shape of the simulated control rods is altered, model 2 uses mixed
compositions in certain core regions.

In selecting the more favourable model for the basis calculation one
has to take in account the well known difficulties occurring in the
treatment of pure Na regions by diffusion theory because of very long
neutron mean free paths.

It was for this reason that in accordance with previous SNEAK cores /8/
model 2 was chosen for the basic k_{eff} calculation although the obviously
somewhat arbitrary choice of the smearing model gives rise to an addi-
tional uncertainty in k_{eff}. An investigation of the influence of the
smeared ring geometry on k_{eff} in SNEAK-10-A yielded the information
that for ring thicknesses between 7 and 15 cm, the k_{eff} variation is
within $\Delta k \sim .2$ % . The ring radii used in the basic calculations of the
different SNEAK-10 cores were obtained from the following models:

In SNEAK-10-A and 10-B the simulated control rods were smeared with
core elements located in the shaded areas of Fig. 10, resulting in a
thickness of $\sim$ 9.8 cm for both rings.

The ratios of control rod to core material (smearing degree) in the
mixed compositions were in the

inner ring: $\dfrac{FO}{CI} = \dfrac{16}{24} = .666$

outer ring: 10-A $\frac{FO}{CA} = \frac{48}{88} = .545$

10-B $\frac{FO}{CA} = \frac{16}{120} = .133$

with   FO: Follower composition
       CI: Inner core composition
       CA: Outer core composition

An additional problem in SNEAK-10-C arose from the fact that rods belonging to the same "ring" were not all located at the same radius. Therefore a mean radius was determined for each ring by taking the mean value of the different radii of one "ring" weighted with the number of rods belonging to them.

The irregular distribution of the rods in 10-C furthermore impeded the choice of a suitable smearing model.

In order to obtain those corrections being correlated with the smearing degree in the same magnitude as in SNEAK-10-A, it was assumed reasonable to smear the rods of 10-C in the same way as in the logically corresponding rings of 10-A. For the central rod of 10-C the smearing degree was chosen in accordance with the inner control rod ring.

The following calculated corrections were added to the basic k_{eff} value.

a) Heterogeneity

The heterogeneity correction takes into account a possible difference in reactivity between the homogenized cell compositions as they are used in the basic calculation, and the actual heterogeneous plate structure of the core loading.

This correction was deduced in the following way: Using the cell code KAPER /9,10/, cell-averaged cross sections of the inner and outer core unit cells were prepared for both the actual cells (Fig. 1) with their heterogeneous platelet arrangement and for cells containing the same homogenized cell compositions in all platelets.

Subsequently two RZ-diffusion calculations were performed using the same geometry as in the basic calculation, but the homogenized cell cross sections initially being prepared by the NUSYS module 446 were substituted:

    i) by the KAPER cross sections of the heterogeneous (actual) cell geometry

    ii) by the homogenized cross sections prepared by KAPER.

The relative deviation of the resulting k_{eff} values

$$\frac{k_{eff}, \; HET - k_{eff}, \; HOM}{k_{eff}, \; HOM}$$

was taken as the heterogeneity correction and added to the basic k_{eff} value.

It has to be emphasized that a direct comparison of the k_{eff} values from calculations using homogenized NUSYS 446 cross sections and those using heterogeneous KAPER cross sections is generally not accurate since the f-factor treatment is slightly different for both codes.

A precise k_{eff} comparison therefore requires a preparation of <u>both</u> cross section types by use of the same code.

b) Condensation ΔK_{cond}

These corrections were derived from 2-dim. diffusion calculations in identical RZ geometry by comparing k_{eff} results for 26, 12, and 6 energy groups. The purpose of these corrections is to normalize all k_{eff} values to 26 groups.
The geometrical model was similar to that of the basic calculation, but wider mesh widths were used in order to reduce computational costs.

c) Elastic removal correction ΔK_{REMO}

The REMO correction /11/ improves the elastic removal cross sections
by weighting them with the spectra of the investigated compositions.
This correction is necessary since the elastic removal cross sections
of the KFKINROO1 set are optimized for a spectrum of the SNR-300 type.

d) Geometry correction ΔK_{Geo}

The geometry correction takes into account that in the basic RZ
calculation

   i) the core and blanket boundaries were not treated
      according to their actual irregular shape but
      were assumed to have cylindrical faces

  ii) the simulated control rods were not treated in accordance
      with their actual location and composition but were
      represented by mixed sodium-core regions.

This correction was deduced from the comparison of a 2-dim. diffusion
calculation in XY geometry and a 1-dim. cylindrical diffusion calcu-
lation, both using the same axial composition and energy group dependent
bucklings.

In SNEAK-10-B this correction was calculated separately for the upper
core portion, containing absorber material in the inner control rod
ring, and for the lower core portion with sodium in all control rod
positions. Subsequently both corrections were combined according to the
relative contribution of these core portions to the normalization
integral, to form the desired global geometry correction.

The KASY k_{eff} values need no geometry correction as in these calcula-
tions the cores were treated in accordance with their actual geometry.

d) Transport correction ΔK_{tr}, ΔK_{tr},rod

This correction accounts for transport effects occurring in neutron propagation which are neglected in the basic diffusion calculation.

All transport calculations were performed using the 2-dim. transport code SNOW /12/ to the order S8 in RZ geometry.

The transport corrections were determined from the k_{eff} difference of a transport and a diffusion calculation both carried out in the same geometry. The geometrical models were essentially the same as in the basic RZ calculations, but mesh widths between 2 and 3 cm were used to accelerate the transport code iteration convergence.

The global transport correction of each configuration was synthesized from a contribution of the core without simulated control rods and a contribution which accounts for additional transport effects caused by the presence of the rods. In order to reduce computational costs these transport corrections were only calculated for a few significant configurations, and the results were transferred to all other configurations as will be described below.

Table 3.2 gives a survey of these configurations and the following parameters:

column 1:   Total transport correction

column 2:   Rod transport correction,
            i.e. the difference between the total transport correction and the one obtained for the clean core without any rods (config. 1).

            The quoted figures therefore represent the rod contribution to the respective total transport correction.

Table 3.2   Survey of Transport Calculation Results in SNEAK-10

Config. No.	Configuration	Total Transport correction [%]	Rod Transport correction [%]	Contribution/ Rod [%]
1	SNEAK-10-A without simulated control rods (also valid for 10-B, 10-C)	.420	0.	0.
2	as No. 1, but with a pure central Na follower	.502	.082	.082
3	as No. 1, but with pure inner follower ring (4 rods) [a]	.724	.304	.076
4	as No. 1, buth with pure outer follower ring (12 rods) [a]	.646	.226	.019
5	as No. 1, buth with central half inserted absorber	.485	.065	.065

[a] Here a ring of control rod positions loaded with follower material (Na) is represented by a narrow ring with the same cross section area, loaded with the same material.

Table 3.3 Comparison of Rod Transport Corrections and Reactivity Effects
(Figures designated with * were extrapolated from the central-rod
transport correction in accordance with the corresponding reactivity worth ratios)

		Inner ring (4 rods)	Outer ring (12 rods)	Reduction inner → outer ring [%]	Total rod transp.corr. [%]
SNEAK-10-A	Reactivity effect [$] 1)	4.67	3.53	75,6	
	Rod transp.corr. [%] 2)	.304	.226	74,3	.530

		Inner ring (4 rods)	Outer ring (4 rods)		Total rod transp.corr. [%]
SNEAK-10-B	Rod transp.corr. [%]	.241	.075		.316

		Central rod	Inner ring (6 rods)	Outer ring (8 rods)	Total rod transp.corr. [%]
SNEAK-10-C	Reactivity effect [$] 1)	1.15 $	5.98 $	3.67 $	
	Rod transp.corr. [%] 2)	.082	.426 *	.262 *	.770

1) values taken from Table 5.5   2) values taken from Table 3.2

column 3: <u>Contribution/Rod</u>

i.e. the rod transport correction divided by the number of rods in the investigated configuration.

The figures of config. 2, 3 and 4 demonstrate the dependence of the single Na-follower transport correction on radial position.

The core contribution (config. 1) was found to have the same value of .420 % in all SNEAK-10-assemblies.

The figures given in column 2 of configuration 3 and 4 represent the rod transport corrections of the inner and outer ring of SNEAK-10-A.

The rod corrections of SNEAK-10-B and 10-C were derived in the following way: Comparing the rod transport corrections of the inner and outer ring of SNEAK-10-A with the reactivity effects of these rings (section 5, table 5.5) one finds that both parameters exhibit nearly the same dependence on radial position (table 3.3 top).

Assuming that this correlation is valid for all control rod locations of interest in SNEAK-10 it is possible to deduce the transport correction of any control rod from the value of the central rod, under consideration of the respective reactivity worth ratios.

In SNEAK-10-C, the rod transport corrections of the individual rings were consequently determined from the transport correction of the central rod by multiplying its value with the ratio of the reactivity worth of the ring in question over the worth of the central rod (Table 3.3 bottom).

In SNEAK-10-B, the transport correction for the rods of the inner ring was derived in a similar way from the correction found for a central half inserted absorber (Config. Nr. 5 in table 3.2). Comparing the

"contribution/rod" values of configuration Nr. 2 and 3 in table 3.2,
which correspond to a transition central $\rightarrow$ rod of inner ring, a
decrease of the rod transport correction from .082 % to .076 % is
observed. Therefore a correction factor corresponding to this reduc-
tion was applied to the transport correction of the central half in-
serted absorber. The resulting value was multiplied by 4, according
to the number of rods in the inner ring.

The transport correction of the outer ring of SNEAK-10-B was obtained
by reducing the corresponding value of SNEAK-10-A by a factor of 3,
according to the smaller number of rods in SNEAK-10-B.

3.3 Comparison of calculated and experimental criticality

A summary of the results of all criticality calculations and the applied
corrections is given in table 3.4.

In order to facilitate the k_{eff} comparison of the different assemblies,
the basic k_{eff} values given in row 1 are already corrected for the
individual excess reactivities of the calculated cores (see section 3.1).
Hence, all k_{eff} values correspond to an experimental k_{eff} = 1.0000.

The final k_{eff} values of the DIXY-RZ calculations show a slight over-
estimation of criticality, which is in good agreement with the experiences
of earlier SNEAK assemblies. The highest overestimation is obtained for
the core with partially inserted absorbers SNEAK-10-B. [+)]

The KASY calculations yield k_{eff} values being .12 % lower than the
corresponding DIXY-RZ results in both follower cores. Only in SNEAK-10-B,
the KASY k_{eff} exceeds the one obtained from DIXY-RZ by .08 %. These
tendencies are in agreement with the experiences of an earlier SNEAK
core 9A-2 (SNR-300 control rod mock up) /8/.

[+)] This is probably due to the underestimation of the reactivity effect
of the partially inserted inner control rod ring (see also section 5.3).

Table 3.4 Criticality Prediction of the SNEAK-10 Assemblies
(the k_{eff} values correspond to an experimental k_{eff} = 1.0000)

	SNEAK-10-A			SNEAK-10-B		SNEAK-10-C		
	DIXY-RZ 12 gr.	KASY 6 gr.	D3D 6 gr.	DIXY-RZ 12 gr.	KASY 6 gr.	DIXY-RZ 12 gr.	KASY 6 gr.	D3D 6 gr.
Basic k_{eff}	1.0027	.9919	.9935	1.0003	.9984	1.0010	.9903	.9919
ΔK_{geo}	-.0104			-.0035		-.0103		
ΔK_{cond}	+.0003	-.0005	-.0005	+.0003	-.0005	+.0003	-.0005	-.0005
Basic k_{eff} + ΔK_{geo} + ΔK_{cond}	.9926	.9914	.9930	.9971	.9979	.9910	.9898	.9914
ΔK_{REMO}	-.0015			-.0018		-.0015		
ΔK_{het}	+.0011			+.0011		+.0011		
Final diffusion k_{eff}	.9922	.9910	.9926	.9964	.9972	.9906	.9894	.9910
$\Delta K_{tr,core}$	+.0042			+.0042		+.0042		
$\Delta K_{tr,rods}$	+.0053			+.0032		+.0077		
Final k_{eff}	1.0017	1.0005	1.0021	1.0038	1.0046	1.0025	1.0013	1.0029

For SNEAK-10-A and 10-C the k_{eff} values of 3-dim. diffusion calculations using the code D3D /18/ are given in addition. These calculations were performed in the frame of the subcritical control rod measurements using the same 6-group condensed cross sections and step widths of 2.72 cm in all directions as the KASY-calculations.

The basic D3D k_{eff} values given in row 1 of table 3.4 were taken from the reference configurations of the control rod reactivity calculations (section 5.3) which closely resembled the clean critical core configurations.

Comparing the final k_{eff} values with those of the RZ-diffusion calculations one finds the same good agreement within .04 % for both assemblies 10-A and 10-C.

4.   Calculation of the delayed neutron fraction
   ───

The precise knowledge of the delayed neutron fraction β_{eff} is essential for a reliable comparison of calculated and measured reactivity values.

The β_{eff} values of the different SNEAK-10 configurations were determined in the perturbation phase of the 2-dim. diffusion code DIXY, using the neutron flux and adjoint of the corresponding basic k_{eff} calculations in RZ geometry. Two different sets of basic delayed-neutron data were used in these calculations:

   a) Keepin's data /14/ that were employed for the evaluation
      of all previous SNEAK assemblies.

   b) Tuttle's combined data /19/ that were confirmed by SNEAK
      measurements and successfully used to analyze material worth
      measurements from several earlier assemblies, as reported by
      Fischer /15/.

Table 4.1   Delayed-Neutron Group Constants for Fast
             Fission of ^{235}U and ^{238}U

Fission Nuclide	Group Index	Decay Constants λ_i (sec^{-1})	β_i ($\cdot$ 10^3)	
			Keepin	Tuttle
^{235}U	1	.0127	.244	.2574
	2	.0317	1.365	1.423
	3	.115	1.205	1.256
	4	.311	2.609	2.719
	5	1.40	.8205	.8551
	6	3.87	.1667	.1736
^{238}U	1	.0132	.1924	.2307
	2	.0321	2.029	2.431
	3	.139	2.398	2.875
	4	.358	5.740	6.886
	5	1.41	3.330	3.993
	6	4.02	1.110	1.331

Table 4.2   Calculated Effective Delayed Neutron Fractions

Configuration		β_{eff}	
		Keepin	Tuttle
SNEAK-10-A	Reference	.00697	.00764
	Inner Ring inserted	.00695	
	Outer Ring inserted	.00695	
	Inner + Outer Ring inserted	.00691	
SNEAK-10-B		.00696	
SNEAK-10-C	Reference	.00697	
	All Rods inserted	.00691	

A survey of the basic delayed-neutron data in use and the obtained β_{eff} values is given in Table 4.1 and 4.2. As can be seen from the first row of Table 4.2 the transition Keepin → Tuttle combined data causes the β_{eff} value to increase by 9.6 %.

Since all SNEAK-10 configurations had similar geometry and compositions this influence was only computed for SNEAK-10-A. The results should be also representative for all other configurations. Furthermore in SNEAK-10-A and 10-C the variation of β_{eff} was investigated for some typical control rod insertion patterns.

The results listed in Table 4.2 show that the relative change in β_{eff} for all critical and subcritical (approx.-11 $ max.) configurations is less than 1 %.

In the frame of the subcritical control rod experiments, only Keepin's β_{eff} values were used in order to get C/E values being directly comparable to those obtained in previous SNEAK cores, whereas the material worth measurements were evaluated using both Keepin's and Tuttle's β_{eff} values (section 6.2).

5.   Subcritical measurements of control rod worths

According to the main objectives of the SNEAK-10 program, extensive measurements of the reactivity effect of various control rod configurations were performed in SNEAK-10-A and 10-C.

Since the reactivities involved had a magnitude (approx. -11 $ max.) that exceeds the range of convenient applicability of quasicritical compensation methods, subcritical techniques had to be employed.

In order to improve the reliability of the experimental results three different subcritical measuring techniques were utilized:

1. The modified source multiplication method using a ^{252}Cf neutron source

2. The source jerk method using
   a) a ^{252}Cf neutron source
   b) a duoplasmatron neutron generator

A detailed description of the **methods is given below.**

5.1 Modified source multiplication method (MSM)

From the experimental point of view this is the easiest method to measure the subcriticality of a system since it only requires the registration of a steady-state counting rate.

The method was proposed in /14/ where a thorough theoretical treatment is given. Therefore only a short survey of the basic mathematical formalism is given in this report.

The basic equation of the method

$$\rho \cdot f_{eff} = \frac{1-K}{K} = \frac{S}{\nu\Sigma_f \phi} \qquad (1)$$

is a direct consequence of the one-energy-group static point reactor equations with and without external source $-\Sigma_a\phi + \nu\Sigma_f\phi + S = 0$ and $-\Sigma_a\phi + \frac{\nu\Sigma_f}{K}\phi = 0$ where S is an arbitrary neutron source.

Defining the efficiency of a detector used to register the flux as

$$W = \frac{Z}{\nu\Sigma_f \phi} \qquad (2)$$

where Z is the detector count rate, (1) can be written as

$$\rho \cdot \beta_{eff} = S \cdot W \cdot \frac{1}{Z} \qquad (3)$$

This means that, as long as point reactor physics applies, the count rate of any detector in a subcritical reactor is inversely proportional to the subcriticality of the system.

The proportionality factor $S \cdot W$ is usually not known but can be easily assessed by registration of the detector counting rate Z_o at a well-known subcritical state ρ_o. This state usually is generated by a defined insertion of shim rods which have been calibrated by an inverse-kinetics technique. After performing this calibration procedure, any other subcriticality can be determined by measurement of the count rate Z from

$$\rho = (\rho_o \cdot Z_o) \cdot \frac{1}{Z} \qquad (4)$$

However, deviations from the point reactor occur when the neutron flux and adjoint are significantly distorted by the insertion of control rods, as is the case in large decoupled systems like SNEAK-10. Then the source strength and detector efficiency are not constant but become strongly dependent on the individual rod pattern. In such cases, S and W in eq. (3) have to be replaced by the more general expressions:

$$S_{eff} = \frac{\underset{source}{\iint} S\phi^+ dEdV \cdot \underset{reactor}{\iint} \nu\Sigma_f \phi dEdV}{\underset{reactor}{\iint} \{\int \nu\Sigma_f \phi dE \cdot \int \chi\phi^+ dE'\} dV} \qquad (5)$$

and
$$W = \frac{\displaystyle\iint_{detector} \Sigma_d \phi \, dE \, dV}{\displaystyle\iint_{reactor} \nu \Sigma_f \phi \, dE \, dV} \qquad (6)$$

Substituting S and W in Eq. (3) by (5) and (6) one gets

$$\rho \cdot \beta = \frac{\displaystyle\iint_{source} S \phi^+ dE \, dV \cdot \iint_{detector} \Sigma_d \phi \, dE \, dV}{\displaystyle\int \{\int \nu \Sigma_f \phi \, dE \cdot \int \chi \phi^+ dE'\} dV} \cdot \frac{1}{Z} \qquad (7)$$

Consequently the unknown subcriticality can now be determined from

$$\rho = (\rho_o \cdot Z_o) \cdot \frac{1}{Z} \cdot F \quad \text{with} \quad F = \frac{S_{eff} \cdot W}{S_{eff_o} \cdot W_o} \qquad (8)$$

This means that the subcriticality can still be determined in the same
way as in the point reactor model, but an additional calculated
correction factor has to be applied to the results to take into account
changes of detector and source efficiency with respect to the sub-
critical calibration point characterized by ρ_o, Z_o, S_{eff_o} and W_o.

In SNEAK-10 the subcritical multiplication experiments were carried
out using a ^{252}Cf neutron source with a source strength of $\sim 2 \cdot 10^7$ n/s.
This source was positioned in the core midplane one element pitch
(5.44 cm) away from the core centre.

The neutron flux was recorded by four ionization chambers (D1 ... D4)
located in the vicinity of the outer radial blanket boundary (Fig. 11).

The subcritical calibration point was established in the following
way: In the reference cores of the subcritical measurements (Figs. 11,12),
exact criticality was established by partially inserting the absorber
part of three calibrated shim rods, designated by T in the figures.
The locations of these were selected as symmetrically as possible in
order to minimize flux tilts.

Subsequently three shim rods were fully inserted, driving the core to
a defined subcritical state that could be determined from the shim
rod calibration curves:

$$\text{SNEAK-10-A: } \rho_{CAL,A} = -58.1 \, \cancel{c}$$
$$\text{SNEAK-10-C: } \rho_{CAL,C} = -64.3 \, \cancel{c} \qquad \pm \, 3 \, \% \quad (1\sigma)$$

The quoted error mainly arises from inaccuracies in the inverse-kinetics
calibration procedure of the shim rods.

The first column of tables 5.1 and 5.2 shows the uncorrected results
for various control rod insertion patterns as they were obtained by
use of Eq. (4). The designation of the rods is in accordance with
Figs. 11 and 12.

Four values are given for each configuration according to the four
detectors in use, with the following sequence

$$D1, \; D2, \; D3, \; D4.$$

The significant difference (up to 60 %) between the reactivities obtained
for the different detectors in most rod configurations proves the in-
ability of the point reactor model to interpret the experimental results.

The calculation of configuration and detector dependent correction factors
can basically be divided into two branches:

5.1.1 Determination of homogeneous correction factors

For each subcritical configuration (including the subcritical calibration
core) a 2-dim. homogeneous diffusion calculation of the real and adjoint
flux in XY-geometry was performed in order to derive the correction fac-
tor F in Eq. (8). 6-group condensed KFKINR001 cross sections were used
with the same condensation structure as was described in section 3.2.

Table 5.1 Experimental Results of Control Rod Worth Measurements in SNEAK-10-A
Source Multiplication Method   (Errors are 1σ standard dev.)

Rods inserted	Uncorr. Results [%]	Detector Efficiency Correction W/W_o		Source Efficiency Correction $S_{eff}/S_{eff,o}$		Total Correction $F = \dfrac{W \cdot S_{eff}}{W_o \cdot S_{eff,o}}$		Corrected Results $\rho = \rho_o \cdot Z_o \cdot \dfrac{1}{Z} \cdot F$ [%]		Final Results (mean values of inhom.-corr. results) [%]
		hom	inhom	hom	inhom	hom	inhom	hom	inhom	
4	.281	.955	.979	.998	1.004	.953	.983	.268	.276	.274±3%
	.288	.921	.954			.919	.958	.265	.276	
	.257	1.034	1.064			1.032	1.068	.265	.274	
	.260	1.025	1.039			1.023	1.043	.266	.271	
4+5	.496	.975		1.004		.979		.486		
	.690	.711				.714		.493		
	.460	1.051				1.055		.485		
	.449	1.069				1.073		.482		
4+7	.558	1.000		1.009		1.009		.563		
	.630	.894				.902		.568		
	.612	.923				.931		.570		
	.520	1.071				1.081		.562		
4+10	.587	.999	1.010	1.004	1.006	1.003	1.016	.589	.596	.597±3%
	.604	.964	.982			.968	.987	.585	.596	
	.572	1.026	1.040			1.030	1.046	.589	.598	
	.617	.953	.963			.957	.968	.590	.597	
4+B	1.54	1.006		.964		.970		1.49		
	1.89	.853				.820		1.55		
	1.47	1.087				1.048		1.54		
	1.33	1.160				1.119		1.49		
B	1.25	1.030	1.028	.961	.958	.990	.985	1.24	1.23	1.23±4%
	1.43	.932	.904			.896	.866	1.28	1.24	
	1.26	1.046	1.027			1.005	.984	1.27	1.24	
	1.16	1.106	1.102			1.063	1.056	1.23	1.22	
B+D	2.77	1.098	1.063	.864	.858	.948	.912	2.63	2.53	2.54±4%
	3.08	1.060	.963			.916	.826	2.82	2.54	
	2.91	1.117	1.020			.965	.875	2.81	2.55	
	2.98	1.053	.992			.910	.850	2.71	2.53	
2,4,6,8,10,12	2.25	.834		1.033		.861		1.94		
	2.03	.945				.977		1.98		
	2:31	.849				.877		2.03		
	1.99	.940				.971		1.93		
2,4,6,8,10,12 A,C	6.73	.899		.920		.827		5.57		
	6.04	1.078				.992		5.99		
	7.20	.915				.842		6.06		
	5.41	1.076				.990		5.36		
1-12	4.63	.772	.713	1.063	1.039	.820	.741	3.80	3.43	3.53±5%
	4.89	.788	.696			.838	.723	4.10	3.54	
	4.83	.788	.701			.838	.728	4.05	3.52	
	4.86	.772	.721			.820	.749	3.99	3.64	
A-D	6.18	1.163	1.028	.727	.723	.845	.743	5.22	4.59	4.67±5%
	6.89	1.183	.939			.860	.679	5.93	4.66	
	6.83	1.183	.954			.860	.690	5.87	4.71	
	6.14	1.167	1.054			.848	.762	5.21	4.68	
A-D 1-12	16.37	.960	.717	.829	.796	.796	.570	13.03	9.33	9.54±6%
	19.35	.980	.613			.812	.488	15.71	9.44	
	16.65	.980	.629			.812	.501	15.14	9.34	
	16.96	.962	.744			.798	.592	13.53	10.04	

Table 5.2 Experimental Results of Control Rod Worth Measurements in SNEAK-10-C
Source Multiplication Method   (Errors are 1σ standard dev.)

Rods inserted	Uncorr. Results $[\$]$	Detector Efficiency Correction $\bar{W}/W_o$ hom	inhom	Source Efficiency Correction $S_{eff}/S_{eff,o}$ hom	inhom	Total Correction $F = \dfrac{\bar{W}\cdot S_{eff}}{W_o\cdot S_{eff,o}}$ $[\$]$ hom	inhom	Corrected Results $\rho = \rho_o\cdot Z_o\cdot\dfrac{1}{Z}\cdot F$ $[\$]$ hom	inhom	Final Results (mean values of inhom.-corr. results) $[\$]$
3	.504	.906	.931			.909	.936	.458	.472	
	.484	.951	.971	1.003	1.005	.954	.976	.462	.472	.465±3%
	.427	1.067	1.078			1.070	1.083	.457	.462	
	.431	1.045	1.051			1.048	1.056	.452	.455	
3+4	.759	.924				.932		.707		
	.918	.783		1.009		.790		.725		
	.640	1.101				1.111		.711		
	.628	1.105				1.115		.700		
3+7	1.03	.982	.983			.991	.990	1.02	1.02	
	1.01	1.027	1.007	1.009	1.007	1.036	1.014	1.05	1.02	1.02±3%
	1.01	1.023	.999			1.032	1.006	1.04	1.02	
	.994	1.005	1.005			1.014	1.012	1.01	1.01	
M	1.32	1.015	1.022			.863	.872	1.14	1.15	
	1.34	1.047	1.004	.850	.853	.890	.856	1.19	1.15	1.15±4%
	1.33	1.045	1.013			.888	.864	1.18	1.15	
	1.29	1.024	1.047			.870	.893	1.12	1.15	
C	.954	1.007	1.011			.991	.993	.945	.945	
	1.12	.896	.879	.984	.982	.882	.863	.988	.967	.947±3%
	.927	1.054	1.040			1.037	1.021	.961	.946	
	.863	1.100	1.094			1.082	1.074	.934	.927	
1-8	4.21	.911	.825			.985	.868	4.15	3.65	
	4.35	.973	.819	1.081	1.052	1.052	.862	4.58	3.75	3.67±4%
	4.22	.974	.822			1.053	.865	4.44	3.65	
	3.92	.958	.883			1.036	.929	4.06	3.64	
A-F	7.97	1.196	.967			.911	.743	7.26	5.92	
	9.32	1.215	.674	.762	.768	.926	.671	8.63	6.25	5.98±5%
	8.60	1.227	.907			.935	.697	8.04	5.99	
	7.26	1.207	1.028			.920	.790	6.68	5.74	
A-F 1-8	16.24	1.179	.774			1.013	.652	16.45	10.59	
	19.97	1.232	.666	.859	.843	1.058	.561	21.13	11.20	10.65±6%
	17.83	1.258	.695			1.081	.586	19.27	10.45	
	14.10	1.247	.873			1.071	.736	15.10	10.38	
A-F 1-8 M	20.01	1.229	.809			.871	.579	17.43	11.59	
	27.63	1.280	.608	.709	.716	.908	.435	25.09	12.02	11.49±6%
	23.35	1.311	.662			.929	.474	21.69	11.07	
	16.62	1.302	.949			.923	.679	15.34	11.28	

The mesh width used in these calculations was 2.72 cm, i.e. half the
SNEAK fuel element pitch.

To describe the axial leakage behaviour of the core, composition and
energy-group dependent bucklings were employed. These bucklings were
deduced from the second derivative of the flux in Z direction in the
core midplane of a 2D diffusion calculation in RZ geometry similar
to the basic k_{eff} calculation of section 3.2. Since the RZ model does
not contain pure sodium nor absorber regions the bucklings for these
areas were taken from additional calculations in RZ geometry of
configurations with a central follower or absorber.

The correction factors thus obtained are designated "hom" in Tables
5.1 and 5.2. As can be seen from the columns "Corrected Results hom"
there is still, in most cases, a strong discrepancy between the results
of the different detectors. Considering the reasons of these discre-
pancies one finds that the homogeneous calculations so far performed
only took into account the different geometrical situations of the
various rod patterns.

An effect which was completely neglected so far is the presence of
higher spatial flux modes, induced by the insertion of the ^{252}Cf
point source.

In order to find out whether these harmonic flux modes cause severe
changes in the detector efficiency corrections a second set of cal-
culations was performed in the subsequently described way.

5.1.2 Determination of inhomogeneous correction factors

In these calculations the same geometrical models and bucklings were
used as in the initially described homogeneous runs.

The only difference consisted in the insertion of a point source in a
position that was nearly identical with the actual experimental
location.

Since diffusion codes with source singularities exhibit extremely bad convergence behaviour - especially in the vicinity of k_{eff} = 1.000 - the fission source distributions of the corresponding homogeneous runs were used as a first guess input.

Although the application of this procedure yielded a considerable reduction of computer time consumption the costs were still very high and only some control rod configurations of major interest were evaluated in this way.

Correcting the reactivity values with the obtained "inhom" correction factors, the agreement of the results of the different detectors was remarkably improved. The remaining discrepancies are probably due to the fact that the source location in the inhom calculations was not accurately identical with the experimental set-up because of geometrical restrictions in the diffusion code input.

In the last column of Tables 5.1 and 5.2 the mean values of the "inhom"-corrected results of all detectors are listed as "final results".

The quoted errors are 1σ standard deviations containing the following contributions:

a) error of the calibration procedure: 3 %

b) error of 10 % in the calculated correction factors: 0.2 .. 5.5 %

c) counting statistics: 0.1 .. 1 %

These errors are in the same order of magnitude as the ones being found in similar measurements in SNEAK-9A-2 /16/.

5.2 Source jerk measurements

In this method the subcriticality is not deduced from the steady-state
flux signal produced by the presence of a neutron source but from
the decrease of this signal when the source is removed from the sub-
critical reactor.

The time behaviour of the flux decrease is governed by two components:

a) The die-out of prompt neutrons, occurring within less
   than 1 sec, which in the fundamental mode causes a
   flux drop that is directly proportional to the sub-
   criticality of the system:

$$\rho[\$] = \frac{\phi_o - \phi_1}{\phi_1}$$

   ϕ_o is the flux level prior to, and ϕ_1 the level after the
   source jerk.

b) The decay of delayed-neutron precursors which is des-
   cribed by the kinetic equations.

Since the subcriticality cannot be determined from the prompt flux drop
alone with sufficient accuracy the delayed neutron decay is included
in the evaluation, using the inverse kinetic equations. The mathema-
tical formalism of this evaluation method closely resembles that for
rod drop experiments. A detailed description is for instance given
in /17/.

In the SNEAK-10 measurements, the source jerk was accomplished by two
different techniques.

5.2.1 Pile oscillator method

A ^{252}Cf neutron source with a source strength of approx. $2\cdot10^7$ n/s
being attached to a pneumatic pile oscillator was positioned close
to the core center (Fig. 11). After leaving the source in this posi-
tion for several minutes, allowing the neutron precursors to establish
an equilibrium concentration, it was driven out of the core to a
position above the upper axial blanket. In this position the source
was screened by surrounding B_4C boxes in order to diminish the in-
fluence of stray neutrons on the detector signal level.

The time span needed by the pile oscillator for the source removal
was in the order of $\sim$ 1 sec.

5.2.2 Neutron generator method

In the second method a duoplasmatron neutron generator was used,
allowing continuous operation at a neutron emission level of up to
$5\cdot10^8$ n/sec.

The tritium target of the generator, which is used to produce 14 MeV
neutrons by ^{3}T(d,n)^{4}He reactions, was positioned close to the core
centre (Fig. 11). Since the main part of the neutron generator had to
be installed outside the reactor matrix, the beam of accelerated
deuterons had to be focused onto the target through a drift tube of
$\sim$ 2 m length.

The radial channel that was necessary for the insertion of the drift
tube had a geometrical cross section of 21 x 53 mm^2.

In this method the instantaneous change of the source strength was
achieved by switching off the generator.

5.2.3 Survey of source jerk results and applied corrections

All measurements were evaluated with a program which is based upon the inverse kinetics equations. The kinetic neutron parameters needed as an input to this evaluation program were taken from the diffusion calculations described in section 4, using Keepin's delayed-neutron yields.

The evaluation of experimental data was considerably complicated by:

   a) the presence of higher flux modes when the source was in
      the "in-core" position, which was already discussed in
      section 5.1,

   b) stray neutrons, influencing the detector signal level
      when the source was in the "out-of-core" position
      (pile oscillator measurements only).

to a) As the evaluation program is based upon point reactor kinetics
      it only takes into account the time dependence of the fundamental
      flux mode. In reality, however, the starting flux profile as
      well as the precursor distribution after the source jerk is
      influenced to a certain degree by the presence of higher flux
      modes.

      An accurate treatment of this problem would therefore require a
      correction of the detector count rates at all instants in such
      a way that the time behaviour of a fundamental flux mode is
      simulated. Subsequently these corrected count rates could be
      evaluated by the above mentioned point kinetics program.

      In order to derive an exact correction one would have to know
      to what extent higher modes persist in the flux and precursor
      distribution after the source jerk. This is a quite difficult
      problem which is still under discussion. Therefore a simplified
      correction procedure was utilized which yielded reasonable
      results up to subcriticalities of ~ 5 $\$$.

This was done by applying corrections to the reactivity values resulting from the evaluation of the original counting rates, rather than correcting these count rates themselves.

These correction factors were derived from the ratio of "hom" and "inhom" detector efficiency corrections which were calculated for the evaluation of the MSM measurements (section 5.1). For a given rod configuration this ratio represents the change in detector count rate relative to the fundamental mode amplitude when a point source is introduced into the core. Application of this correction factor to $\rho\left[\$\right]$ measured by source jerk corresponds for large ρ approximately to reducing the starting flux ϕ_o to its fundamental-mode contribution.

It has to be emphasized that this correction method represents only a rough approximation. A precise treatment of this problem will be a task of further investigation.

to b) In the pile oscillator measurements an additional problem arose from the effect of stray neutrons reaching the detectors when the source was in the "out-of-core" position.

These stray neutrons cause a contribution to the detector signal level that is nearly independent of the subcritical state of the reactor.

This effect was accounted for in the evaluation by reducing all detector count rates after the source jerk by a certain constant amount: the "background correction". This correction was taken as the difference of the detector count rates in the following situations:

1. Source in "out-of-core" position of the pile oscillator

2. Source removed from the reactor building

The "background correction" reached a magnitude of $\sim$ 35 %
of the recorded count rate in the configurations with the
highest subcriticality.

The results of all source jerk measurements and the applied corrections
are summarized in Tables 5.3 and 5.4.

Since only two detectors (D1, D2) could be operated with automatic
sensitivity control, which means that the sensitivity is automatically
increased by a factor of 10 when the signal level decreases below 10 %
of full scale, only two values are given for each subcritical confi-
guration. An automatic sensitivity control is necessary to track the
decrease of the signal level after the source jerk with sufficient
accuracy.

Comparing the final results of the pile oscillator method with the ones
obtained from the modified source multiplication, an agreement within
3 % is observed for reactivities up to $\sim$ 5 $. For higher subcriticali-
ties the agreement becomes significantly worse. This effect is assumed
to be correlated with the rapidly increasing influence of higher flux
modes on the kinetic process, which has not been accurately accounted for.

For the neutron generator measurements a similar agreement is observed
in most cases. The slightly larger discrepancy in some configurations
may be due to the fact that the "inhom" correction factors were only
calculated for the position of the ^{252}Cf source, which is not identical
with the location of the neutron generator target. This causes an
additional inaccuracy in the neutron generator corrections which was
accounted for by an adequate increase of the error bars (see below).

The quoted errors contain the following contributions:

1. The background correction is assumed to have a possible inaccuracy
   of 10 %, leading to an error contribution in the range of

$$0.1 \ldots 3.5 \%$$

Table 5.3 Experimental Results of Control Rod Worth Measurements in SNEAK-10-A
Source Jerk Method   (Errors are 1σ standard deviations)

Rods inserted	Pile oscillator measured [ß]	Pile oscillator with background corr. [ß]	Neutron-generator measured [ß]	Corr.-factor for presence of higher flux modes	Final Results (corr. for higher modes) mean values Pile oscill. [ß]	Neutr.Gen. [ß]	Comparison Source jerk / MSM Pile oscill.	Neutr.Gen.
4	.284 .261	.287 .263	.284 .265	.975 .964	.276±3%	.276±2%	1.01	1.01
4+5	.501 .497	.509 .505	.513 .510					
4+7	.582 .578	.592 .586	.598 .596					
4+10	.603 .596	.614 .603	.608 .607	.989 .982	.600±3%	.599±2%	1.00	1.00
4+B	1.39 1.35	1.46 1.40	1.51 1.48					
B	1.18 1.14	1.23 1.17	1.23 1.21	1.002 1.031	1.22±4%	1.24±4%	.99	1.01
B+D	2.31 2.21	2.52 2.35	2.52 2.45	1.033 1.101	2.60±5%	2.65±5%	1.02	1.04
2,4,6,8,10,12	1.80 1.75	1.93 1.83	1.86 1.81					
2,4,6,8,10,12,A,C	3.37 3.39	4.20 3.83	4.12 4.07					
1-12	2.84 2.77	3.27 3.06	3.21 3.16	1.083 1.132	3.50±5%	3.53±5%	.99	1.00
A-D	3.50 3.22	4.31 3.75	4.22 4.11	1.131 1.260	4.80±8%	4.98±7%	1.03	1.07
A-D 1-12			7.62 7.47	1.339 1.600		11.08±15%		1.16

Table 5.4 Experimental Results of Control Rod Worth Measurements in SNEAK-10-C
Source Jerk Method   (Errors are 1σ standard deviations)

Rods inserted	Pile oscillator measured [$]	with back-ground corr. [$]	Neutron-generator measured [$]	Corr.factor for presence of higher flux modes	Final Results (corr. for higher modes) mean values Pile oscill. [$]	Neutr.Gen. [$]	Comparison Source jerk / MSM Pile oscill.	Neutr.Gen.
3	.477 .463	.483 .466	.477 .467	.973 .979	.463±3%	.461±2%	1.00	.99
3+4	.711 .696	.720 .700	.717 .705					
3+7	.998 .966	1.015 .974	1.025 .984	.999 1.020	1.00±3%	1.01±2%	.99	1.00
M	1.11 1.06	1.13 1.07	1.10 1.07	.993 1.043	1.12±4%	1.11±4%	.97	.96
C	.931 .906	.946 .914	.938 .916	.996 1.019	.937±3%	.934±3%	.99	.99
1-8	3.05 2.95	3.28 3.07	3.26 3.10	1.104 1.188	3.63±5%	3.64±5%	.99	.99
A-F	4.27 4.02	4.91 4.37	4.50 4.36	1.237 1.390	6.07±8%	5.81±9%	1.02	.97
A-F 1-8	6.26 5.39	8.52 6.51	7.26 6.78	1.523 1.850	12.51±18%	11.80±20%	1.17	1.11
A-F 1-8 M			7.84 7.27	1.519 2.105		13.61±24%		1.18

2. Statistical errors yield an inaccuracy of

       1 % ... 6 % for the pile oscillator method

   and 0.2 % ... 2 % for the neutron generator method

3. As the higher-mode correction procedure was only a rough approxi-
   mation, possible inaccuracies in the correction factors of

       25 % in the pile oscillator method

   and 30 % in the neutron generator method

  were assumed.

Comparing the results of MSM and source jerk measurements in general,
one finds that - except for very small reactivities - the MSM results
contain significantly smaller errors. This is due to the more precise
correction procedure applied in this method. Therefore only MSM results
are used for comparison with calculated reactivity worths.

5.3 Calculation of control rod worths

As a first approach, the reactivities of the control rods were extracted
from the same diffusion calculations in XY geometry which were used for
the determination of homogeneous correction factors in the source multi-
plication evaluation (see section 5.1.1).

The reactivity of a given rod configuration was determined from the
fractional change of the k_{eff} value:

$$\rho = \frac{k_1 - k_2}{k_2} \qquad [\%]$$

where

    k_1 is the calculated k_{eff} value of the reference core with
    sodium in all rod positions

and

    k_2 is the calculated k_{eff} value of the subcritical configuration.

Table 5.5 Comparison of measured and calculated Control Rod Worths
in SNEAK-10

Measurement: Modified source multiplication (MSM)

Calculation: 2D-XY geometry, 6 energy groups,
mesh: $\Delta s = 2.72$ cm, composition and
group dependent B^2

Conversion: by Keepin $\beta_{eff} = .00697$

SNEAK-10-A

Rods inserted	MSM [$]	Calc. [$]	C/E
4	.274	.238	.87
4+10	.597	.505	.85
B	1.23	1.04	.85
B+D	2.54	2.15	.85
1-12	3.53	2.98	.84
A-D	4.67	3.98	.85
A-D 1-12	9.54	8.16	.86

SNEAK-10-C

Rods inserted	MSM [$]	Calc. [$]	C/E
3	.465	.398	.86
3+7	1.02	.870	.85
M	1.15	.888	.77
C	.947	.782	.83
1-8	3.67	3.16	.86
A-F	5.98	4.79	.80
A-F 1-8	10.65	8.81	.83
A-F 1-8 M	11.49	9.44	.82

Table 5.5 shows a comparison of calculated and measured subcriticalities.
In accordance with section 2.1 all calculated values were reduced by
$\sim$ 1 % in order to take into account that in the experiment the absorber
loading of the simulated control rods only covered the upper axial blanket
and the core region. This correction was deduced from a comparison of
two diffusion calculations in RZ geometry, one with the inner control
rod ring totally inserted and another with the actual experimental in-
sertion depth. It was assumed that this correction is representative
for all control rod configurations.

Furthermore the same β_{eff} value (Keepin) needed for the conversion of
$\Delta K/K$ into $ was used in all cases, although it was shown in section 4
that there is a slight influence of the subcriticality on the delayed-
neutron yield.

The experimental results were taken from the source multiplication
measurements since these could be evaluated more accurately and are
therefore supposed to be more reliable.

Looking at the C/E-values one finds that in the case of SNEAK-10-A the
values are rather low   but quite consistent for all rod configurations:

$$.85 \pm 2 \text{ %}$$

In SNEAK-10-C, however, the C/E-values surprisingly range between

$$.77 \text{ and } .87$$

depending on the distance between the respective rod or rod group and
the core center.

The C/E ratio may have been influenced by various causes:

On the experimental evaluation side, the efficiency correction factors
could contain larger uncertainties than in SNEAK-10-A since the point
source was located in the close vicinity of a follower or absorber. The
treatment of neutron propagation in this core region by diffusion
calculations is therefore obviously less accurate than in 10-A.

On the calculational side, the bucklings utilized which were deduced
from the core-midplane flux shape of RZ-diffusion calculations ob-
viously overestimate the axial leakage of the Na-follower regions.

Furthermore the calculated reactivities could be influenced by the
applied mesh width, the number of energy groups, and the calculational
geometry (2-dim. XY, 2-dim. RZ, 3-dim., etc.).

As the true reasons of the C/E shift were not known extensive cal-
culations were performed with the objective to assess the respective
influence of the above mentioned parameters on the calculated reac-
tivity.

Tables 5.6 and 5.7 give a survey of the parameters which were changed,
and the resulting C/E values.

In order to avoid excessive computational costs, particularly in the
3D-diffusion calculations, only few rod configurations of major
interest were investigated.

The quoted figures are C/E values with respect to the MSM measurements.

The observed influences are subsequently described in detail.

a) Mesh widths Δs

A variation of Δs from 1.81 cm to 5.44 cm (SNEAK-element pitch) caused
increases in C/E in the following range:

$$\text{SNEAK-10-A: } \Delta(C/E) = + .03 \ldots + .05$$
$$\text{SNEAK-10-C: } \Delta(C/E) = + .03 \ldots + .05$$

The C/E shift is not significantly reduced by changes of mesh width.

Table 5.6 Comparison of measured and calculated Control Rod Worths in SNEAK-10-A
Parametric Study of C/E values

Rods inserted	2D-XY-Diff. 12 Groups			2D-XY-Diff. 6 Groups					3D-Diff. 6 Groups	
	Δs = 1.81 cm			Δs=1.81 cm	Δs=2.72 cm	Δs = 5.44 cm			Δs=5.44 cm	Δs=2.72 cm
	B^2=1.80-3	B^2=1.92-3	B^2(M,E)	B^2(M,E)	B^2(M,E)	B^2(M,E)	B^2=1.80-3	B^2=1.92-3		
1-12	.80	.78	.84	.83	.84	.86	.83	.81	.94	.92
A-D	.83	.81	.86	.85	.85	.88	.86	.84	.97	.93
A-D 1-12	.82	.79	.85	.85	.86	.89	.85	.82	.98	.95

B^2: All bucklings given in cm^{-2}

B^2(M,E): Group and composition dependent bucklings

Table 5.7 Comparison of measured and calculated Control Rod Worths in SNEAK-10-C

Parametric Study of C/E-values

Rods inserted	2D-XY-Diff. 6 Groups				3D-Diff. 6 Groups		2D-RZ-Diff.			2D-RZ-Transport
	$\Delta s = 1.81$ cm		$\Delta s=2.72$ cm	$\Delta s=5.44$ cm	$\Delta s=5.44$ cm	$\Delta s=2.72$ cm	6 Groups	12 Groups		12 Groups
	$B^2=1.80-3$	$B^2(M,E)$	$B^2(M,E)$	$B^2(M,E)$			$\Delta s \approx 1$ cm	$\Delta s \approx 1$ cm	$\Delta s \approx 2...4$ cm	$\Delta s \approx 2...4$ cm
M	.73	.77	.77	.81	.94	.92	.93	.94	.95	.97
1-8	.85	.86	.86	.89	.97	.95				
A-F	.76	.79	.80	.84	.94	.92				
M A-F 1-8	.79	.82	.82	.86	.96	.94				

B^2: All bucklings given in cm^{-2}

$B^2(M,E)$: Group and composition dependent bucklings

b) Number of energy groups

A transition from the initially used 6-group condensed cross sections to
12 groups causes a maximum increase in C/E of + .01. This influence was
only checked for SNEAK-10-A as it was assumed to be representative for
both assemblies.

c) Bucklings

In addition to the initially used composition and group dependent buck-
lings (subsequently referred to as $B^2(M,E)$), the influence of two diffe-
rent universal bucklings was investigated:

B^2 = 1.80-3   This buckling shifts the k_{eff} value of the SNEAK-10-A

    cm^{-2} reference core to approx. unity. Since in the eva-

               luation of the BIZET control rod experiments a uni-

               versal buckling was chosen under the same aspect, a

               comparison of C/E values in both assemblies is facili-

               tated.

B^2 = 1.92-3   This buckling was used in all 1-dim. calculations, as

    cm^{-2} it adjusted the k_{eff} value of these calculations

               approx. to the k_{eff} of the 2-dim. basic RZ calculation.

With respect to the calculations using $B^2(M,E)$, the application of these
universal bucklings yielded C/E changes in the following range:

    SNEAK-10-A:
        $B^2(M,E) \rightarrow B^2 = 1.80-3$ $\Delta(C/E) = - .02 \ldots - .03$
        $B^2(M,E) \rightarrow B^2 = 1.92-3$ $\Delta(C/E) = - .05 \ldots - .06$

    SNEAK-10-C:
        $B^2(M,E) \rightarrow B^2 = 1.80-3$ $\Delta(C/E) = - .01 \ldots - .04$

The C/E shift in SNEAK-10-C is slightly enlarged by the use of $B^2 = 1.80-3 \ cm^{-2}$.

d) Geometry

Since the parameter variations so far described failed to diminish the
C/E shift it was assumed that there may be a principal error in the
treatment of transversal neutron propagation.

In order to circumvent the application of probably inaccurate buck-
lings 3-dim. diffusion calculations were performed with the code
D3D /18/.

Using this code, the prediction of control rod worths was not only
remarkably improved (increase in C/E) but also the C/E shift in
SNEAK-10-C was nearly eliminated. The C/E values of both assemblies
are now for the smaller mesh widths of $\Delta s = 2.72$ cm consistently in
the region of .94 $\pm$ 2 %.

As a backup check of the D3D calculations, additional 2-dim. calcula-
tions in RZ geometry were performed for the central rod in SNEAK-10-C.
The results should closely resemble those of D3D since the treat-
ment of axial neutron propagation is the same in both codes. Comparing
column 6 and 7 of Table 5.7 one finds that, for similar mesh widths
and equally condensed cross sections, the C/E values are in fact in
good agreement.

In order to check the influence of transport effects on the control
rod reactivity prediction, the central rod worth was also determined
using the 2-dim. transport code SNOW to the order S8 in RZ geometry /12/.

The result of this calculation which is given in the last column of
Table 5.7 shows a further improvement of the rod worth prediction. The
difference of C/E values in the last two columns reflects the effect
of transport mechanisms in the central rod.

5.4   Conclusions

5.4.1 General remarks on experimental and calculational techniques

It was found in both cores SNEAK-10-A and 10-C that the modified source multiplication method offers the easiest and most precise tool to measure subcriticalities. The corrections which have to be applied to the experimental results could be determined with sufficient accuracy from diffusion calculations with point-source singularities.

The evaluation of source jerk measurements proved to become very complicated above subcriticalities of $\sim 5\ \$$. This is due to the increasing influence of higher harmonic flux modes on the distribution and time dependence of delayed neutron precursors after the source jerk.

The most reliable subcriticality prediction in both SNEAK-10 assemblies was obtained from 3-dim. diffusion calculations using the code D3D. The C/E-bias factor was found to have the same value of .94 $\pm$ 2 % in both assemblies and for all rod configurations investigated.

Using 2-dim. diffusion calculations in XY geometry for the subcriticality prediction, C/E values of .85 $\pm$ 2 % were found for SNEAK-10-A.

In SNEAK-10-C such calculations yielded C/E values in the range of .77 for the central rod to .87 for rods in the outer ring. Since this C/E shift is nearly removed by the application of 3-dim. calculations it appears to be caused by an incorrect treatment of the transversal neutron propagation.

Further investigations of this problem, which are planned for the future, will show whether the C/E shift can be reduced when the bucklings are derived from 2-dim. transport calculations in RZ geometry.

5.4.2 Control rod interaction (antishadowing effects)

One of the major goals of the SNEAK-10 program was to find out whether a compact core exhibits similar control rod interaction effects as one expects for large breeder reactors.

An information about the magnitude of those interactions can be obtained by comparing the reactivity of a certain group of control rods with the arithmetic sum of the individual reactivity effects of the components in this group.

In Table 5.8 such comparisons are given for the rod combinations of major interest in SNEAK-10-A and 10-C.

For the combination of inner and outer control rod ring in SNEAK-10-A one observes an antishadowing effect of + 16 %. In SNEAK-10-C this effect is reduced to + 10 %, due to the more uniform distribution of the simulated control rods. If in addition the central rod is inserted the interaction effect decreases to + 6 %.

Comparing these values with the corresponding calculated ones a general slight overprediction is observed.

Table 5.8 Control Rod Interaction Effects in SNEAK-10-A and 10-C

Measurement: Modified source multiplication

Calculation: 3-dim. diffusion D3D, 6 groups,
                step width Δs = 2.72 cm

SNEAK-10-A

Rod combination	Measurement	Calculation	C/E
$\dfrac{\rho_{i+a}}{\rho_i + \rho_a}$	1.16	1.18	1.02

SNEAK-10-C

Rod combination	Measurement	Calculation	C/E
$\dfrac{\rho_{i+a}}{\rho_i + \rho_a}$	1.10	1.11	1.01
$\dfrac{\rho_{i+a+m}}{\rho_i + \rho_a + \rho_m}$	1.06	1.08	1.02

ρ_i: Reactivity of inner control rod ring

ρ_a: Reactivity of outer control rod ring

ρ_m: Reactivity of central rod

6.   Central reactivity worth

6.1   Description of the experiment

In the reference core SNEAK-10-A central reactivity worth measurements
of ^{10}B and the fuel isotopes ^{235}U and ^{238}U were performed.

The experiment was carried out with a pneumatic pile oscillator which
was positioned adjacent to the core center element (POS. 17/20). The
upper part of the pile oscillator element tube is subdivided into
18 partitions separated by steel partings. Each partition can be loaded
with 15 SNEAK platelets of normal thickness (.315 cm) and a cross section
of 4.6 x 4.6 cm^2.

The lower part of the pile oscillator is loaded continuously, without
subdivisions.

In order to meet the special loading requirements and to adapt the
neutron spectrum and fuel density of the pile oscillator to the surroun-
ding core region, modified unit cells had to be designed. Fig. 13
shows the 3 cell types in use, the loading scheme of the pile oscillator
element tube and the inner core unit cell for comparison. The investiga-
ted samples were inserted in partition 17, replacing the Al-40 % platelet.

The reactivity effect of the sample movement was determined from the
flux signals by the inverse kinetics method with corrections applied
for the transport of neutron precursors.

6.2 Calculations

The reactivity worth calculations were performed with the perturbation phases of three different codes:

    a) KAPER

    b) 1D-diffusion (NUSYS-2200)

    c) 2D-diffusion (DIXY-PERT)

a) KAPER is a one-dimensional collision probability code in plate geometry. It takes into account the heterogeneity of the sample and its environment. The reactivity worth phase of the program is based on exact perturbation theory using the perturbed flux in the sample and the surrounding cell (Ref. /9,10/).

The geometrical model used in these calculations is shown in Fig. 14. Since the environment of the samples remained unchanged in all calculations, only the geometries of the different samples are shown.

In the KAPER material-worth phase the Al-40 % reference platelet is replaced by the respective sample in close accordance with the experimental procedure.

The atomic compositions of the perturbed cell platelets, as they were used in the KAPER code, took into account the decreased fuel density and increased steel contents due to the double steel walls of the pile oscillator element tube with respect to the surrounding core.

A special branch of KAPER allows to compute reactivity worths in a homogenized cell structure.

The normalization integral that is needed in the program to relate the computed local perturbation to the total reactor was deduced from a 2-dim. diffusion calculation in r-z geometry.

b) 2200 is a first-order perturbation code which is implemented in the Karlsruhe NUSYS program system. It uses unperturbed fluxes and adjoints for the reactivity worth determination.

c) DIXY-PERT is the perturbation phase of the 2D-diffusion code DIXY. This calculation is also based on first-order perturbation theory using the unperturbed fluxes and adjoints of the basic k_{eff} calculation in r-z geometry.

In both calculations b) and c) homogenized cell cross sections were used which had been prepared by the NUSYS module 446. The microscopic cross sections were in all calculations taken from the KFKINROO1 set.

The β_{eff} values needed to convert the calculated reactivities from $\Delta K/K$ into $\$$ were discussed already in section 4 of this report.

6.3 Results

A comparison of measured and calculated material worths is given in table 6.1.

Using the Keepin β_{eff} value (shaded area) one observes the usual overestimation of the material worth of the fuel isotopes and underestimation of ^{10}B.

These results are significantly improved by the use of Tuttle's β_{eff}. The C/E values of the fuel isotopes are decreased to approximate unity.

The extreme underestimation of ^{10}B which is known already from previous assemblies will have to be further investigated.

Table 6.1 Material Worths at the Core Center of SNEAK-10-A

Sample	Sample Weight (gm)	Experiment $[m\$/g]$	Calculation / Experiment $\beta_{eff} \rightarrow$ KEEPIN / TUTTLE				Experimental values normalized to ^{235}U
			KAPER HET	KAPER HOM	2200	DIXY-PERT	
^{235}U	6.69	+.185±3 %	1.10 / 1.00	1.09 / .99	1.06 / .96	1.08 / .98	1.0
^{238}U	123.6	−.0127±3%	1.08 / .98	1.11 / 1.01	1.06 / .96	1.11 / 1.02	−.069
^{10}B	.589	−4.26±2 %	.94 / .85	1.02 / .92	1.01 / .91	1.04 / .94	−23.1

7. Importance measurements in SNEAK-10-A

7.1 Experiments

A pointwise representation of the axial importance distribution in
the core-centre-element (POS 17/19) and of the radial distribution
along the North-South-axis of the reactor in the core midplane was
obtained by application of the source oscillation method. In this
method a ^{252}Cf neutron source is oscillated in an axial or radial
channel between a certain position inside the core for which the
importance is to be determined and a location outside the blanket
where the importance is approx. zero.

The apparent reactivity effect of the source oscillation was deter-
mined by compensation using an automatic control rod, that in turn
was calibrated by the inverse kinetics method using Keepin's relative
group yields.

Assessing the importance function of the neutron source one has to be
aware of the fact that the measured reactivity effect contains two
components of different origin:

1. The desired apparent reactivity of the source neutrons,
   which is inversely proportional to the flux level.

2. The material worth of the source, caused by interaction
   of neutrons with the source and capsule materials, which
   must be corrected for.

In order to extract the effect of the source neutrons, all measurements
were performed at a low power level, ($\sim$ 2.6 W) where the source effect
predominates, and a high power level ($\sim$ 52 W) where the material worth
causes most of the effect.

The desired apparent reactivity at low power can then be determined from

$$\rho_a = \frac{\rho_H - \rho_L}{\dfrac{P_L}{P_H} - 1}$$

where ρ_H and ρ_L are the measured reactivity values for high and low power respectively and P_H, P_L are the corresponding power levels.

7.2 Calculation

The calculation of the importance profiles was based on a 2-dim. adjoint diffusion calculation (DIXY) in r-z geometry using the same geometrical model and cross sections as the basic k_{eff} calculation (see chapter 3.2). In an evaluation phase the adjoint fluxes $\phi^+(E_i)$ were groupwise multiplied with the 12-group source spectrum $S(E_i)$ of the ^{252}Cf source yielding the effective source strength

$$\sum_{i=1}^{12} S(E_i) \cdot \phi^+(E_i)$$

for each mesh point, which is directly proportional to the desired apparent reactivity ρ_a.

7.3 Results

A survey of experimental and calculational results is shown in Figs. 15 and 16. The calculational results were normalized to the respective experimental core centre values.

The statistical error of the experimental values is in the region of ± 1 % (1σ). This value does not contain uncertainties of the automatic control rod calibration.

For the axial traverse the calculation matches the experimental values
with sufficient accuracy. The agreement is generally better than $\pm$ 1 %.

In the radial direction the situation is slightly worse. In sufficient
distance from the Na-followers the agreement is within $\pm$ 2 %. Only in
the vicinity of the inner control rod ring the discrepancy reaches 4 %.
This is probably due to the fact, that in the experiment the neutron
source was moved through a "pure fuel" region while in the calculation
the corematerial was smeared with the Na-followers into rings of
$\sim$ 10 cm thickness. In these regions of reduced fuel density the cal-
culation consequently underestimates the importance of the source
neutrons.

Comparing the core centre values of both traverses one finds a discre-
pancy of $\sim$ 1.4 % (axial: 2.16 ¢, radial 2.19 ¢), that is within the
region of the experimental accuracy.

8. Fission rate distributions

8.1 Experimental techniques

Extensive measurements of the fission rate distributions were performed
in all SNEAK-10-configurations, using experimental techniques which
were already successfully employed in several earlier SNEAK-assemblies.
The experimental program comprised the following points:

Measurement of axial and radial fission rate distributions
of ^{235}U and ^{238}U with fission chambers and foil activations.

Measurement of fission rates at various points distributed
over the core midplane with the foil activation technique.

8.1.1 Fission chamber measurements

In this technique cylindrical fission chambers of $\sim$ 6 mm diameter are moved stepwise through an axial or radial channel. At each position within the core region, the counts of the chambers were sampled up to a total count number of 120000. When this count limit was reached the total number of counts, the sampling time, the position of the chamber, and the count rate of an independent out-of-core detector were recorded on magnetic tape. Subsequently the chamber was automatically moved to the next position.

In the blanket region, the count limit was reduced to 60000 or lower in order to accelerate the data acquisition process.

The active layer of the chambers had a length of $\sim$ 20 mm and consisted of 93 % enriched (^{235}U-chamber) and 0.04 % depleted (^{238}U-chamber) uranium.

The results of the ^{238}U-chamber had to be corrected in the evaluation routine since its ^{235}U content (0.04 %) causes a contribution of

$$0.04 \ \% \cdot \sigma_{f5}/\sigma_{f8} = 0.04 \ \% \cdot 33.3 = 1.3 \ \%$$

to the measured count rate.

A correction to the ^{235}U-chamber results was not supposed necessary, as its ^{238}U content (7 %) only causes a count rate contribution of

$$7 \ \% \cdot \sigma_{f8}/\sigma_{f5} = 7 \ \% \cdot 0.03 = 0.21 \ \%$$

For the axial measurements a special element type was used, which was loaded with platelets having a centre hole. This allowed the insertion of a guide tube through which the fission chambers could be moved. The inner diameter of this guide tube was 11 mm. In order to minimize

flux disturbance and leakage effects, caused by the insertion of this channel element, the probe which held the fission chambers during the traverse was itself fuelled with enriched uranium oxide. A detailed description of the experimental setup is given in /21/.

In order to improve the signal-to-noise ratio in these measurements, miniaturized impedance transformers were installed inside the probe, close to the fission chambers.

For the measurement of radial traverses, a channel at core mid-height was built using the "window cells" described in section 2. This channel is oriented in north-south direction and is indicated in all SNEAK core maps by a horizontal dashed line through the matrix row Y = 19.

During all measurements the flux was kept constant by an automatic control rod.

8.1.2 Foil activation measurements

Uranium metal foils of 25.4 mm diameter and nominally 0.1 mm thickness were used in the activation measurements. Pairs that consisted each of a depleted (0.4 % ^{235}U) and an enriched (20 % ^{235}U) foil were placed between the platelets and exposed to the neutron flux, e.g. for 3 hours at a reactor power of 250 W. Starting about 20 hours after activation, the γ activity of the foils in the energy window 700 ... 1330 keV was measured using an automatic sample changer equipped with two NaI scintillation detectors. Background counts and foil activity not due to fission products were taken into account by including in the measurements a non-activated foil of each kind as well as an empty position of the sample-changer magazine.

The decay of the activity is eliminated by taking the data in a number
of cycles (about 20 ... 30) that are evaluated independently. Each
cycle consists in measuring, for a fixed time per foil, the sequence
of foils first forward and then backward so that every foil is mea-
sured twice. By summing the two count numbers obtained for each foil,
the data obviously become independent of the decay as long as the decay
can be considered linear with time over the duration of the cycle. The
error introduced by the latter approximation can be kept sufficiently
small by using short cycle durations, e.g., 1 hour at 20 hours after
activation.

This method yields relative distributions of the microscopic fission
rate for each isotope separately. In order to obtain the ratios
σ_{f8}/σ_{f5}, an additional pair of foils is placed between the active
layers of two calibrated parallel-plate fission chambers, one en-
riched and one depleted in ^{235}U. The four uranium layers are close
to each other and are thus exposed to the same fluence and spectrum.
By including this pair of foils in the γ-activity measurement, cali-
bration factors for the fission rates can be deduced by comparison
to the counting rate of the chambers.

In each of the three SNEAK-10 assemblies, this pair of fission chambers
was kept at a fixed location in the core. Therefore, the corresponding
activated foils also provided the normalization necessary for comparing
the data from separate activations.

The positioning of the activation foils within the different core unit
cells is indicated in Fig. 17. These positions were selected under the
following aspect:

Slight variations of the foil position within the unit cell, which can
be caused by varying thicknesses of the platelets themselves or of the
foil pairs wrapped in Al-sheets, should not cause severe changes in the
foil fission rate. Thus it appears favourable to insert the foils in

a position where the fission rate fine structure has the smallest
gradient. In order to find out for which position this requirement
is best fulfilled, calculations of the fission rate fine structure
were performed with the cell code KAPER for both unit cells.

The calculated fission rate distributions of ^{238}U are shown in
Fig. 17 along with the unit cell structures. (The fission rate of
^{235}U shows no significant fine structure and is therefore irrelevant
in this consideration.) All fission rate values were normalized to
the minimum value of the respective cell. It can be seen that the
foils are in fact located in the region of the lowest gradient.

In addition to the individual fission rate profiles, the macros-
copic cell average values, as they were calculated by KAPER, are
indicated for each cell. A comparison of the fission rate values
at the foil positions $<\sigma_{f8}\phi>_{Foil}$, $<\sigma_{f5}\phi>_{Foil}$ with the corresponding
cell average values $<\sigma_{f8}\phi>_{Av}$, $<\sigma_{f5}\phi>_{Av}$ shows that the foils in the
inner and outer core zone detect different fractions of the cell
average values:

	$<\sigma_{f5}\phi>_{Foil}/<\sigma_{f5}\phi>_{Av}$	$<\sigma_{f8}\phi>_{Foil}/<\sigma_{f8}\phi>_{Av}$
Inner core zone	1.006	.979
Outer core zone	1.005	.969
Adaptation factor applied to outer core zone results	$\frac{1.006}{1.005} = 1.001$	$\frac{0.979}{0.969} = 1.010$

This means that the results of foil measurements in the inner and
outer core zone can only be compared when an adequate normalization
factor is taken into account. For the horizontal fission rate
distributions, this was achieved by multiplying the results of the
outer core zone with the "adaptation factors" given in the third
row of the above table.

For the measurements of axial fission rate traverses the distances
between the foil pairs were chosen as multiples of the unit cell
height in order to avoid a modulation of the global distribution
by the local cell fine structure.

8.2 Calculational methods

Various 2-dim. and 3-dim. codes were employed for the calculation of
fission rate distributions. The major part of these calculations
closely resembles those already used for the k_{eff} prediction of the
critical cores (section 3.2) and the determination of control rod
worths (section 5.3). Therefore, in general, only a short repetition
of the most important parameters is given here.

Since in the synthesis calculations with KASY the choice of the **trial**
functions is of major importance for the determination of fission
rate distributions, this aspect will be discussed in more detail.

1. <u>KASY</u>   3-dim. synthesis diffusion code /6/.
             Cross sections: 6 groups (section 3.2).
             Mesh widths: $\Delta s = 2.72$ cm in all coordinate directions.
             Geometrical model: as in k_{eff} prediction (section 3.2).

             The **trial** functions needed in the synthesis method
             were determined by 2-dim. diffusion calculations in
             XY geometry.

             In SNEAK-10-A and 10-C two trial functions were prepared:
             a) in the core midplane
             b) in the axial blanket

             In SNEAK-10-B three trial functions were determined:
             a) in the lower core portion, with sodium in all simulated
                control rod positions
             b) in the upper core portion with absorber material in
                the rods of the inner control rod ring
             c) in the upper axial blanket.

The bucklings of the trial function XY calculations were chosen as was proposed in /23/:
In the core trial function calculations a global buckling was chosen in such a way that the k_{eff} value of the XY calculation was shifted to approximately unity.

In the axial blanket region the buckling was always set to 0.0. Some test runs with different negative bucklings did not yield any significant changes in the KASY k_{eff} value nor in the calculated fission rate distributions.

2. <u>AUDI 3</u>   is a 3-dim. evaluation code which yields reaction rate distributions on the basis of threedimensional fluxes from KASY or D3D /22/.

Since in some cases the KASY calculations were not able to predict the fission rate distribution with sufficient accuracy, additional calculations were performed, using the following codes:

3. <u>DIXY-XY</u>   2-dim. diffusion code in XY-geometry.
Cross sections: 6 groups (see section 3.2).
Mesh widths: Δs = 2.72 cm.
The same geometrical model and bucklings (group and composition dependent) were used as in the calculations of section 5.1.1 and 5.3 (subcritical control rod measurements).

4. <u>DIXY-RZ</u>   2-dim. diffusion code in RZ-geometry.
Cross sections: 12 groups (see section 3.2).
Mesh widths: 1 - 2 cm.
The geometrical model was basically the same as the one described in the basic k_{eff} calculations of section 3.2.

However, an additional sodium rod was introduced into the core centre. The size of this central rod was chosen corresponding to the geometrical cross section area of the actual Na-followers used in all SNEAK-10 assemblies.

5. D3D   3-dim. diffusion code /18/.

Cross sections: 6 groups (see section 3.2).

Mesh widths: Δs = 2.72 cm

The geometrical model was chosen in agreement with the calculations performed in the frame of control rod worth calculations (section 5.3).

8.3 Results of the evaluation

8.3.1 Axial traverses

In SNEAK-10-A fission rate traverses of ^{235}U and ^{238}U were measured in several positions of the inner and outer core zone, indicated by 'X' in the core map below:
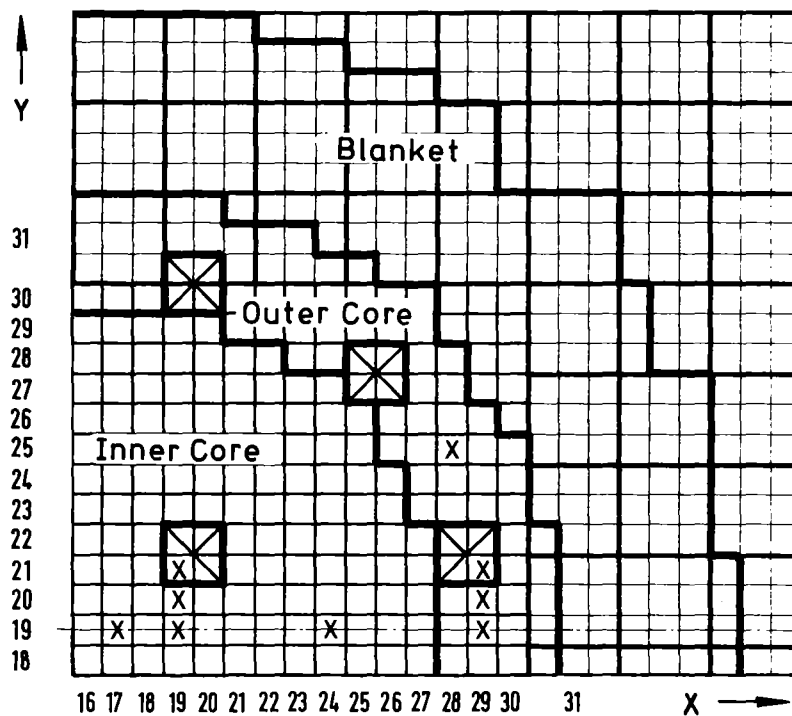
These positions were chosen in order to check the influence of the following parameters on the shape of the traverses:

1. Radial position (different core zones)

2. Distance between measuring position and simulated control rods.

The evaluation of the group of measurements along Y = 19 and at position 28/25 yielded curves with very similar shape, comparable deviations between fission chamber and foil activation measurements, as well as similar discrepancies between measurement and calculational prediction. Therefore, a detailed discussion of the results will subsequently only be given for one of these positions: the core-centre Pos. 17/19 (Fig. 18). The statements given there also apply to the other measurements of the above mentioned group.

Concerning the traverses at positions 19/20 and 29/20, adjacent respectively to followers of the inner and outer simulated control rod ring, one only observes a slight flattening of the traverses due to the influence of increased axial leakage in the neighbouring Na channels.

A significant change in the shape of axial traverses with respect to those measured within fuel regions is found for the measurements inside Na-followers of the inner and outer ring (Pos. 19/21, 29/21). These measurements were only carried out with the foil activation method as the insertion of a channel element would have seriously altered the structure of the Na-follower. As the traverses in both positions had nearly the same shape (max. deviation $\leq$ 1 % in the core region) only the results of Pos. 19/21 are given in Fig. 18 for comparison with the core-centre traverse.

Looking at the results given in Fig. 18, one finds that the agreement of fission chamber and foil measurements is for the core region of the ^{235}U traverse within 1 % and for ^{238}U within 2 %.

In the blanket region, the agreement of both experimental techniques becomes significantly worse; in some points of the ^{238}U traverse the deviation reaches $\sim$ 10 %. Similar discrepancies were already found in earlier SNEAK-cores (e.g. SNEAK-9A-2 /16/, SNEAK-9C-2 /13/). They are possibly caused by leakage effects in the axial channel element, which do not occur in the foil measurements.

The statistical 1σ errors of the measurements are approximately:

	fission chambers	foil activation
^{235}U	0.3 %	0.1 ... 0.6 %
^{238}U	1 %	0.1 ... 1 %

(For error contributions in foil activation measurements see section 8.3.3)

The calculated fission rate distribution of the core centre traverse was obtained from KASY-fluxes (section 8.2.1). A general good agreement between calculated and measured shapes is observed.

As the axial fission rate distribution within the Na-follower could not be described by KASY with sufficient accuracy, it was derived from an RZ-diffusion calculation with a central follower (section 8.2/4.). The calculated axial distribution within the central follower is indicated in Fig. 18 by a dotted line. The distribution thus calculated in general closely matches the measured values.

SNEAK-10-B

Figs. 19 and 20 give a survey of traverses in different positions of SNEAK-10-B. The first traverse was taken adjacent to a half inserted absorber of the inner ring (Pos. 19/20), the second at the boundary of inner and outer core zone (Pos. 27/19). These positions were chosen in order to study the radial dependence of flux shift effects caused by the partial insertion of the inner control rod ring.

All measurements were performed with the fission chamber technique. The calculated curves were obtained from KASY fluxes (section 8.2/1.).

For both isotopes a significant shift of the fission rate maximum to the lower core half is observed in the vicinity of the half inserted absorber (Pos. 19/20). In Pos. 27/19, which is located approx. 35 cm away from the inner control rod ring, the fission rate distribution is found to be nearly symmetrical with respect to the core midplane. This indicates that in the region of the inner-outer-core interface, the partial insertion of the inner ring has no significant influence on the shape of the axial fission rate distribution.

A comparison of measured and calculated values shows for position 27/19 a similar good agreement as for the measurements in SNEAK-10-A. However, for the traverses adjacent to the half inserted absorber of the inner ring a general shift of the calculated distribution to the upper core region was found. A similar effect has already been observed in SNEAK-9A-2 /16/. The reason for this phenomenon, which is particularly distinct in the ^{238}U traverse, is probably related to the underestimation of the control rod worth (less effective control rods cause less intensive flux shifts).

SNEAK-10-C

In SNEAK-10-C only a few axial traverses were measured, in order to check whether the reorganisation of the simulated control rod positions had caused a distinct change in the shape of the traverses with respect to those measured in SNEAK-10-A. As only minor changes were found in the slope of the traverses, and as the quality of the prediction for KASY calculations is comparable with SNEAK-10-A, no detailed description will be given of these results.

8.3.2 Radial traverses

Radial fission chamber traverses of ^{235}U and ^{238}U were performed in all SNEAK-10 assemblies. The location of the radial channel through which the fission chambers were moved is indicated in the core maps of Figs. 4 - 6 by a dashed line through row Y = 19 (N-S-direction). As, in general, the shape of the ^{235}U and ^{238}U traverses was very similar and as on the other hand ^{238}U provides only a relatively small contribution to the total power, only the ^{235}U distributions will be presented subsequently.

A comparison of radial ^{235}U traverses in SNEAK-10-A and SNEAK-10-B is given in Fig. 21. All values are relative to the maximum value of the respective traverse. In SNEAK-10-A this maximum value is located in the core centre. In SNEAK-10-B it is shifted towards the outer zone, due to the partial insertion of the inner control rod ring.

In addition to the experimental results, calculated distributions are given for each assembly. As a basic computational tool the 3-dim. synthesis code KASY was used again. As, however, in the inner core zone of SNEAK-10-A deviations of up to $\sim$ 5 % occured between measured and calculated values the fission rates were recalculated with fluxes obtained from the 3-dim. code D3D (section 8.2/5.). The results of this calculation, which are given in Fig. 21 as a dotted line, show a significantly better agreement with the measured distribution.

A similar improvement of the calculated values was obtained in SNEAK-10-C (Fig. 22) where the discrepancy between measured and KASY values reached a maximum of $\sim$ 7 %. By the use of D3D the maximum deviation was reduced to approximately 3 %.

In general it has to be emphasized that all fission rate distributions shown in Figs. 18 - 22 have been normalized to their respective maximum value and therefore yield informations about the shape of the traverses only. In certain cases the choice of normalization may cause a misleading impression when measurements and calculations are compared.

This is the case in the radial fission rate traverse in SNEAK-10-C.
There, the normalization point is located in a region - the central
follower - which is not accurately treated by diffusion theory: As
the fission rate is underpredicted in this region with respect to the
rest of the core one arrives at a normalization factor which leads
to an apparent general overestimation for the calculated distribution.

8.3.3 Core-midplane distribution

A survey of the results of foil activation measurements, performed
in selected parts of the core-midplane of all SNEAK-10-assemblies,
is given in Tables 8.1 - 8.3. The outer core zone results are correc-
ted for the 'cell fine structure / cell average' ratio according to
section 8.1.2. Again all values were normalized to the respective
maximum value of each distribution. The quoted errors comprise
counting statistics and such equipment fluctuations as are found in
comparing the results of the individual cycles (see sect. 8.1.2).
However, certain additional errors of a few tenths of a percent
cannot always be excluded, e.g. from inaccurately known uranium
masses of the foils.

The measured distributions of SNEAK-10-A and SNEAK-10-C were compared
with the results of KASY, DIXY-XY (section 8.2/4.) and D3D calcula-
tions. In SNEAK-10-B only KASY results were taken for comparison. The
resulting (C-E)/E deviations are listed in Tables 8.1 - 8.3 and for
^{235}U partially in Figs. 23 - 25.

The magnitude of the deviations is similar to those found in the
radial traverses and shows a distinct correlation with the treat-
ment of transverse neutron propagation in the different codes.

Table 8.1 Comparison of measured and calculated Fission Rate Distributions in the core-midplane of SNEAK-10-A

	Position	Radius [cm]	$<\sigma_{f5}\phi>/\text{Max}\{<\sigma_{f5}\phi>\}$ Measurement: Foil activation	$\frac{C-E}{E}$ [%] 2-dim.XY-calcul.	$\frac{C-E}{E}$ [%] 3-dim.synth. calcul.	3-dim. calcul.	$<\sigma_{f8}\phi>/\text{Max}\{\sigma_{f8}\phi>\}$ Measurement: Foil activation	$\frac{C-E}{E}$ [%] 2-dim.XY-calcul.	$\frac{C-E}{E}$ [%] 3-dim.synth. calcul.	3-dim. calcul.
inner core zone	17/19	0.00	.999±0.002	± 0		+)	1.000±0.005	± 0		+)
	18/20	7.69	1.000 "	− 1.3	− 1.3	− 1.1	.962±0.002	+ 0.7	+ 0.8	+ 2.0
	19/19	10.88	.994 "	− 1.0	− 0.9	− 1.0	.962±0.003	+ 0.6	+ 0.9	+ 1.7
	19/20	12.16	.988 "	− 1.3	− 1.3	− 1.1	.931±0.004	− 0.2	+ 0.1	+ 3.1
	21/20	22.43	.971 "	− 0.4	+ 0.4	− 0.2	.936±0.002	+ 2.0	+ 2.6	+ 2.8
	21/22	27.20	.952 "	− 0.6	+ 0.2	− 0.5	.887±0.002	+ 2.3	+ 3.1	+ 5.0
	22/19	27.20	.957 "	+ 0.4	+ 2.2	+ 0.6	.943 "	+ 3.3	+ 4.3	+ 2.5
	22/24	38.47	.876±0.001	+ 1.3	+ 3.3	+ 1.0	.869 "	+ 4.0	+ 5.1	+ 2.3
	23/22	36.49	.892 "	+ 1.3	+ 3.5	+ 1.2	.895 "	+ 2.9	+ 4.0	+ 1.4
	24/19	38.08	.876 "	+ 1.4	+ 3.8	+ 1.5	.881 "	+ 3.1	+ 4.5	+ 1.5
	24/26	53.85	.661 "	+ 0.5	+ 2.3	− 0.4	.662 "	+ 2.1	+ 3.0	0.0
	26/24	56.01	.641 "	+ 1.5	+ 3.1	+ 0.4	.668 "	+ 3.0	+ 3.7	− 1.7
	27/19	54.40	.641 "	+ 0.2	+ 2.2	0.0	.658 "	+ 1.2	+ 2.3	− 1.5
outer core zone	27/25	63.44	.521±0.001	+ 0.7	+ 1.7	− 1.7	.577±0.001	+ 1.0	+ 1.3	+ 4.5
	27/29	76.93	.293 "	+ 1.2	+ 1.4	− 1.3	.283±0.002	0.0	− 0.1	+ 15.8
	29/19	65.28	.472 "	− 0.8	0.0	− 2.2	.515±0.001	− 0.8	− 0.4	+ 4.9
	29/20	65.51	.469 "	− 0.9	− 0.4	− 2.1	.485±0.002	+ 0.4	+ 5.3	+ 9.6
	29/26	75.57	.296 "	+ 0.7	+ 0.7	− 2.9	.288 "	− 1.1	− 1.1	+ 13.6
	30/22	72.58	.366 "	− 0.3	− 0.3	− 1.9	.355 "	+ 0.4	+ 3.9	+ 15.1
	30/23	73.99	.332 "	− 0.3	− 0.3	− 2.4	.326 "	− 0.6	− 1.1	+ 13.5

+) Normalization point

Table 8.2   Comparison of measured and calculated Fission Rate Distributions in the core-midplane of SNEAK-10-B

Position	Radius [cm]	$<\sigma_{f5}\phi>/Max\{<\sigma_{f5}\phi>\}$ Measurement : Foil activation	3-dim.synth. calculation	$\frac{C-E}{E}$ [%]	$<\sigma_{f8}\phi>/Max\{<\sigma_{f8}\phi>\}$ Measurement : Foil activation	3-dim.synth. calculation	$\frac{C-E}{E}$ [%]
17/19	0.00	.896±0.001	.896	0.0	.911±0.002	.882	− 3.2
19/19	10.88	.894 "	.888	− 0.7	.901 "	.866	− 3.9
22/19	27.20	.963 "	.974	+ 1.2	.988 "	.968	− 2.1
24/19	38.08	1.000 "	1.000	± 0 +)	1.000 "	1.000	± 0 +)
27/19	54.40	.855 "	.879	+ 2.8	.904 "	.909	+ 0.6
21/22	27.20	.916 "	.908	− 0.9	.898 "	.874	− 2.7
22/24	38.47	.942 "	.947	+ 0.5	.959 "	.945	− 1.5
23/22	36.49	.979 "	.970	− 0.9	.985 "	.968	− 1.7
24/26	53.85	.795 "	.758	− 4.7	.789±0.001	.757	− 4.0
26/24	56.01	.791 "	.788	− 0.4	.845 "	.820	− 2.9
29/19	65.28	.666 "	.677	+ 1.7	.768 "	.759	− 1.2
27/25	63.44	.654 "	.636	− 2.8	.751 "	.702	− 6.5
29/26	75.54	.379 "	.362	− 4.5	.385 "	.347	− 9.9
27/29	76.93	.363 "	.340	− 6.2	.363 "	.324	− 11.0

(rows 17/19 through 26/24 are in the inner core zone; rows 29/19 through 27/29 are in the outer core zone)

+)   Normalization point

Table 8.3 Comparison of measured and calculated Fission Rate Distributions in the core-midplane of SNEAK-10-C

Position	Radius [cm]	$\langle\sigma_{f5}\phi\rangle/Max\{\langle\sigma_{f5}\phi\rangle\}$ Measurement: Foil activation	$\frac{C-E}{E}$ [%] 2-dim.XY-calcul.	3-dim.synth. calcul.	3-dim. calcul.	$\langle\sigma_{f8}\phi\rangle/Max\{\langle\sigma_{f8}\phi\rangle\}$ Measurement: Foil activation	$\frac{C-E}{E}$ [%] 2-dim.XY-calcul.	3-dim.synth. calcul.	3-dim. calcul.
18/20	8.60	1.000±0.001		± 0	+)	.934±0.001	+ 2.1	+ 2.3	+ 5.4
18/21	13.87	.996 "	+ 1.1	+ 1.2	+ 0.5	1.000±0.002		± 0	+)
18/22	19.23	.983 "	+ 1.7	+ 1.9	+ 0.6	.984 "	+ 0.9	+ 1.0	+ 0.5
18/26	40.89	.886 "	+ 2.8	+ 4.1	+ 0.9	.850±0.001	+ 2.9	+ 3.8	+ 3.6
18/27	46.32	.827 "	+ 4.4	+ 6.1	+ 1.4	.831 "	+ 3.8	+ 4.7	+ 1.0
18/28	51.75	.752 "	+ 4.2	+ 6.0	+ 0.7	.739 "	+ 4.3	+ 5.5	+ 2.0
19/22	20.71	.980 "	+ 1.5	+ 1.8	+ 0.4	.984 "	+ 0.1	+ 0.3	- 0.1
21/24	35.46	.940 "	+ 3.7	+ 5.4	+ 1.7	.949 "	+ 3.2	+ 4.0	+ 1.0
22/26	47.58	.874 "	+ 7.7	+ 10.1	+ 3.7	.906 "	+ 6.9	+ 8.3	+ 1.2
23/27	55.08	.801 "	+ 9.5	+ 12.3	+ 3.9	.859 "	+ 8.8	+ 10.5	- 0.6
19/30	63.09	.614 "	+ 6.0	+ 7.5	+ 0.6	.658 "	+ 3.0	+ 4.4	+ 10.9
24/28	62.62	.695 "	+ 10.3	+ 13.2	+ 2.3	.804 "	+ 8.1	+ 10.2	+ 5.6
26/30	77.79	.386 "	+ 10.1	+ 13.5	- 2.2	.409 "	+ 6.8	+ 9.2	+ 10.7

(The first ten rows belong to the "inner core zone"; the last three rows belong to the "outer core zone".)

+) Normalization point

In general the highest discrepancies between measured and calculated distributions are observed for KASY calculations where the axial leakage, found by synthesizing trial functions which were calculated using a universal buckling (section 8.2/1.), is apparently not sufficiently accurate.

Somewhat better results were obtained from 2-dim. diffusion calculations in XY geometry where group and composition dependent bucklings were employed.

For most cases, the best agreement was achieved by 3-dim. calculations (D3D) where the transverse neutron propagation is not accounted for by bucklings but is included in the calculation. However, large discrepancies were found using this method for the ^{238}U fission rate in the outer core zones. A definite reason for this specific problem was not found.

8.3.4 Spectral indices

Table 8.4 gives a survey of cell averaged fission rate ratios σ_{f8}/σ_{f5} (subsequently referred to as spectral indices) in different positions of SNEAK-10-A.

The experimental values given in the first row were derived from foil activation measurements. Absolute fission rates, necessary for the determination of the spectral indices, were obtained from the foil activation data by relating them to the counting rates of calibrated parallel-plate fission chambers (see section 8.1.2 and /24/). Also, the desired cell average values were derived from the activation at the individual foil positions according to sect. 8.1.2 and Fig. 17.

The corrected experimental data are compared in Table 8.4 with the results of KASY /6/ calculations with homogenized cross sections and KAPER /9/ cell calculations.

In the fuel regions of the inner and outer core zone (column 1, 2, 4 of Table 8.4), the KASY calculations underpredict the spectral indices by 6 ... 7 %. The numbers given in column 3 and 5 shed some light on the shift of the neutron spectrum inside the Na followers. In these regions, the spectral indices are overestimated by KASY.

In the KAPER calculation the inner zone unit cell was embedded in an environment of the same composition as the cell itself. The result is therefore representative for a cell located in a 'clean core region', i.e. an area with sufficient distance from zone boundaries and other disturbances (e.g. Na followers).

Comparing the KAPER result of the inner core unit cell (given in column 1) with the measured spectral index of the core centre, one observes approx. the same underestimation as for the corresponding KASY calculation.

Fig. 26 shows this underestimation of the spectral index (calculated by KAPER) versus the experimental spectral index at the core centre of SNEAK-10-A and two earlier uranium-fuelled SNEAK assemblies: SNEAK-9A-0 /8/ and SNEAK-9C-1 /13/. It can be seen that the underestimation in SNEAK-10-A is - within the experimental accuracy - in good agreement with a tendency which has already been observed in earlier SNEAK assemblies:

An underestimation of the core-centre spectral index σ_{f8}/σ_{f5}, increasing with the experimental value of this quantity.

Table 8.4 Cell averaged Spectral Indices σ_{f8}/σ_{f5} in SNEAK-10-A

Position		Inner core zone		Outer core zone	
	17/19 Core centre	19/20 adjacent to Na-foll.	19/21 Na-follower	29/19	29/21 Na-follower
Experiment	.0324	.0305	.0246	.0353	.0269
KASY	.0301	.0288	.0261	.0327	.0277
C/E (KASY)	.93	.94	1.06	.93	1.03
KAPER	.0305				
C/E (KAPER)	.94				

Calculation

Inner Core Unit Cell

- 77 -

Acknowledgements

References
_____

/1/   F. Helm, G. Jourdan
        Die Kompakte Anordnung - eine neue Methode zur Simulation
        schneller Brutreaktoren in Kritischen Anlagen
        Reaktortagung Nürnberg 1975, S. 233

/2/   F. Helm, H. Giese
        Measurements at SNEAK of control rod worth and control rod
        influence on power distributions in fast reactors
        Specialists Meeting on Control Rod Measurement Techniques:
        Reactivity Worth and Power Distribution, Cadarache, April 1976

/3/   E. Eisemann, R. Fröhlich, E. Kiefhaber, H. Küsters, A. Polch
        private note

/4/   U. Wehmann
        Private note, 1974

/5/   W. Hoebel
        "DIXY", a 2-dim. multigroup diffusion program,
        unpublished computer program

/6/   G. Buckel
        Approximation der stationären dreidimensionalen Mehrgruppen-
        Neutronen-Diffusionsgleichung durch ein Syntheseverfahren
        mit dem Karlsruher Syntheseprogramm KASY
        KFK 1349 (June 1971)

/7/   E. Kiefhaber
        The KFKINR Set of Group Constants
        KFK 1572 (March 1972)

/8/   M. Pinter
       Physics Investigations of Sodium-Cooled Fast Reactors:
       SNEAK-Assembly 9A
       KFK 2028 (July 1974)

/9/   P.E. McGrath, E.A. Fischer
       Calculation of Heterogeneous Fluxes, Reaction Rates and
       Reactivity Worths in the Plate Structure of Zero Power
       Fast Critical Assemblies
       KFK 1557 (March 1972)

/10/   P.E. McGrath
       KAPER - Lattice Program   for Heterogeneous Critical
       Facilities (User's Guide)
       KFK 1893 (December 1973)

/11/   H. Huschke
       Gruppenkonstanten für dampf- und natriumgekühlte schnelle
       Reaktoren in einer 26-Gruppendarstellung
       KFK 770 (1968)

/12/   C. Günther, W. Kinnebrock
       SNOW, Ein zweidimensionales S_N-Programm zur Lösung der
       Neutronentransportgleichung in Platten- und Zylinder-
       geometrie
       KFK 1826 (July 1973)

/13/   W. Scholtyssek
       Physics Investigations of Sodium-Cooled Fast Reactors:
       SNEAK-Assembly 9C
       KFK 2361 (April 1977)

/14/   G.R. Keepin
       Physics of Nuclear Kinetics
       Addison-Wesley Publishing Company, Inc., Reading,
       Massachusetts (1965)

/15/   E.A. Fischer
       Integral Measurements of the Effective Delayed Neutron
       Fractions in the Fast Critical Assembly SNEAK
       Nucl. Sci. Eng. 62, 105 (1977)

/16/   M. Pinter et al.
       Control Rod Worth and Power Distribution Measurements
       in the SNR Mock up SNEAK-Assembly 9A
       KFK 2077 (November 1974)

/17/   H. Walze
       Systematische Fehler und Korrekturmöglichkeiten bei
       inverskinetischen Kontrollstabeichungen
       KFK 1701 (November 1972)

/18/   B. Stehle
       D3D - Ein FORTRAN-Programm zur Lösung der stationären
       dreidimensionalen Multigruppendiffusionsgleichungen
       KFK 2118 (March 1975)

/19/   R.J. Tuttle
       Delayed-Neutron Data for Reactor-Physics Analysis
       Nucl. Sci. Eng. 56, 37 (1975)

/20/   J. M. Stevenson
       private note

/21/   R. Böhme
       Messung des Einflusses von Kontrollstäben auf die
       Leistungsverteilung in der SNR-300 Nachbildung SNEAK-9A-2
       - Spaltkammertraversen -
       PSB-Vierteljahresbericht 1/1973 (pp 121-15)
       KFK 1273/1 (1973)

/22/   G. Willerding
       AUDI-3, private note

/23/   S. Pilate et al.
       A Three-dimensional Synthesis Method Tested and Applied
       in Fast Breeders
       KFK 1345 (August 1971)

/24/   R. Böhme et al.
       Messung von Reaktionsraten im schnellen Nulleistungsreaktor
       SNEAK
       atw, July 1971, S. 360
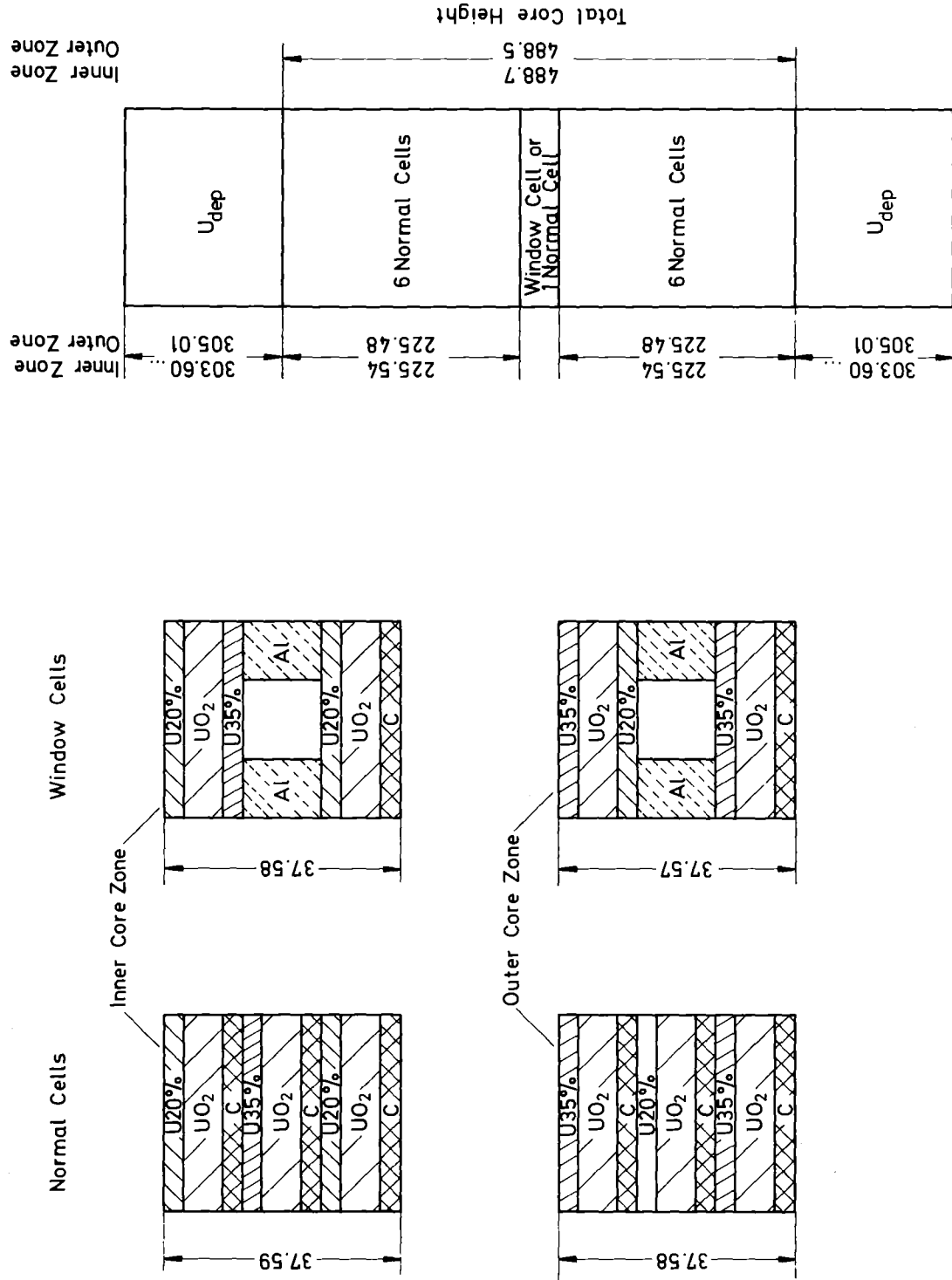
Fig.1 Core Cells and Element Loading Schemes of SNEAK-10

Total Height of Core Portion

Outer Zone
Inner Zone

490.31
490.93

| U_{dep} | 15x Normal Cell | 1x Rest Cell | U_{dep} |

303.84
471.45
472.05
303.84

Outer Zone
Inner Zone

Rest Cell

Normal Cell

Inner Core Zone

Outer Core Zone

U20% / C / Unat / Al2O3 / U35% / C

U35% / Al2O3 / UO2 / U20% / Al2O3

U20% / C / Unat / Al2O3 / U35% / C / Unat / Al2O3 / U20% / C

U35% / Al2O3 / UO2 / U35% / Al2O3 / UO2 / U20% / C

18.88
18.86
31.47
31.43
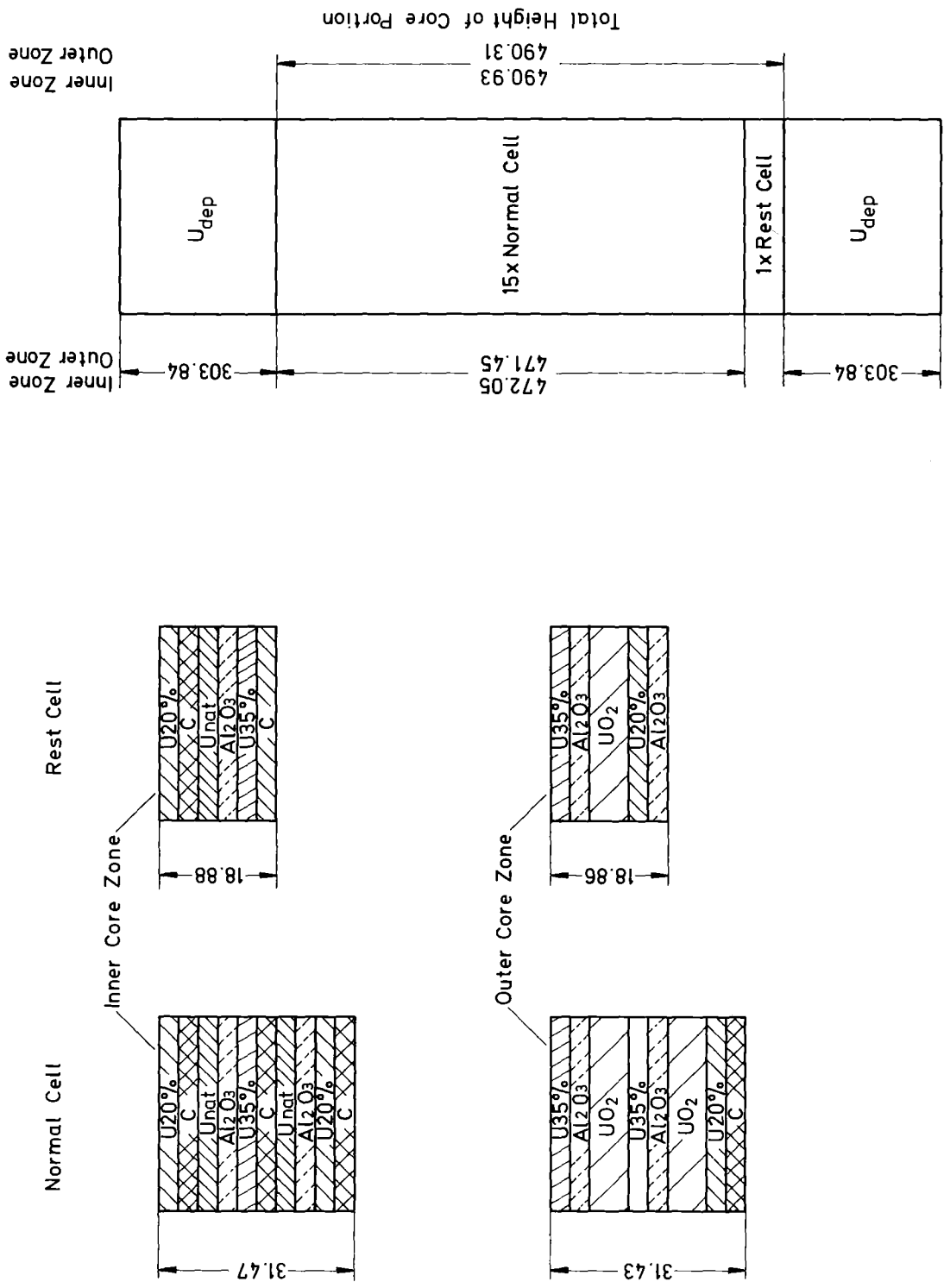
Fig. 2 Cells and Loading Schemes of Shim Rods in SNEAK-10
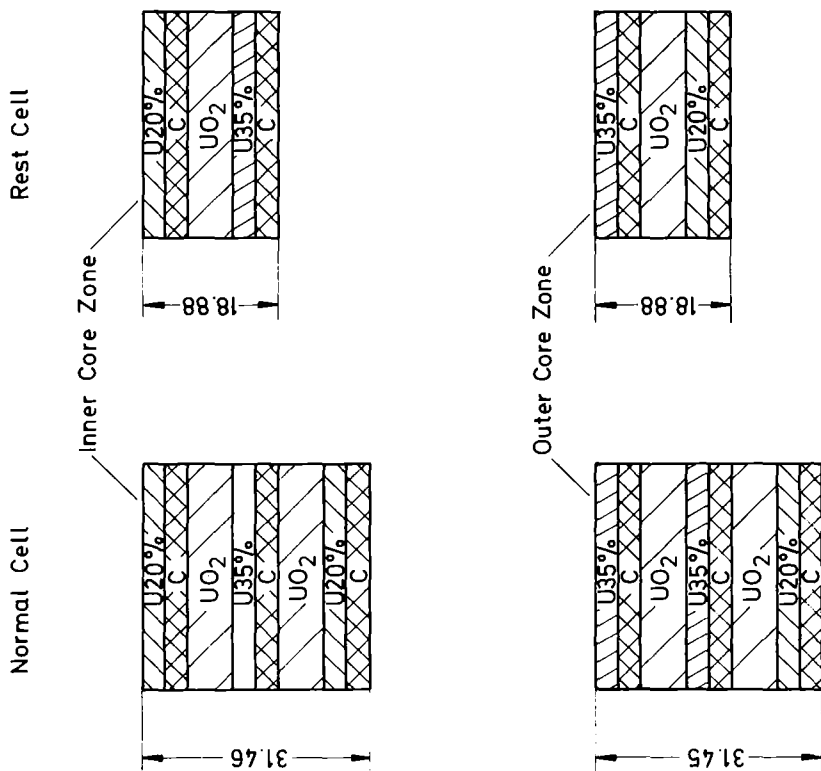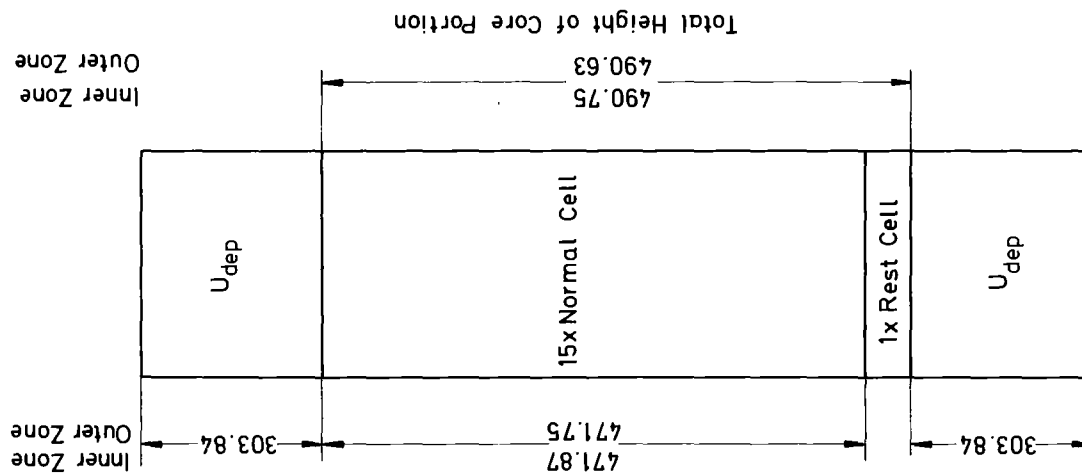
Fig. 3 Cells and Loading Schemes of Safety Rods in SNEAK-10
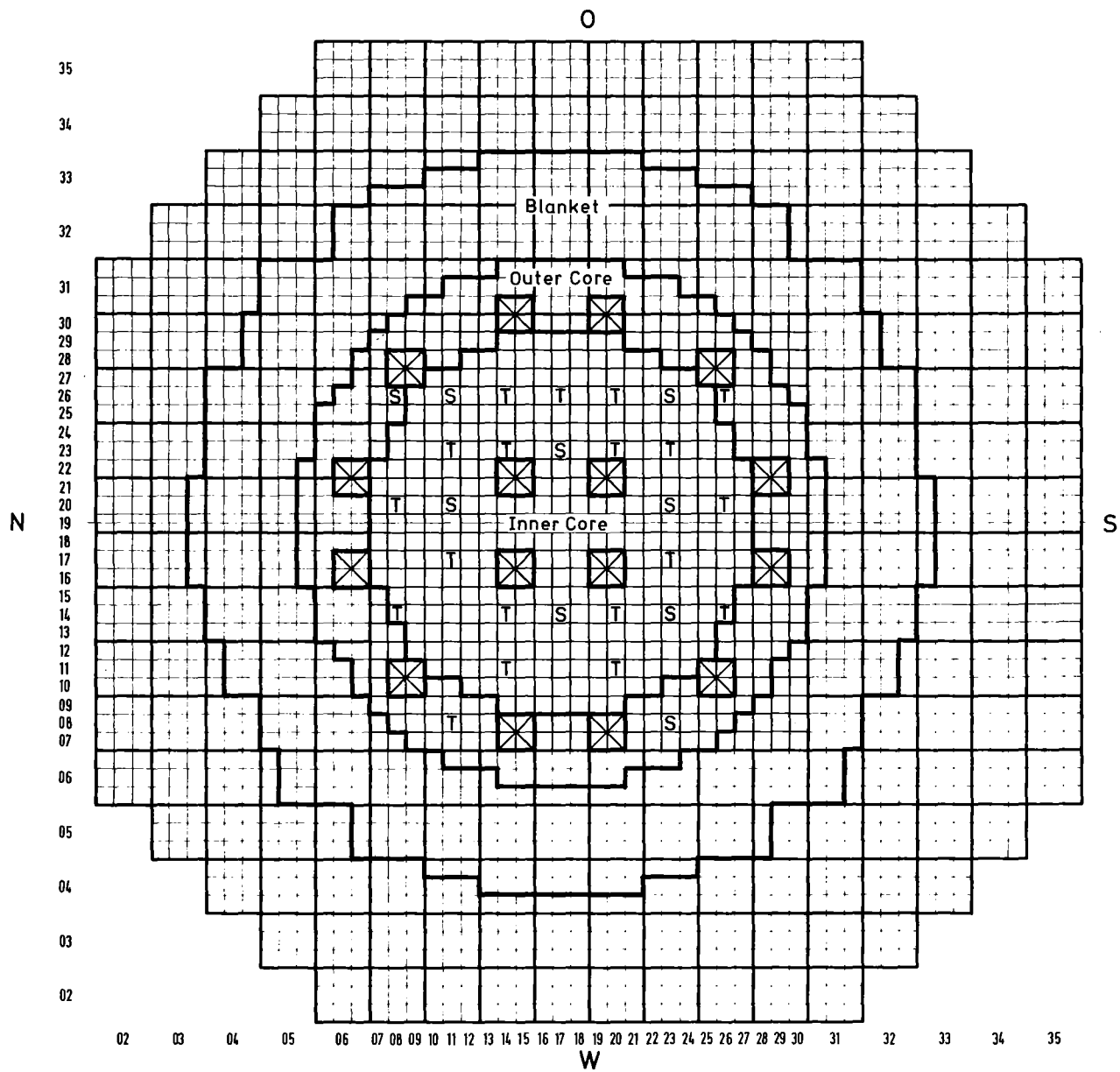
Fig. 4   Horizontal Cross Section of Critical Core
SNEAK-10-A

T   SNEAK shim rod

S   SNEAK safety rod

⊠   Simulated control rod (Na-follower)
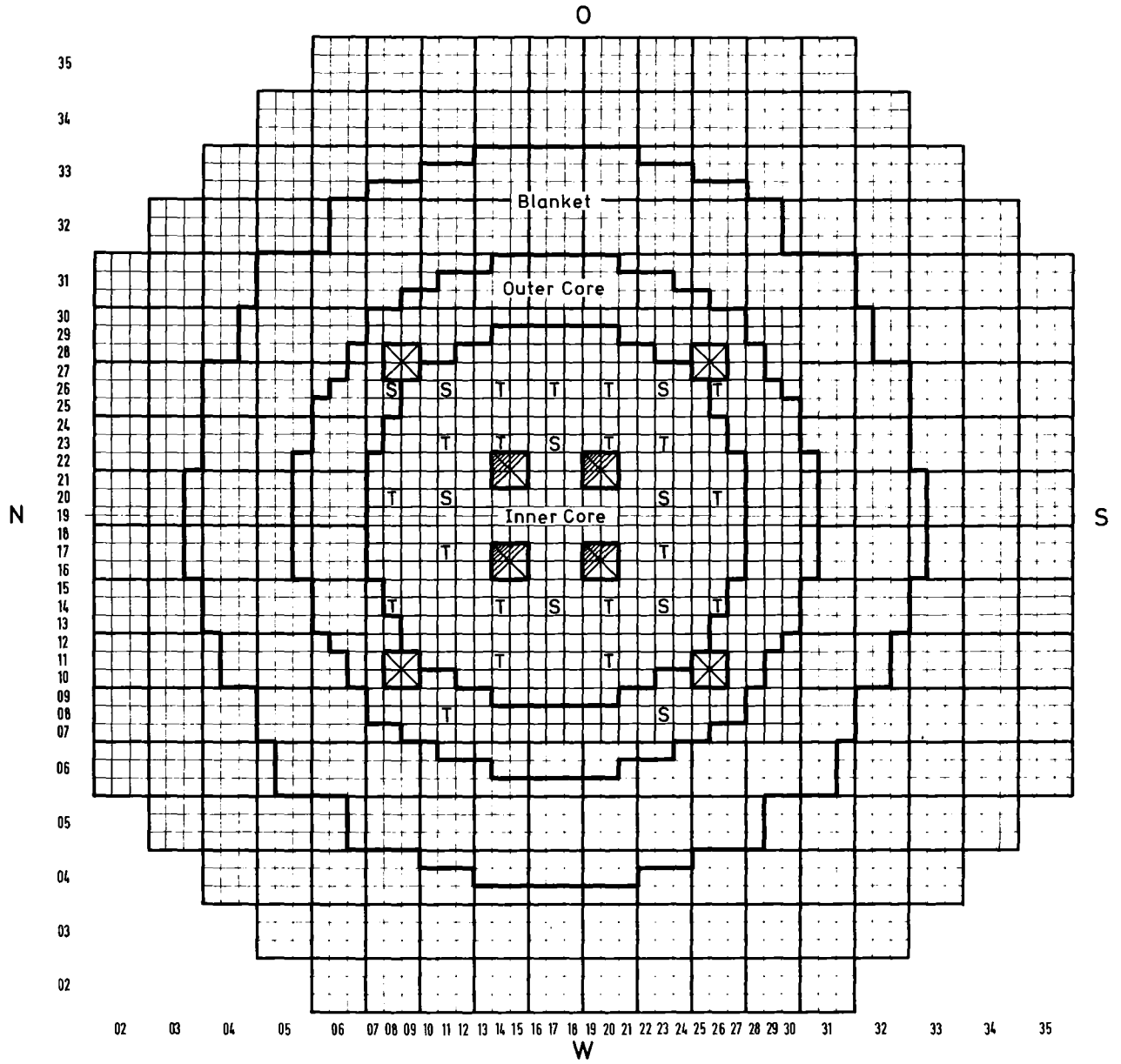
Fig. 5 Horizontal Cross Section of Critical Core
SNEAK-10-B

T   SNEAK shim rod

S   SNEAK safety rod

Simulated control rod

Na- follower

Absorber inserted to
5cm above core midplane
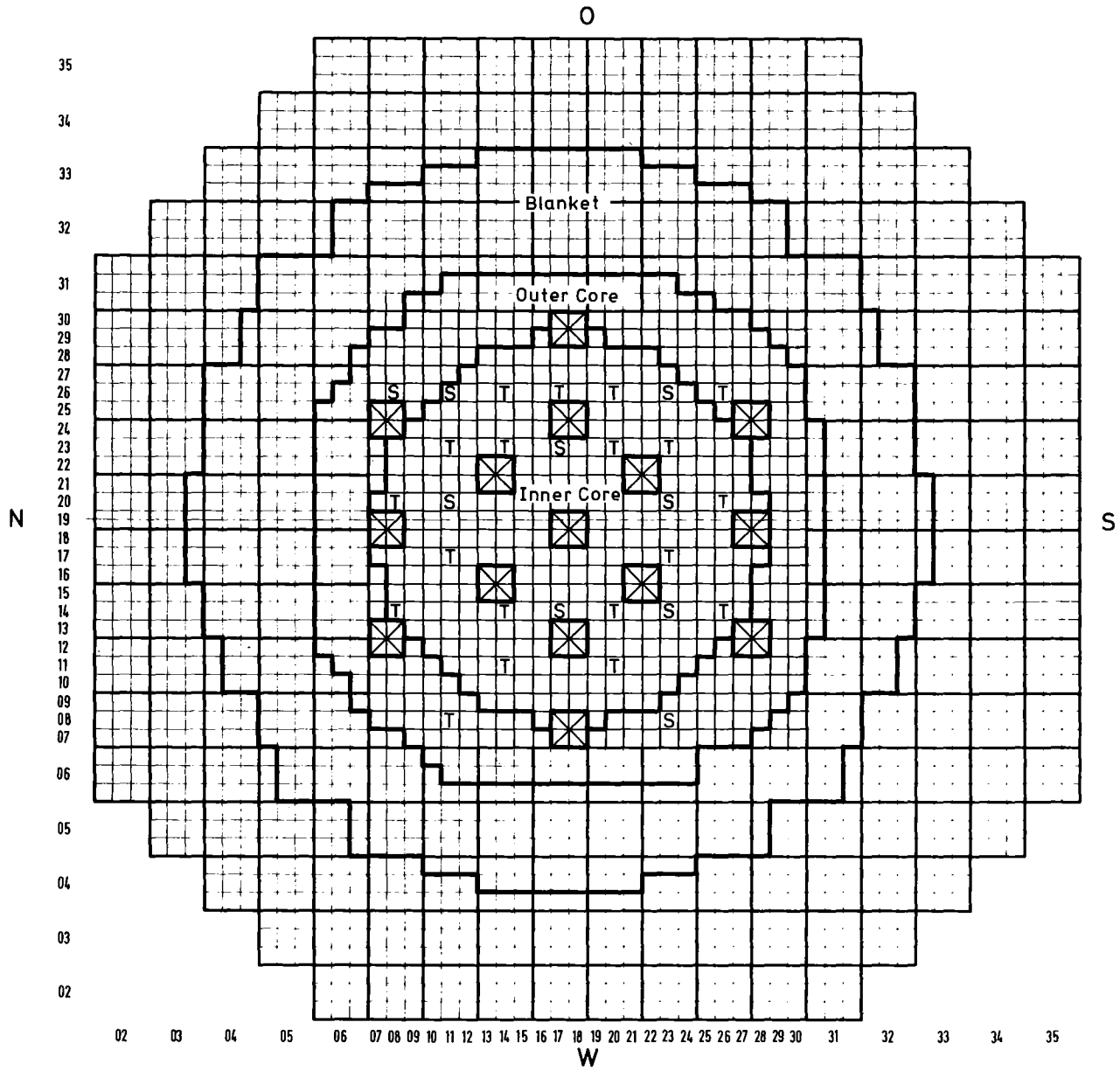
Fig. 6 Horizontal Cross Section of Critical Core
SNEAK-10-C

T   SNEAK shim rod

S   SNEAK safety rod

⊠   Simulated control rod (Na-follower)
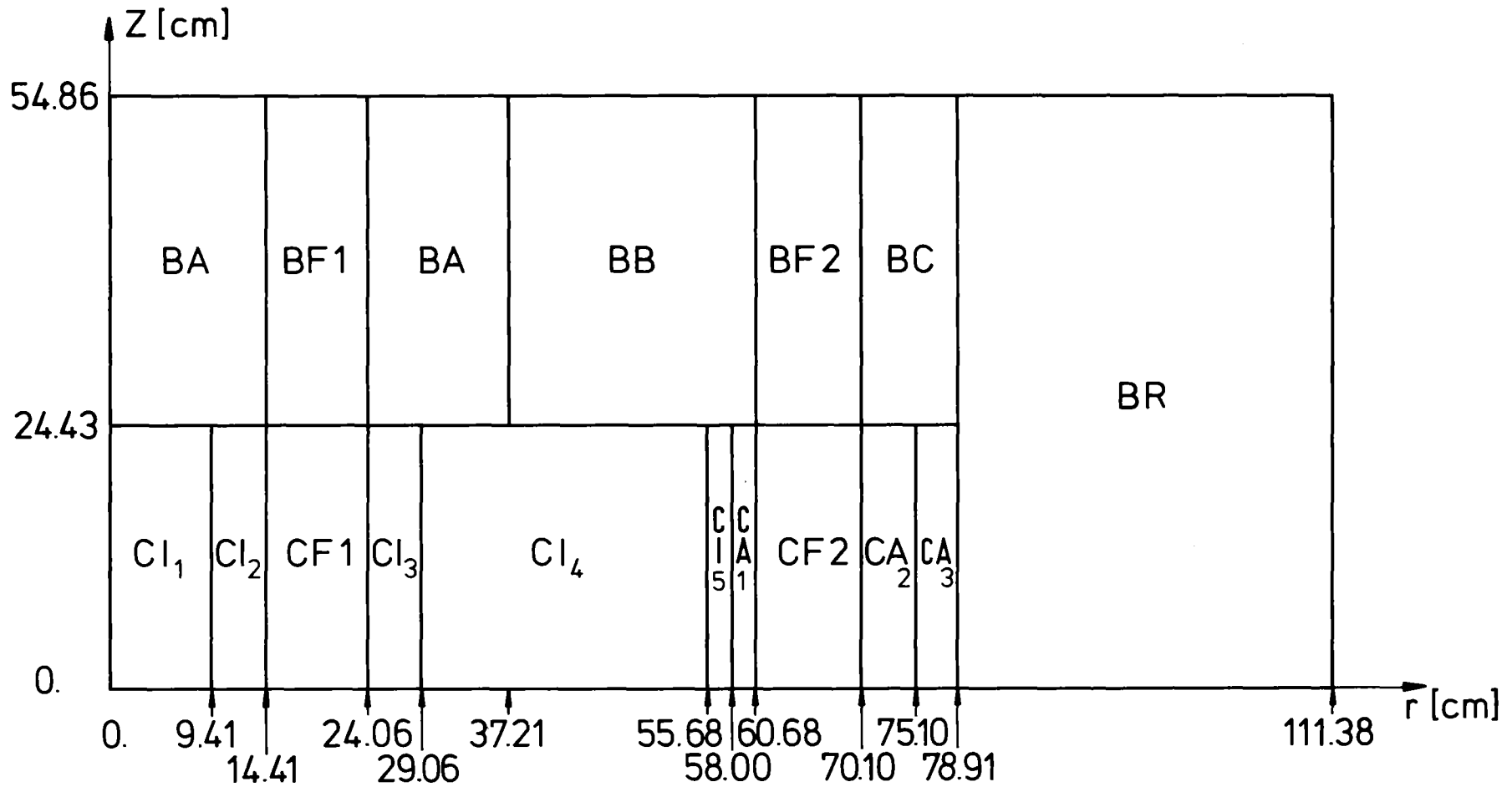
Fig.7 Geometrical Model for RZ–Diffusion Calculation in SNEAK-10-A
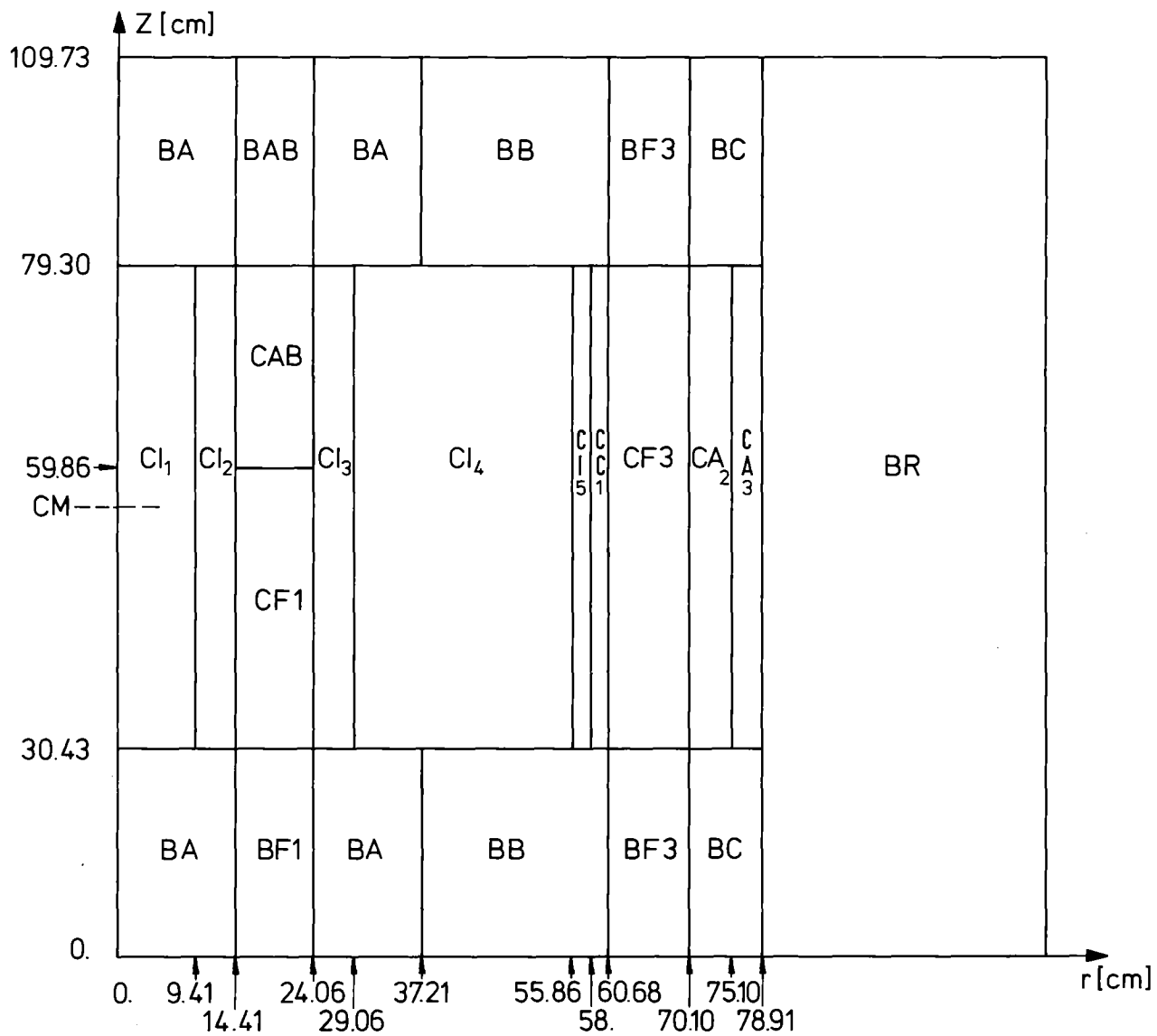
Fig.8 Geometrical Model for RZ-Diffusion Calculation in SNEAK-10-B
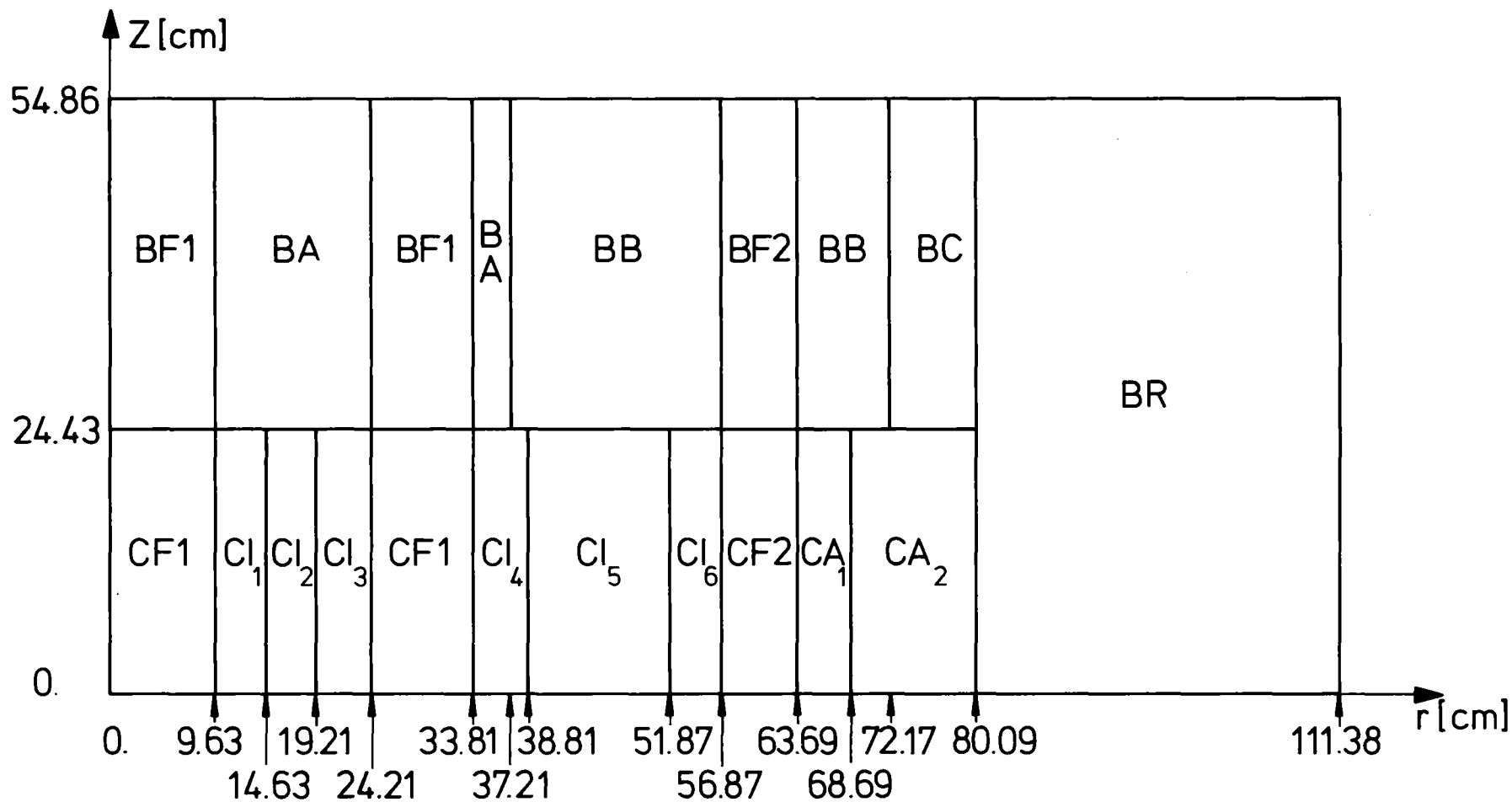
Fig. 9 Geometrical Model for RZ-Diffusion Calculation in SNEAK-10-C
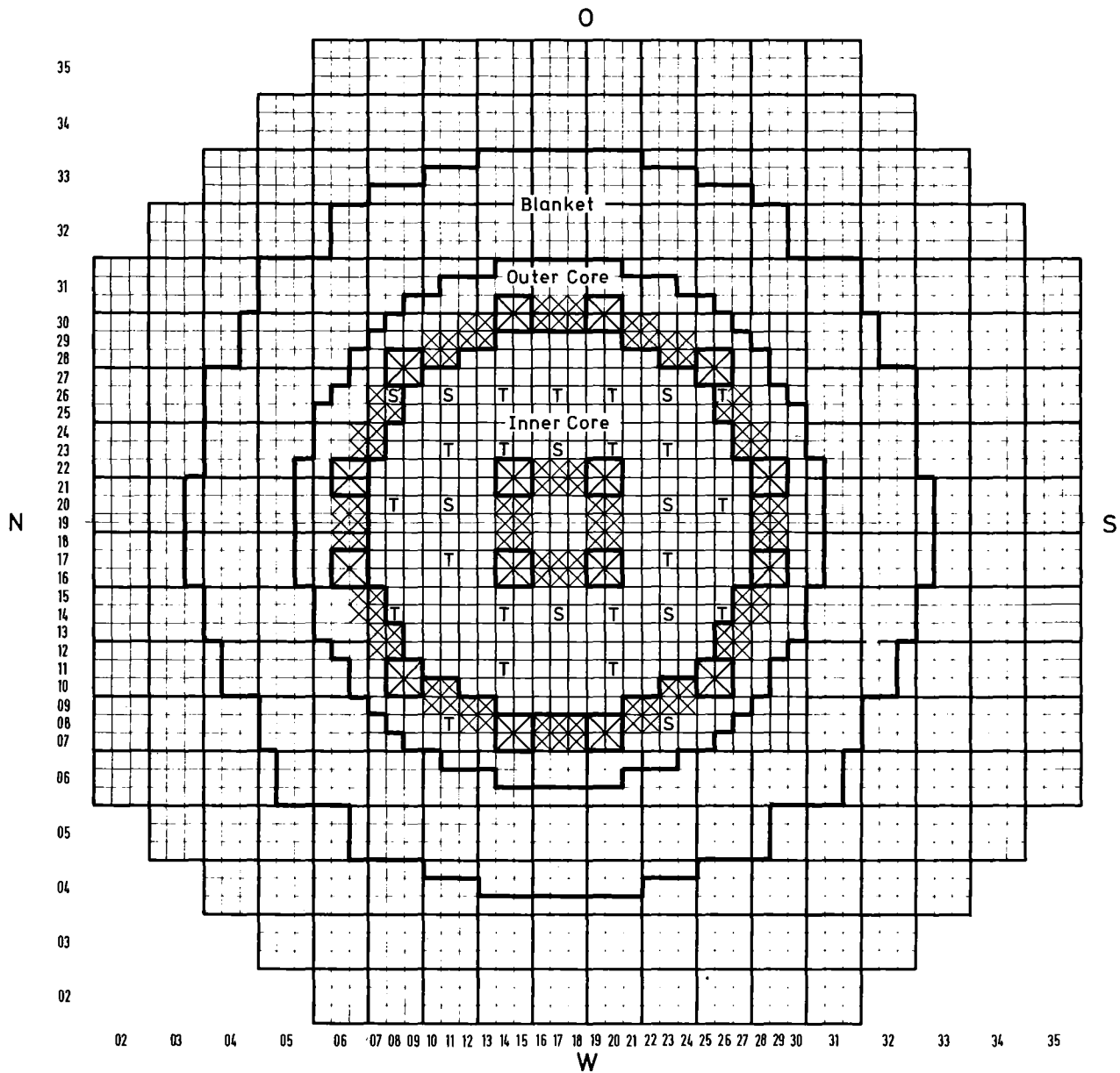
Fig. 10 Geometrical Model of basic Diffusion
Calculation (DIXY-RZ) in SNEAK-10-A
and SNEAK-10-B

Followers and absorbers were smeared into
rings with core elements according to the
number contained in the shaded areas

T   SNEAK shim rod

S   SNEAK safety rod

⊠   Simulated control rod
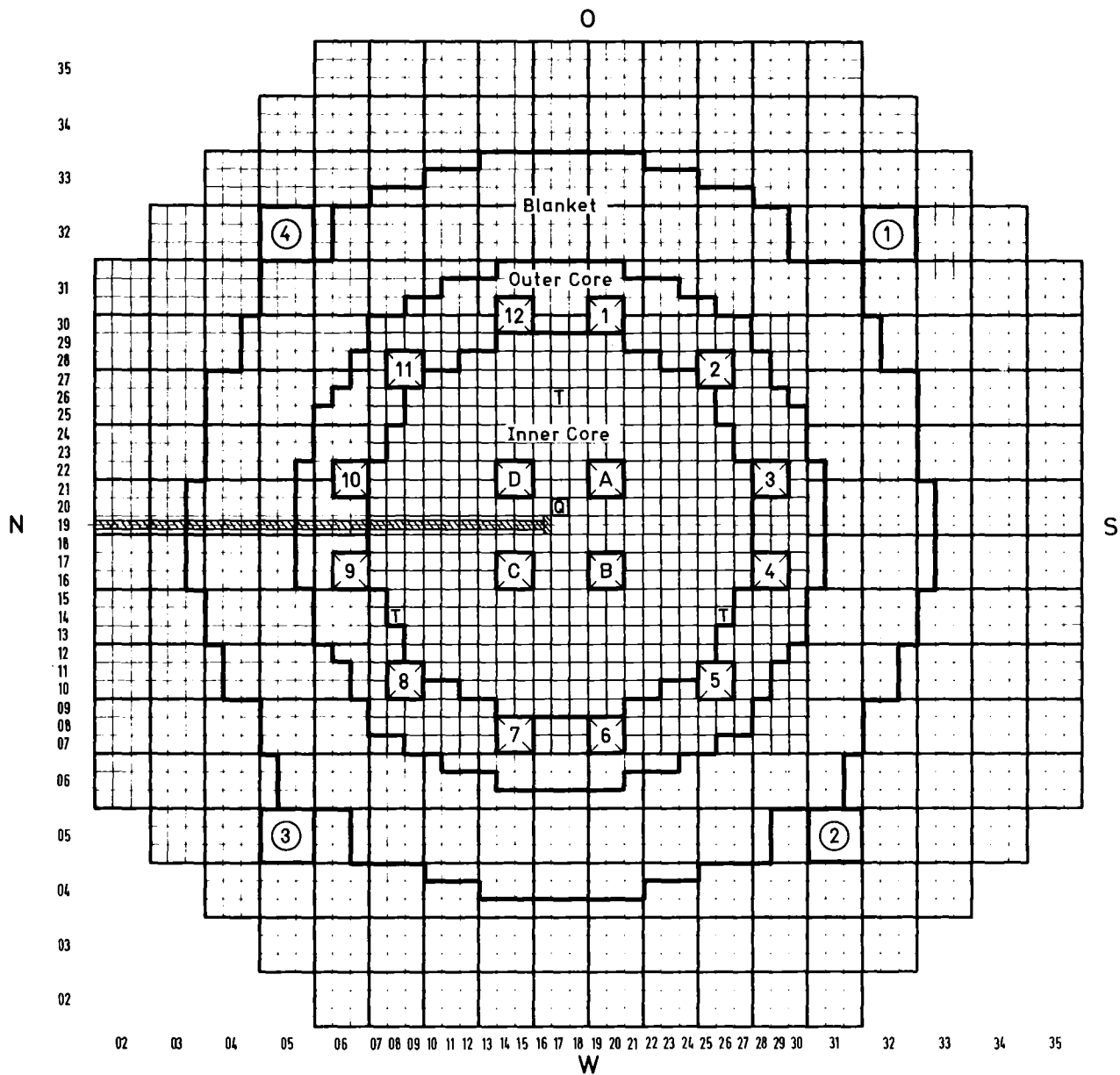
Fig. 11 SNEAK-10-A modified for subcritical
Control Rod Measurements

T SNEAK shim rods used to establish
subcritical calibration point

Q Location of ^{252}Cf-neutron source

[1] Simulated control rods

① Detector Locations

Neutron generator drift tube and target
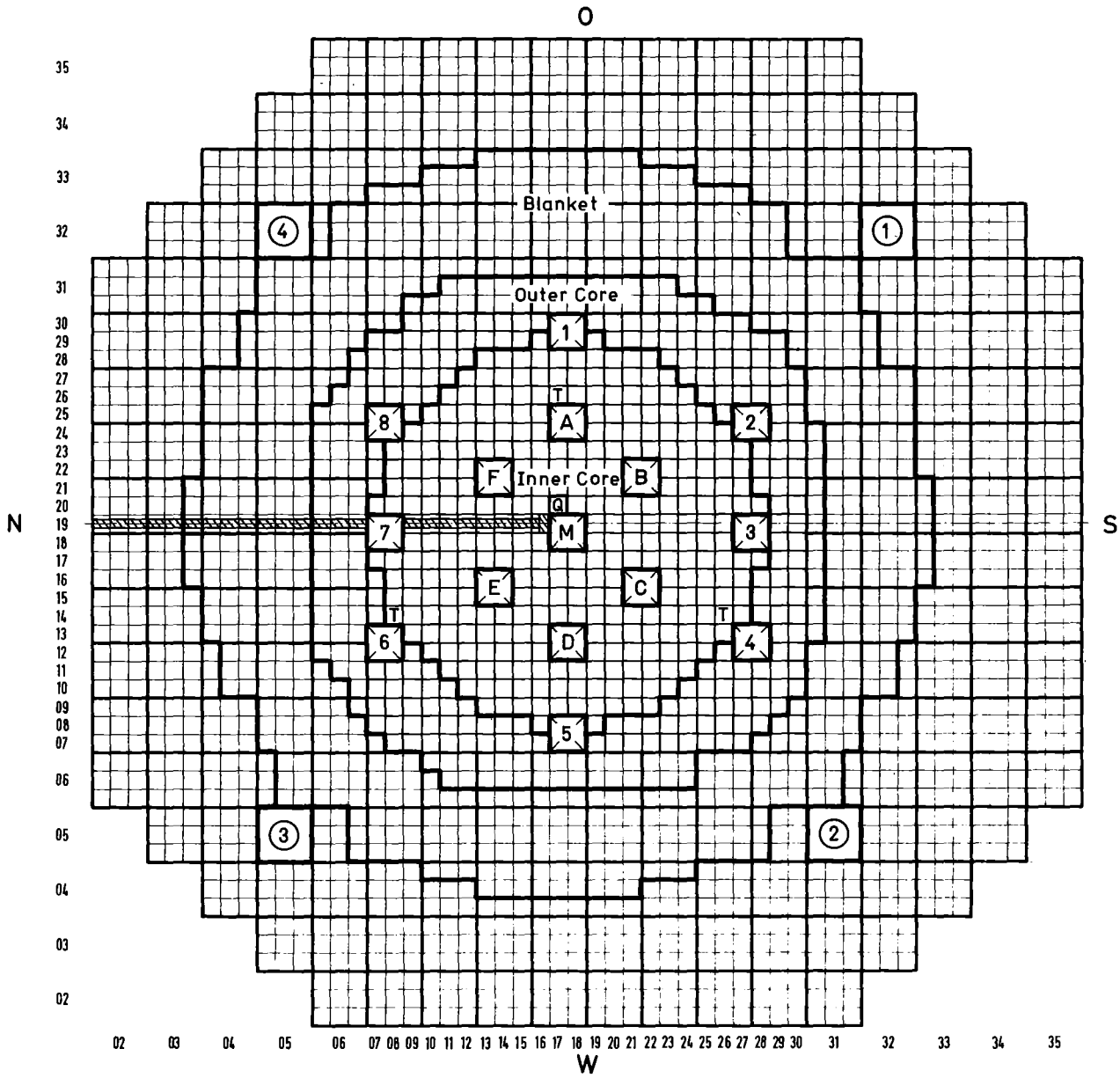
Fig. 12 SNEAK-10-C modified for subcritical
Control Rod Measurements

T   SNEAK shim rods used to establish
subcritical calibration point

Q   Location of ^{252}Cf-neutron source

[1]   Simulated control rods

①   Detector Locations

▨   Neutron generator drift tube and target

Fig. 13 Pile Oscillator Cells and Element Configuration in SNEAK-10-A

Pile oscillator cells

Type 1

| U20% |
| C |
| UO₂ |
| U35% |
| C |
| UO₂ |
| U20% |
| C |
| U20% |
| C |
| UO₂ |
| U35% |

Type 1a

| U20% |
| C |
| UO₂ |
| U35% |
| UO₂ |
| Al40% | ←— Sample position
| U20% |
| C |
| U20% |
| C |
| UO₂ |
| U35% |

Type 2

| C |
| UO₂ |
| U20% |
| C |
| U20% |
| C |
| UO₂ |
| U35% |
| C |
| UO₂ |
| U20% |
| C |

Normal core cell

| U20% |
| UO₂ |
| C |
| U35% |
| UO₂ |
| C |
| U20% |
| UO₂ |
| C |

Cell type	Partition	
1	1	
2	2	
1	3	
2	4	
2	16	
1a	17	Sample cell
2	18	
1		
2		2 x SS 25%
1		
2		

Element loading scheme

etc

- 95 -

- 96 -
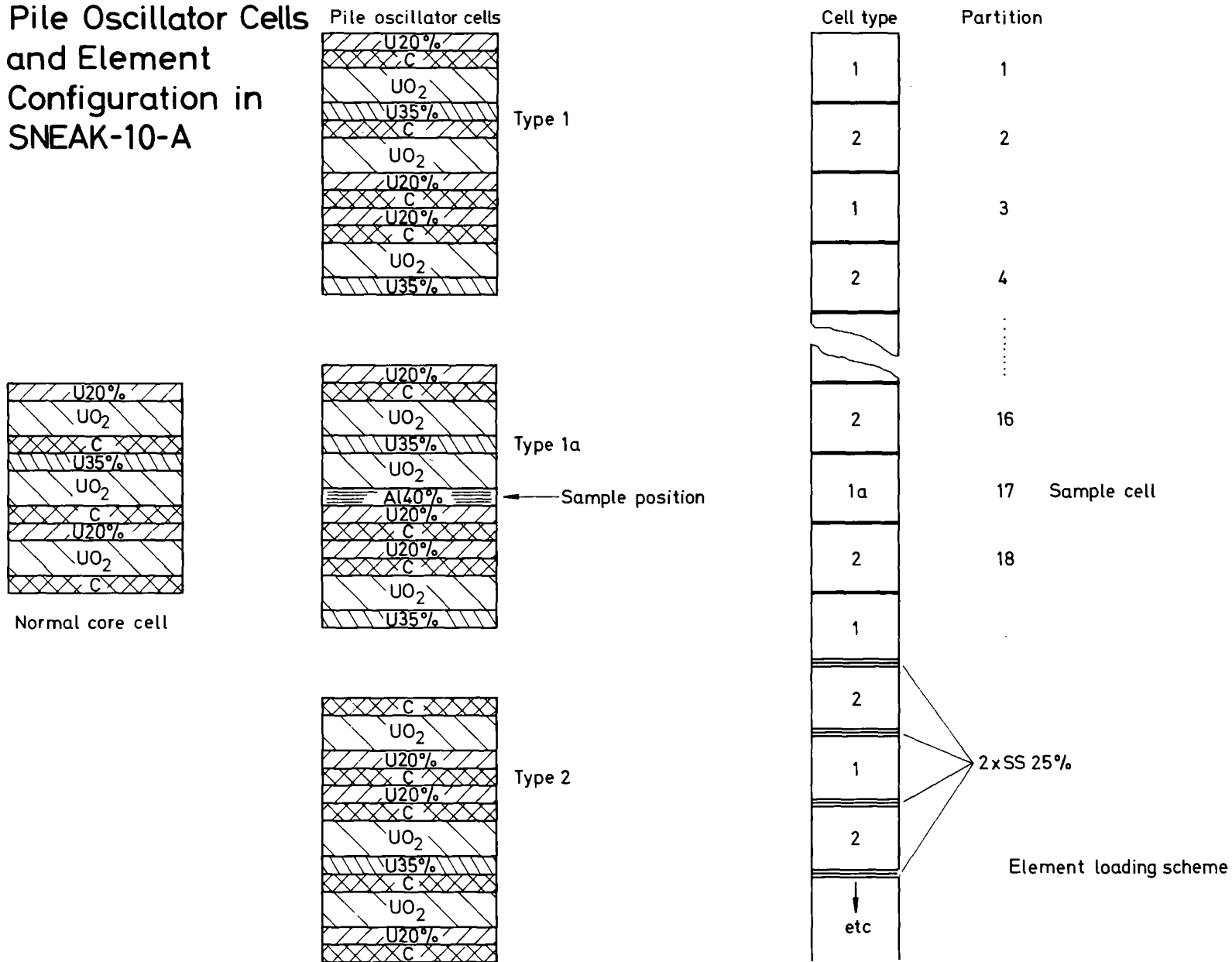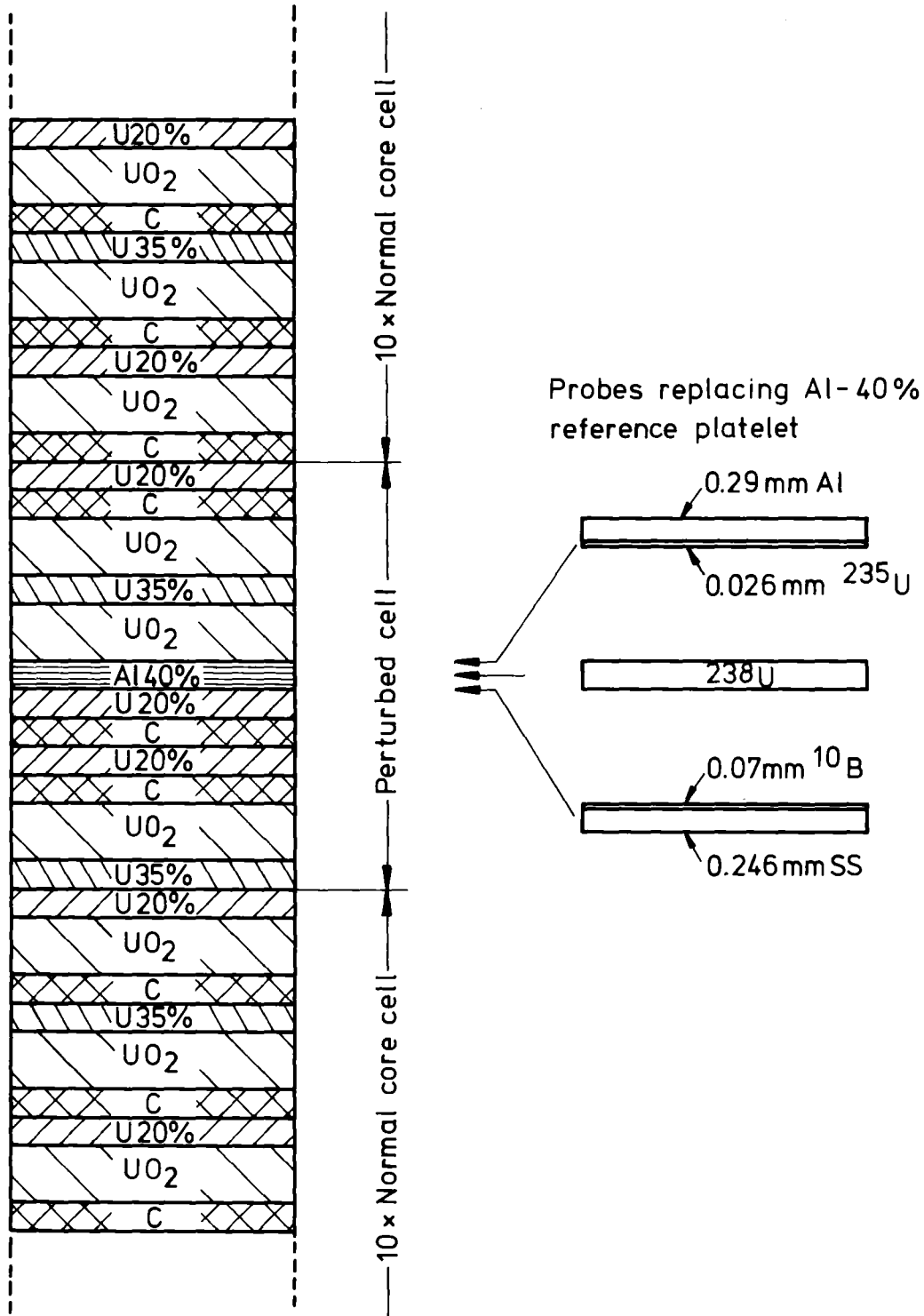
Fig.14 Geometrical Model of heterogeneous
Material Worth Calculations (KAPER)
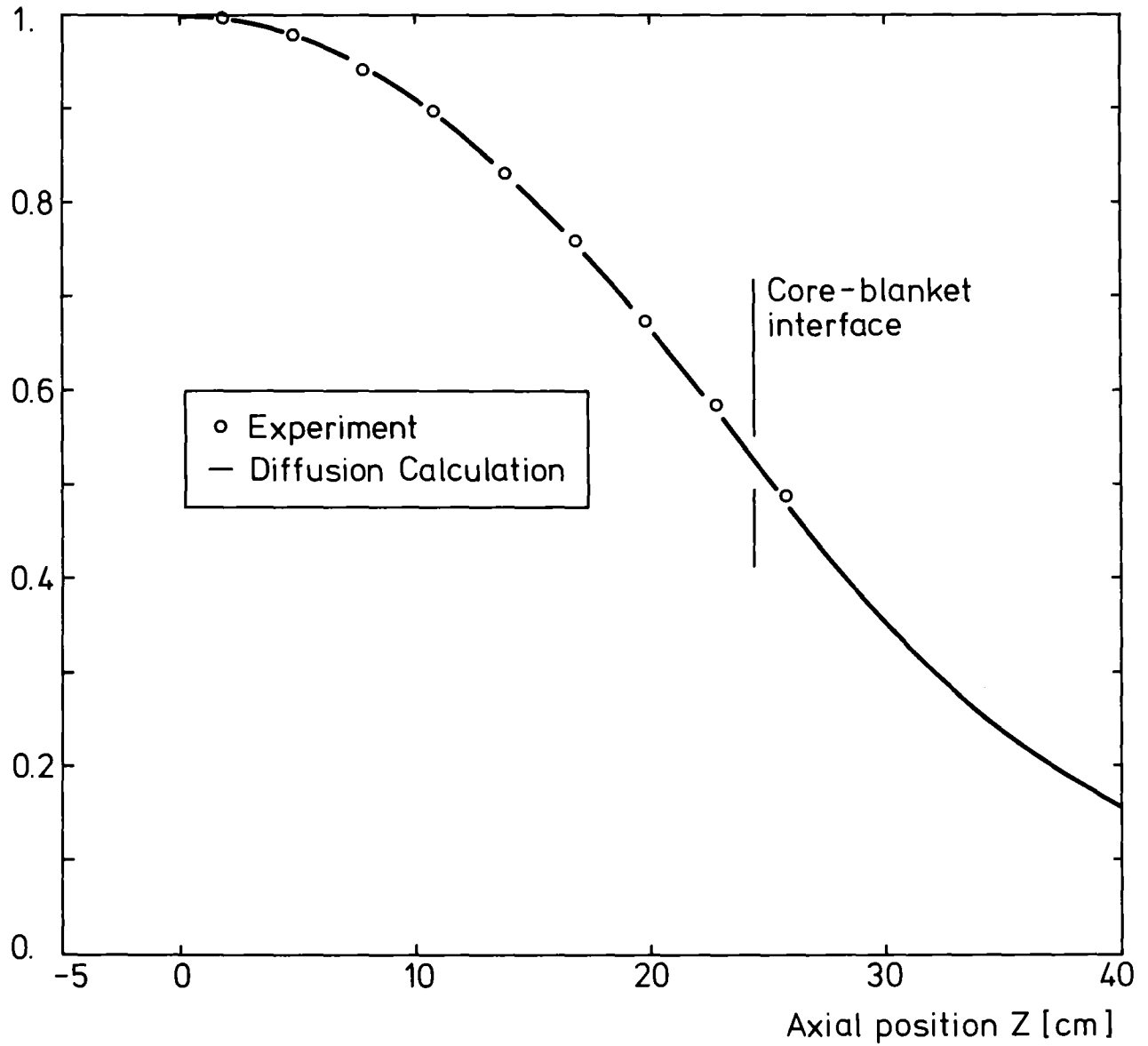
Fig.15 Axial Importance Traverse in the Core Centre of SNEAK-10-A
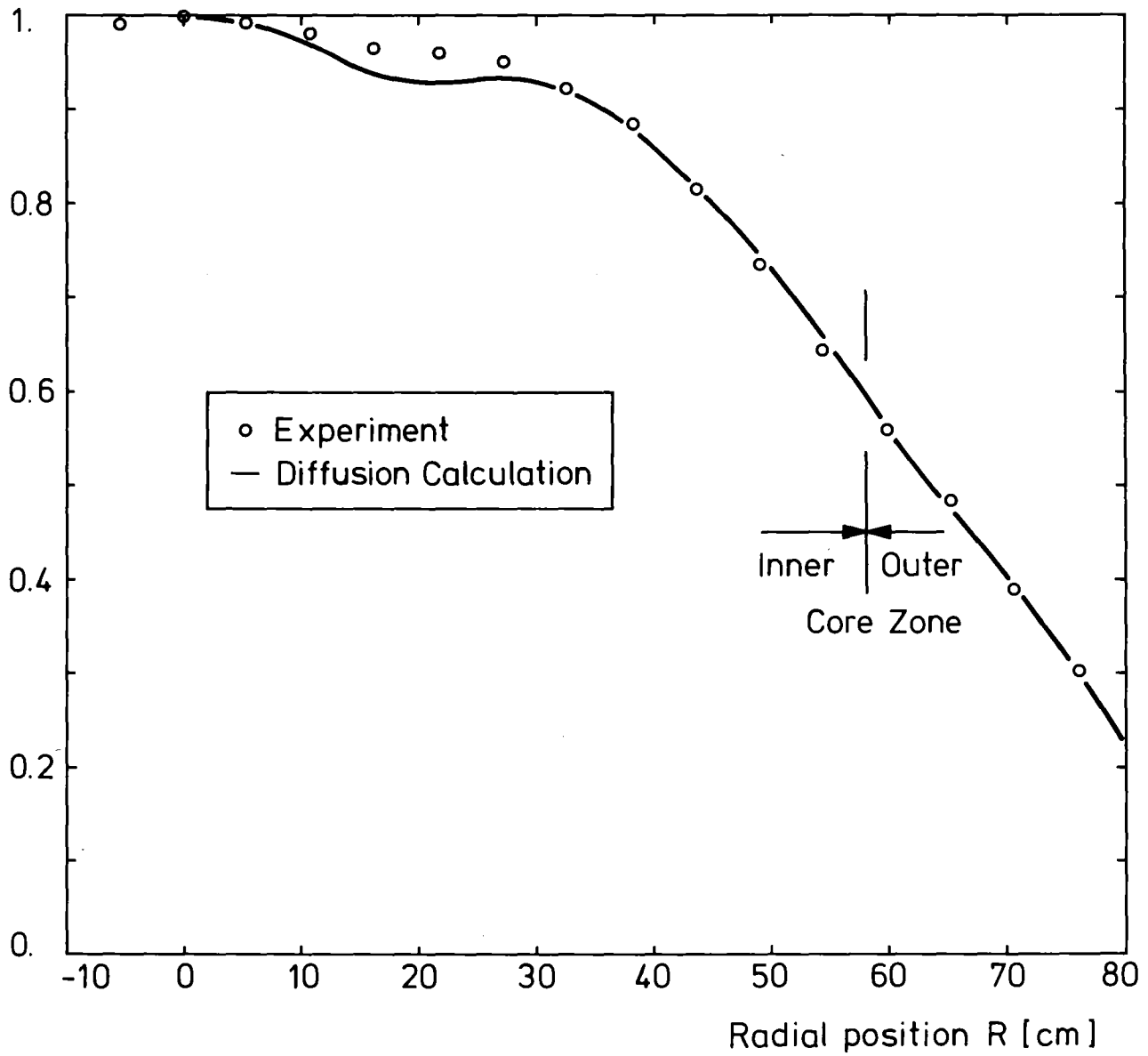
Fig. 16 Radial Importance Traverse in SNEAK-10-A

Inner Core Unit Cell   Outer Core Unit Cell

| U-20% |
| UO₂ |
| C |
| U-35% |
| UO₂ |
| C |
| U-20% |
| UO₂ |
| C |

$U-20\%$ ... text within boxes:

Inner Core Unit Cell:
U-20%
UO₂
C
U-35%
UO₂ — core midplane
C — foil position — 2‰
U-20%
UO₂
C

macroscopic fission
rate cell average

1.0   1.05   1.10

$<\sigma_{f8}\phi>/_{Min \{<\sigma_{f8}\phi>\}}$

Outer Core Unit Cell:
U-35%
UO₂
C — 3‰ — foil position
U-20%
UO₂ — core midplane
C
U-35%
UO₂
C

macroscopic fission
rate cell average

1.0   1.05   1.10

$<\sigma_{f8}\phi>/_{Min \{<\sigma_{f8}\phi>\}}$

- 99 -
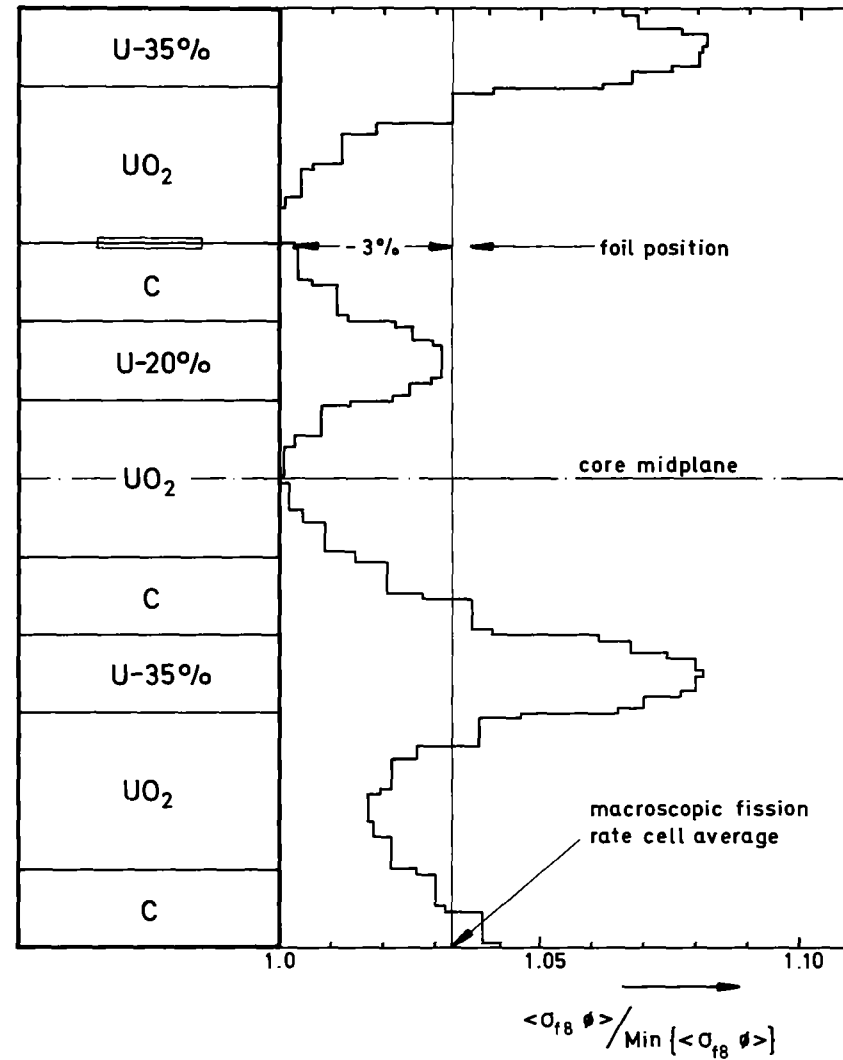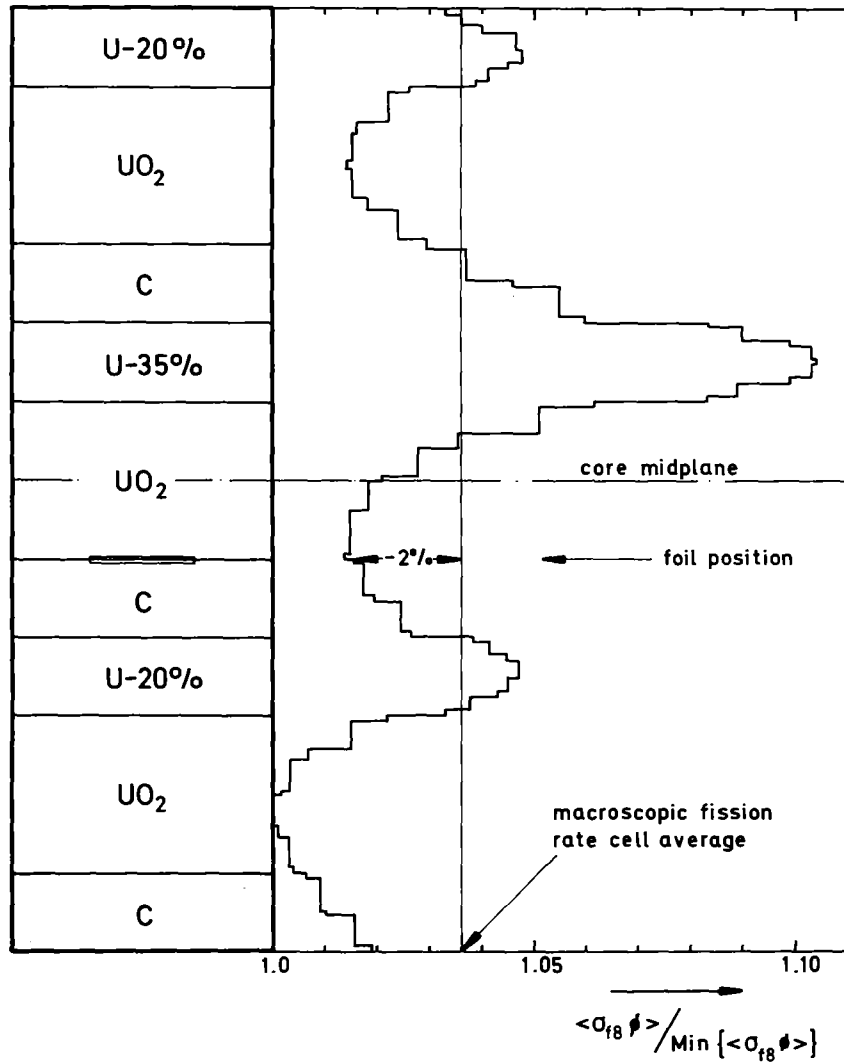
Fig.17 Calculated Fission Rate Fine Structures of ^{238}U and Activation Foil Positions in the Core Unit
Cells of SNEAK-10
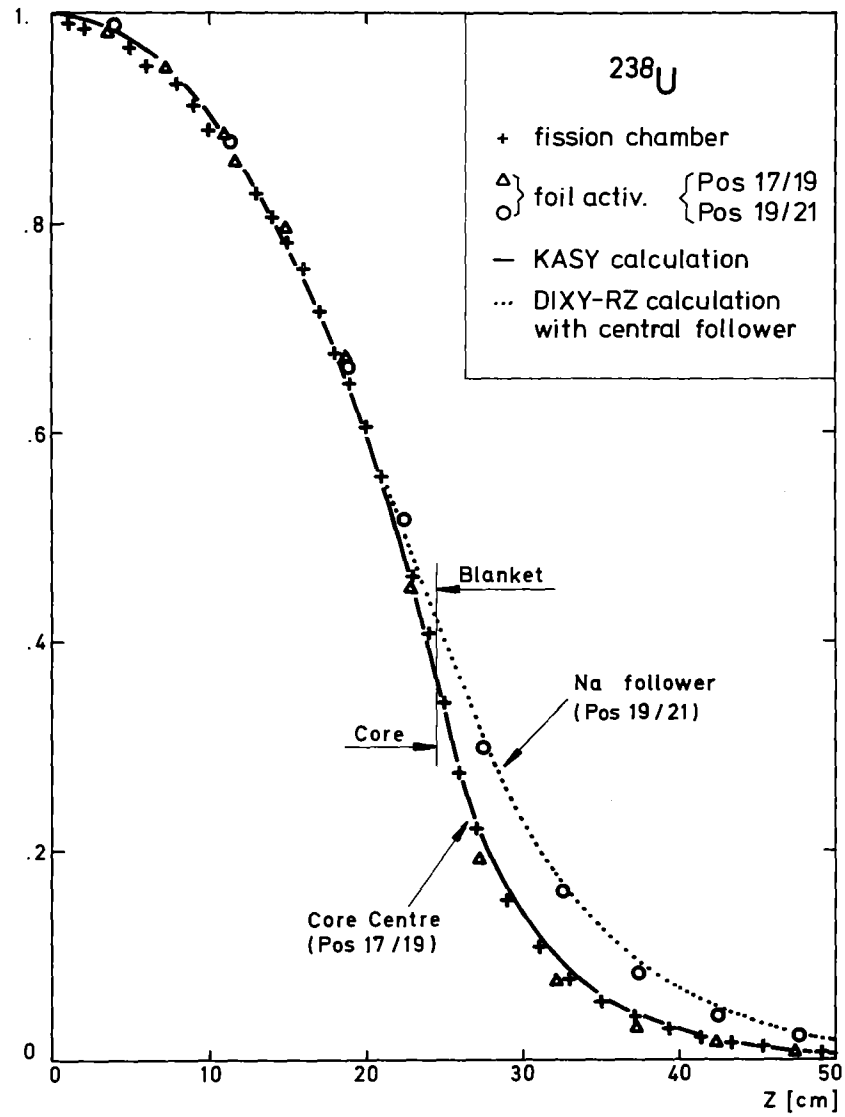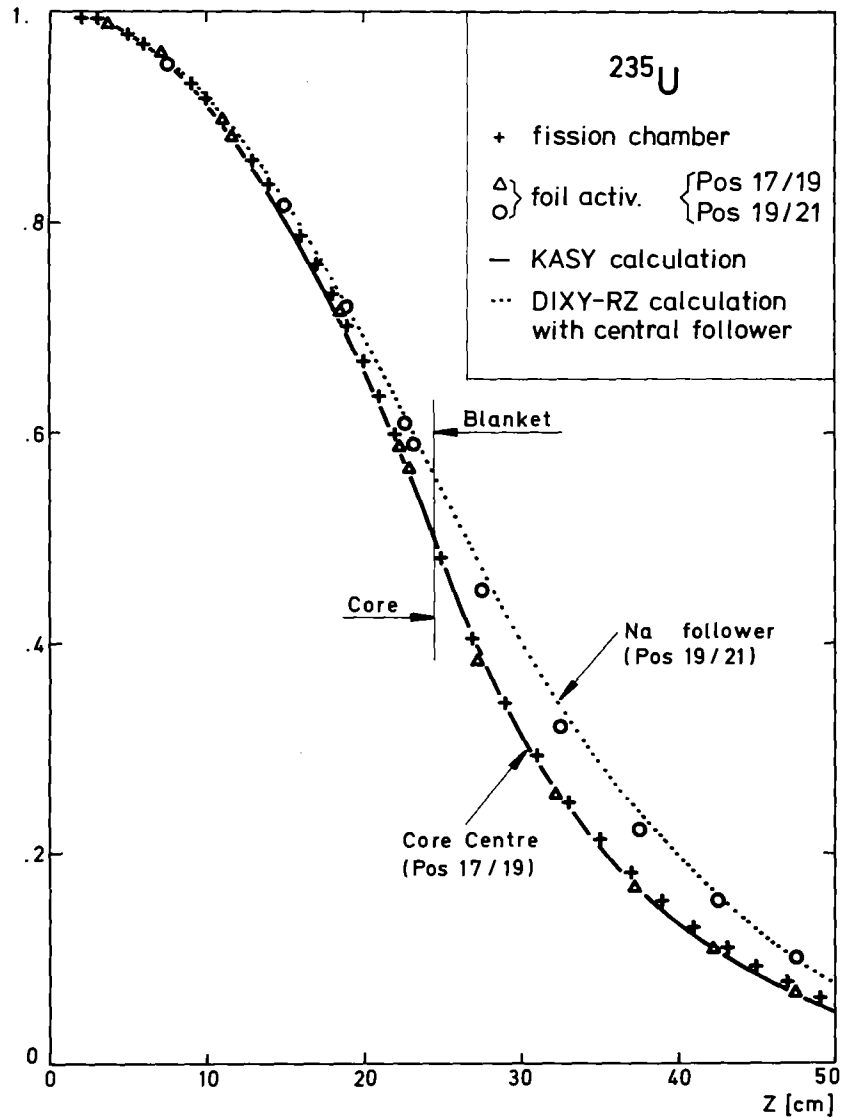
Fig.18 Comparison of Axial Fission Rate Traverses in Different Positions of SNEAK-10-A

Δ fission chamber Pos 19/20

+   "   "   Pos 27/19

— 3-dim synth. diffusion
        calculation

Rod insertion depth

Pos 19/20   Pos 27/19

Blanket

Core

Y

Outer Core   Blanket

Inner Core

27
25
23
21
19

17 19 21 23 25 27   X →

1.

.8

.6

.4

.2

0.

-50 -40 -30 -20 -10 0 10 20 30 40 50

Distance Z from core midplane [cm]
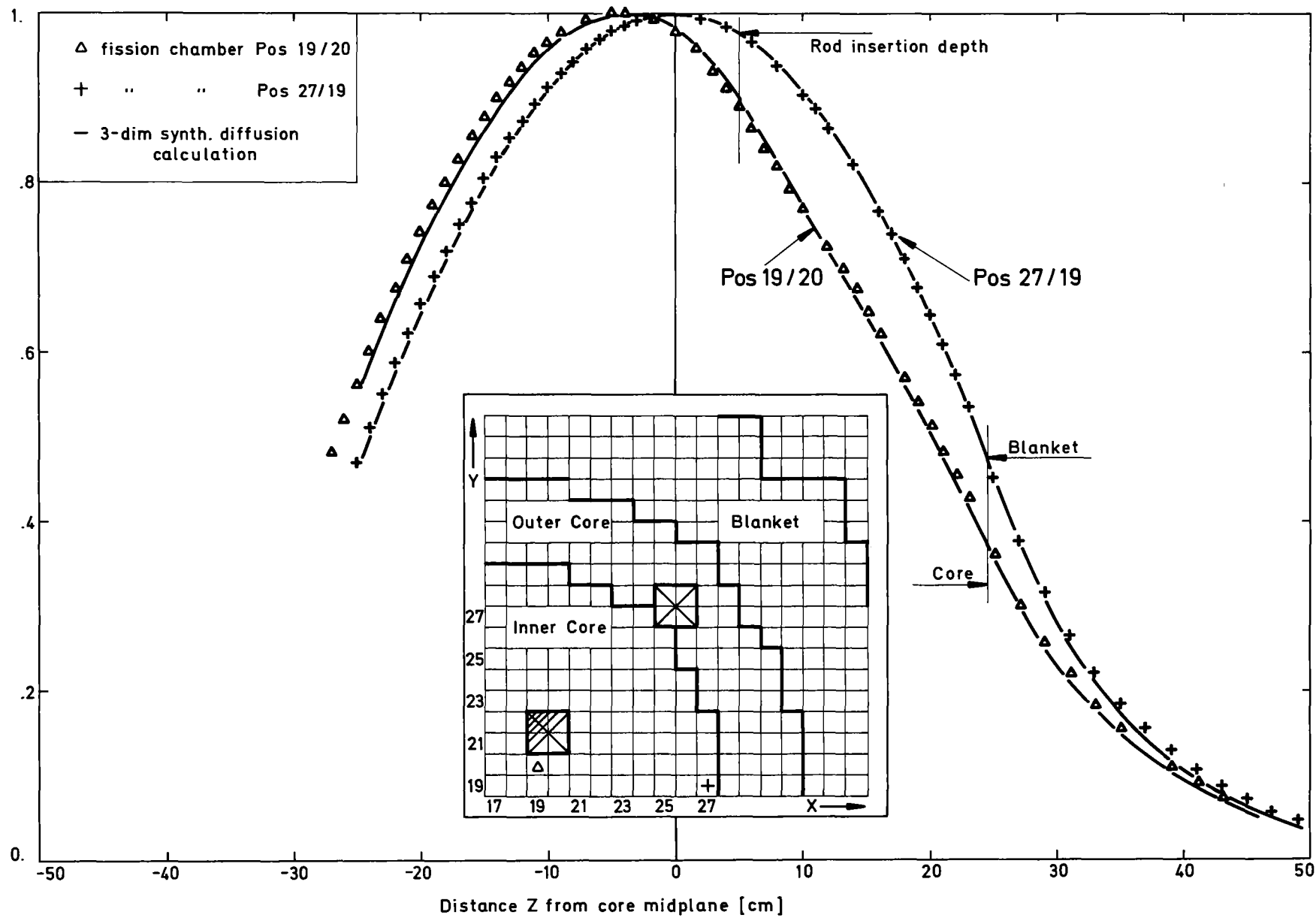
Fig. 19 Comparison of Axial Fission Rate Traverses of ^{235}U in Different Positions of SNEAK-10-B
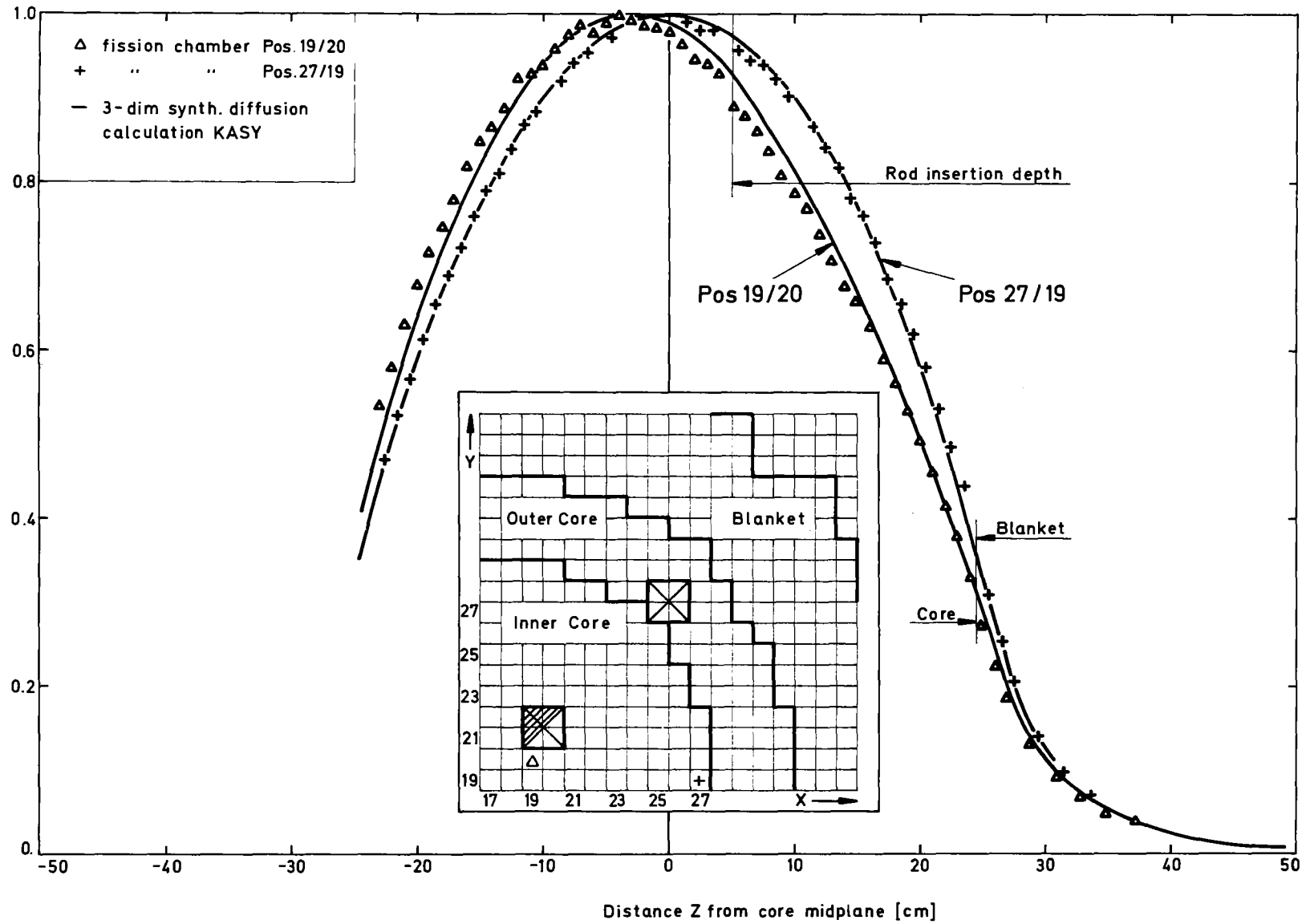
Fig. 20 Comparison of Axial Fission Rate Traverses of ^{238}U in Different Positions of SNEAK-10-B
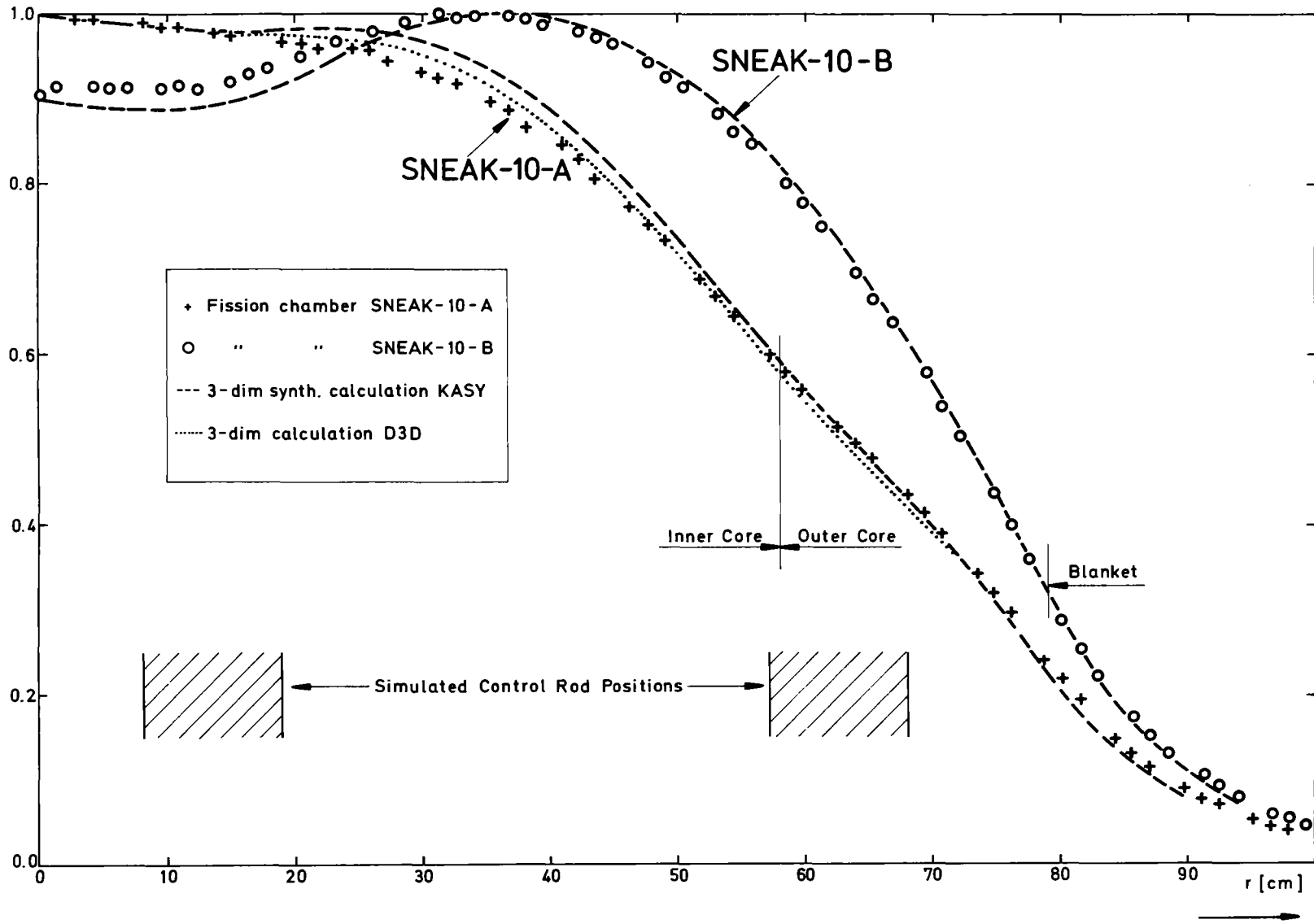
Fig. 21 Comparison of Radial Fission Rate Traverses of ^{235}U in SNEAK-10-A and SNEAK-10-B

(normalized to respective maximum value)
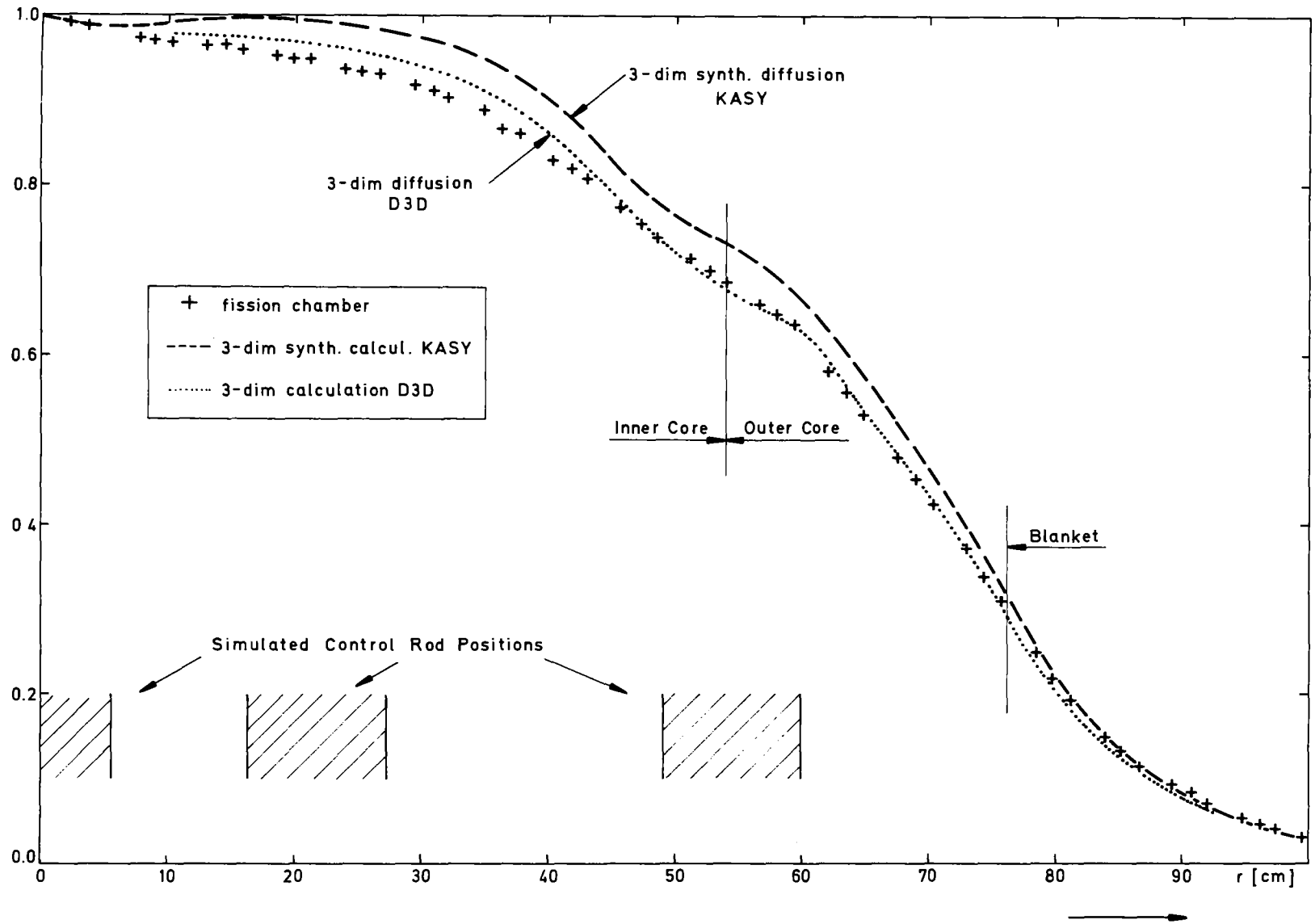
Fig. 22 Radial Fission Rate Traverse of ^{235}U in SNEAK-10-C

(normalized to maximum value)
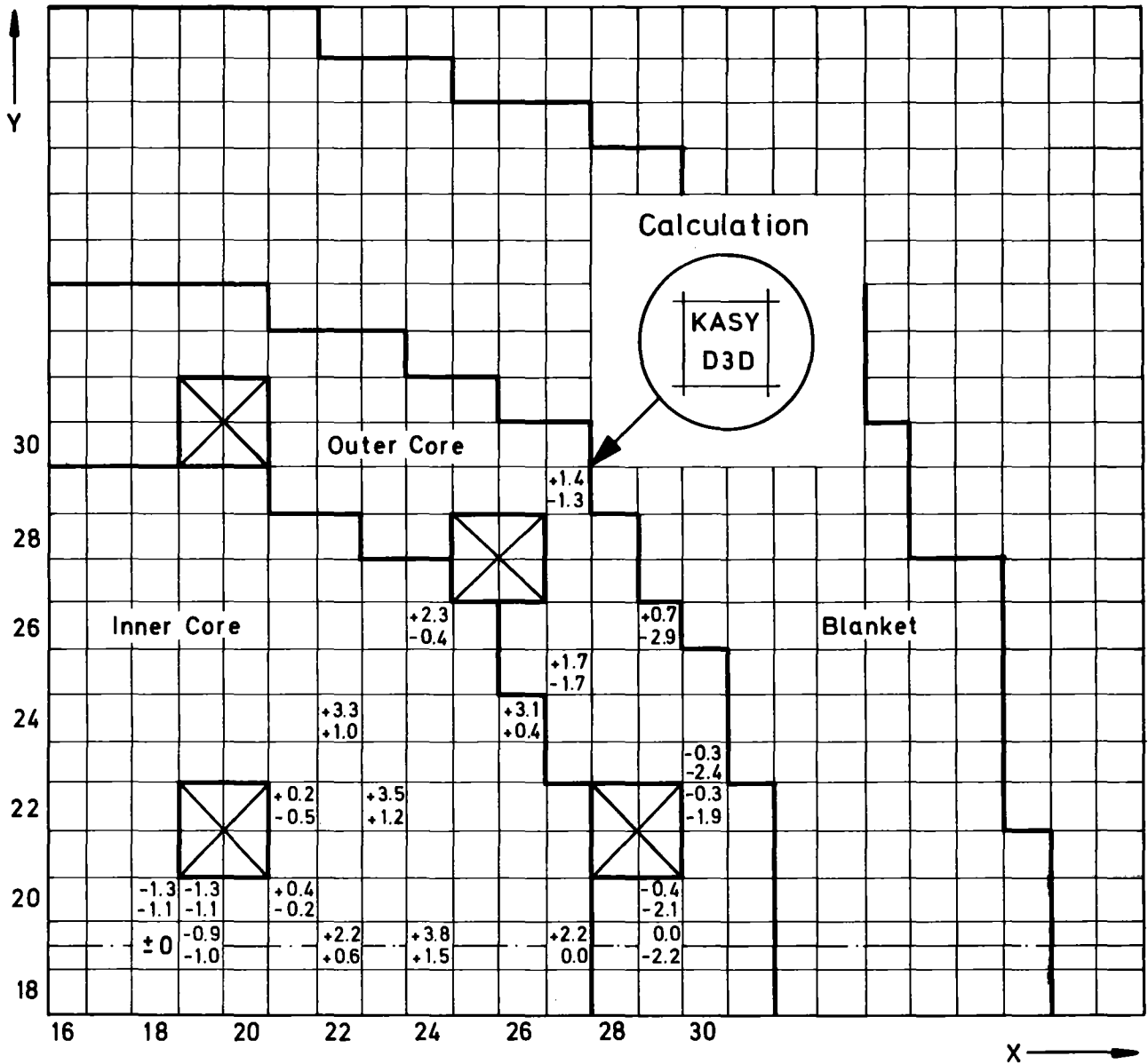
Fig. 23 Relative Deviations $\dfrac{C-E}{E}$ [%] of ^{235}U Fission Rates in the Core-midplane of SNEAK-10-A

Normalization point indicated by '±0'
Calculation : KASY, D3D
Experiment : Foil Activation
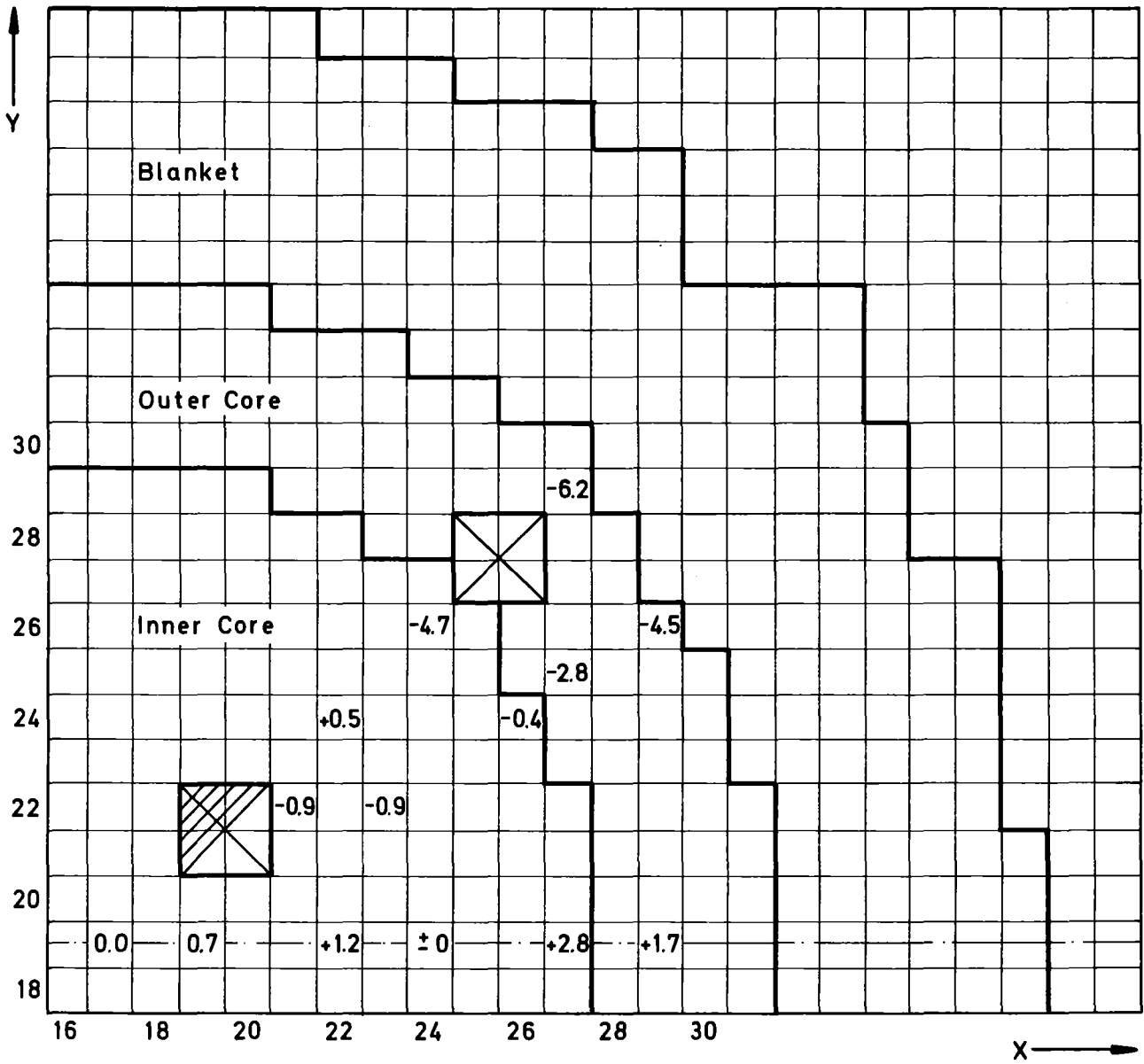
Fig. 24 Relative Deviations $\frac{C-E}{E}$ [%] of ^{235}U Fission
Rates in the Core-midplane of SNEAK-10-B

Normalization point indicated by '±0'
Calculation : KASY
Experiment : Foil Activation
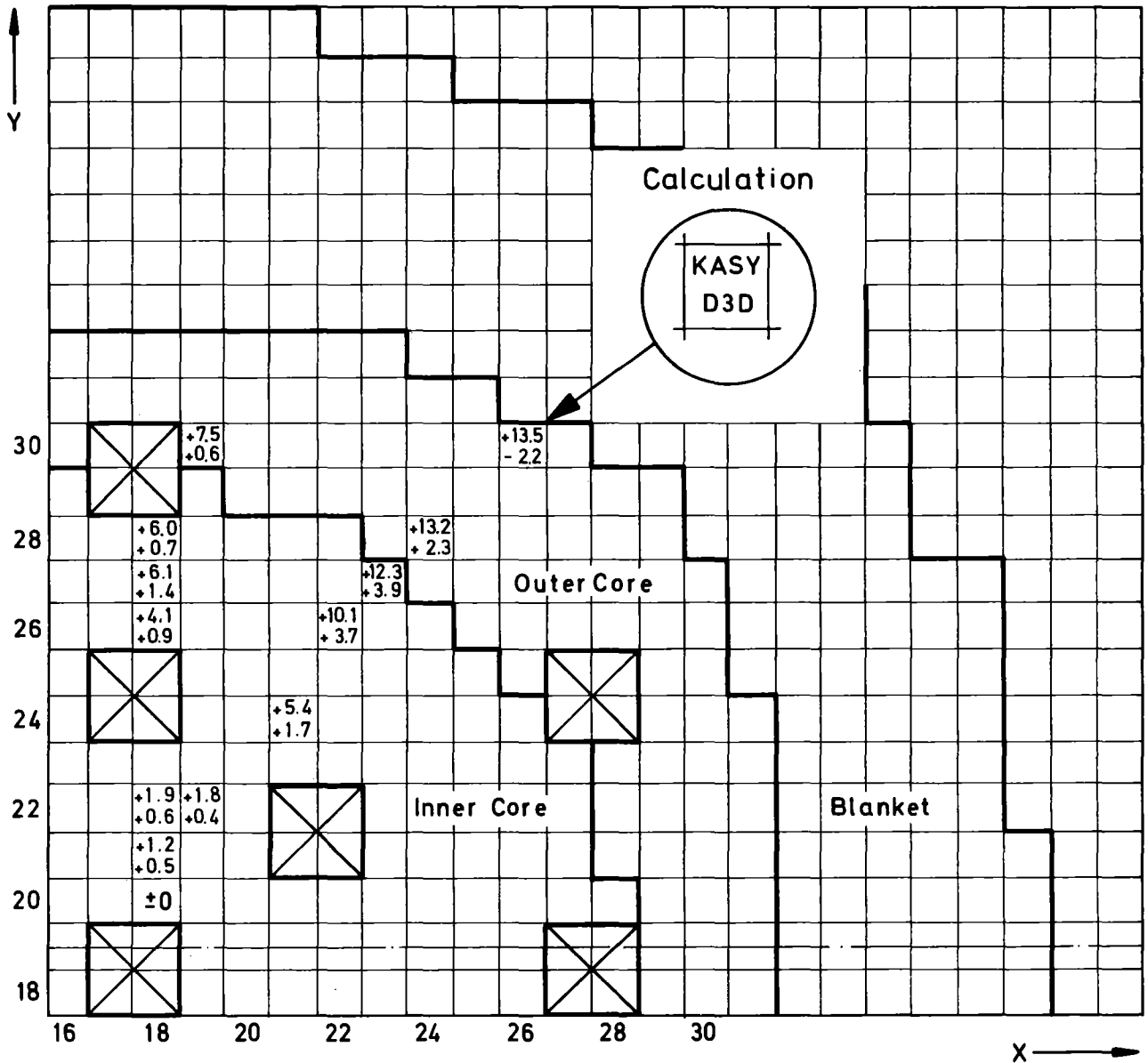
Fig. 25 Relative Deviations $\dfrac{C-E}{E}$ [%] of ^{235}U Fission Rates in the Core-midplane of SNEAK-10-C

Normalization point indicated by '±0'
Calculation : KASY, D3D
Experiment : Foil Activation
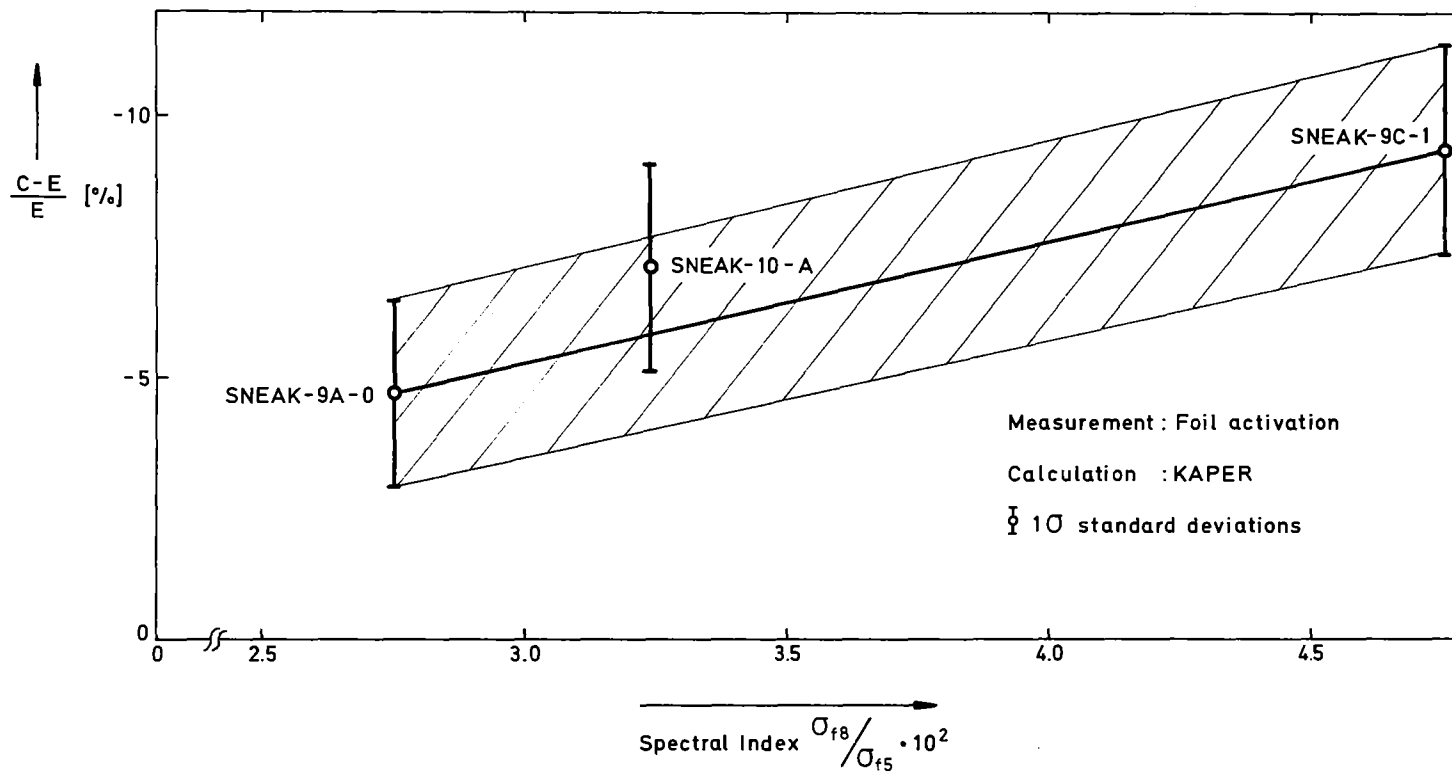
Fig. 26 Underestimation of Spectral Index σ_{f8}/σ_{f5} in the Core Centre of Different Uranium Fuelled SNEAK Assemblies